UNIVERSITY OF TRENTO

DOCTORAL RESEARCH IN

CIVIL, ENVIRONMENTAL AND MECHANICAL ENGINEERING

Cycle XXXII

Curriculum B: Mechanics, Materials, Chemistry and Energy

New Multi-Doped Apatites as 3-D Porous Devices With Multifunctional Ability for Regenerative Medicine

A dissertation by

Lorenzo Preti

Ph.D. candidate

Supervisors

Prof. Nicola Pugno

Dott. Simone Sprio

Esame finale Anno 2020

Contents

Abstract

The research activity described in the present thesis is devoted to the design and development of porous bioactive ceramic scaffolds addressed to the regeneration of bone tissue and was mainly carried out at the Institute of Science and Technology for Ceramics, belonging to the National Research Council of Italy (ISTEC-CNR), during my Ph.D. in Civil, Environmental and Mechanical Engineering (Curriculum B: Mechanics, Materials, Chemistry and Energy).

The regeneration of critical size bone defects is still an unmet clinical need and since decades the development of bioactive scaffolds, capable to instruct and guide bone cells to tissue regeneration is a major research area in material science, including interdisciplinary approaches spanning from the field of chemistry, engineering, biology and medicine. In fact, the currently used bio-inert devices (e.g. metallic devices) can merely provide a mechanical support without regenerating the damaged bone tissue and often inducing adverse side effects such as infections while forcing the patient to frequent revision surgeries, with relevant socio-economic impact.

The main aim of my work was the design and optimization of new materials and processes to produce bioactive ceramics implants as potential solution for the treatment of large and load-bearing bone defects, particularly suitable for cranio-maxillofacial, orthopaedic and spinal surgery.

In my activity I synthesized new hydroxyapatite-based materials, $Ca_{10}(PO_4)_6(OH)_2$, exhibiting ionic substitutions designed to mimic the inorganic part of bone, particularly magnesium, strontium, zinc and carbonate, which increase the osteogenic ability and the bio-resorbability, promote the physiological bone turnover, thus suitable also for osteoporotic patients, as well as the antibacterial ability.

After a general introduction of bone tissue physiology and an overview on the analytical methods involved in the research (Chapter I and Chapter II, respectively), my thesis focuses on the development of various hydroxyapatite nanophases showing multiple ionic substitutions including strontium or zinc ions, in association with magnesium and carbonate, with the purpose to provide synergistic biological effects such as osteogenic and antibacterial ability, and induce microstructural changes,

potentially improving the mechanical performance (Chapter III). In this Chapter, an important role was played by sintering, that was investigated varying different parameters like temperature and atmosphere (Air, CO_2). The influence of doping ions and conditions of sintering was evaluated by chemical-physical, biological and mechanical characterization in order to understand how the presence of doping ions and different conditions of sintering influence the osteogenic properties and the mechanical behavior of the hydroxyapatite scaffolds.

Then, Chapter IV describes novel nanocrystalline, multi-doped hydroxyapatite phases with excellent osteoinductive character and anti-infective properties, evaluated in collaboration with University of Pavia. Physico-chemical analysis highlighted the role of the surface state and charge, as induced by the ion doping, in the enhancement of the biological features.

Finally, Chapter V describes the preparation of 3-D devices endowed where the porosity could be controlled and tailored to achieve suitable compromise between mechanical properties and porosity extent, relevant for bone invasion and osteointegration. The devices are obtained via direct foaming of multi-doped hydroxyapatite ceramic suspension with high-energy planetary ball milling. This method enabled the development of large and complex shape porous scaffolds, recapitulating composition, porosity and structure of the natural bone, thus promising for future practical applications in bone surgery. A better understanding of how dopant ions affect the mechanical properties of these scaffolds has been made possible thanks to the several mechanical and microstructural tests performed on them.

Chapter 1
Introduction

1.1 Human Skeleton

The skeletal system is the rigid framework that support the soft tissues of our body and it includes system of joints and levers that allow the body to move (Fig. 1.1). Simple actions like standing, sitting, walking and taking a breath would not be possible without our skeleton.

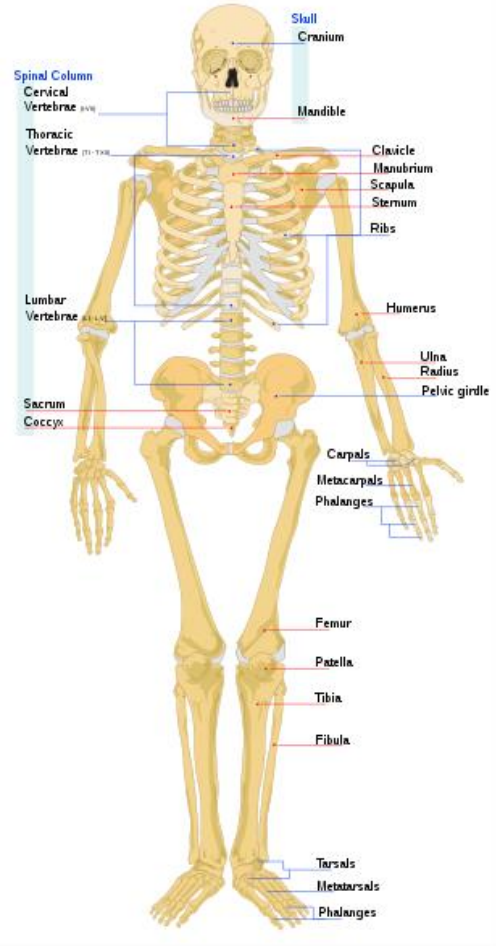

Fig. 1.1 – The human skeleton

At birth the human skeleton is composed of 270 bones, during the growth some of them fuse together thus decreasing the total number of bones at 206, in the adulthood. The skeleton is not only the rigid framework of our body but have complex functions as listed below:

1) *support*: the skeleton provides the framework that support the body and together with muscle allow the body to maintain its shape.
2) *movement*: the joints between bones allow movement. Movements are powered by skeletal muscles, attached to the skeleton with ligaments at various sites. Muscles, bones and joints provide the principal mechanics for movement.
3) *protection*: the skeleton protects our vital internal orgasm from external damage. Particularly skull protect brain, vertebrae protects the spinal cord and the rib cage, and the sternum protects lungs, heart, the major blood vessels and liver.
4) *production of bone cells and lymphocytes*: blood cells productions is a process called haematopoiesis that take place in the bone marrow, which is in the head of long bones and is also responsible of the production of lymphocytes, a support of the immune system.[1]
5) *storage of mine*rals: bones are composed mainly of calcium phosphate and are involved in calcium metabolism. Instead bone marrow contains ferritin, involved in iron homeostasis.
6) *endocrine regulation*: osteocalcin is a hormone involved in the insulin regulation, in the release of sugar and in fat deposition. Bone cells could release osteocalcin.[2]

In order to performs all their functions, bones need to have a lot of different and contrasting properties. They must be strong enough to protect the body but light enough to avoid overloading of it. It must be hard to avoid breakage but porous in order to host cells within it and can be repaired. The human skeleton can combine these different features, thanks to its structure and morphology, hierarchically organized, able to distribute the individual loads on many different points and composite, that is formed from different materials able to give them different properties.

1.1.1 Types of Bones

Bones have different shape, according to their different and specific role in the body. In the human body there are 5 different types of bones: long, short, flat, irregular and sesamoid.

Long bones have the function of support the weight of the body and maintain the correct distance between the different part of the body, to do this they have an

elongated shape. Long bones are composed of a central elongated part, called diaphysis, a middle tubular part composed of compact bone which surrounds a central cavity which contains red or yellow marrow and fat tissue, and two rounded heads, called epiphysis, that is filled with red bone marrow, which produces erythrocytes. Example of long bones are femur, humerus and tibia (Fig. 1.2).

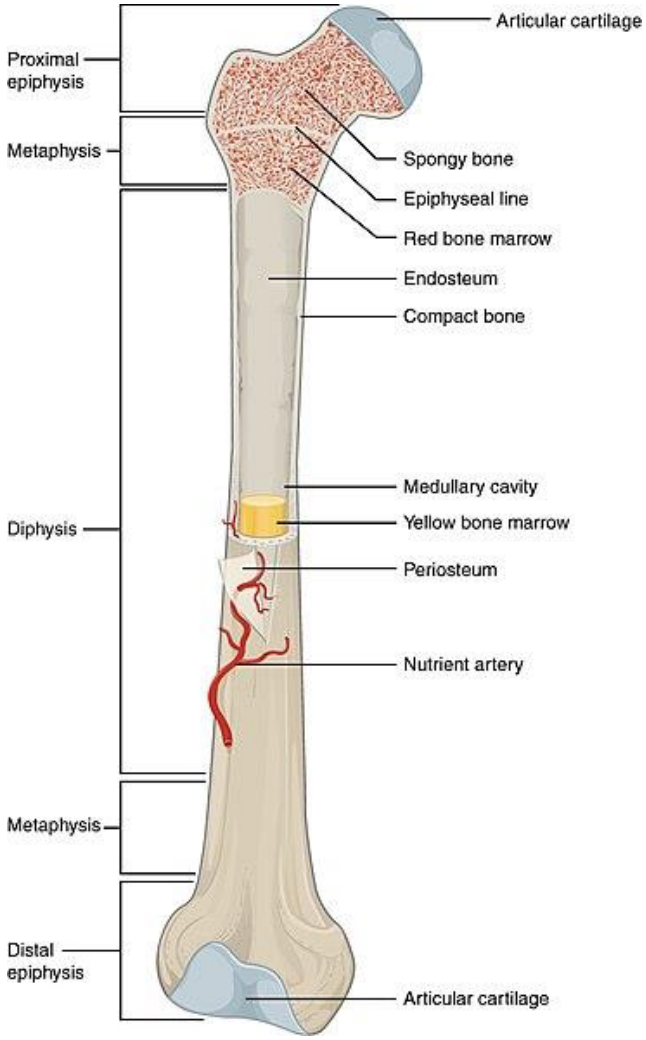

Fig. 1.2 - Structure of a long bone (openstax.org)

Short bones have the function to support they weight with their almost cubical shape, without cavity so they do not contain any marrow. Short bones are concentrated in ankles, like the tarsus, and wrist, like carpus.

Flat bones have the function of protecting the soft organs and providing a broad surface for muscular attachment. They have a planar shape, composed of two layers of planar compact bones enclosing between them a strait of cancellous bone, containing

red marrow, responsible for the creation of new red blood cells. Examples of flat bones are the cranium, the ilium and the rib cage.

Sesamoids are small bones located almost in the joints. They act like pulleys, providing a smooth surface for tendons to slide over and their shape depends from the strain which they are subject.[3]

Irregular bones cannot be grouped as long, short, flat or sesamoid bones. Irregular bones serve various purposes in the body, such as protection of nervous tissue, affording multiple anchor points for skeletal muscle attachment. They consist of cancellous tissue enclosed within a thin layer of compact bone.

1.2 Bone Structure

1.2.1 Bone Tissue

The bone tissue is the connective tissue, that is mainly present in the body, with function of structural support. The bone tissue is made of an organic matrix reinforced by deposits of calcium salts, forming the mineral phase. In the organic matrix are presents several ions, the most present are calcium and phosphate ions, forming a crystalline salt called *hydroxyapatite* $Ca_{10}(PO_4)_6(OH)_2$.[4] Bone tissue is made of organic matrix (about 30wt%) and hydroxyapatite (about 70wt%). The organic phase is mainly composed of collagen fibres and the residual (5-10wt%) is *extracellular matrix* (ECM), that favour the nucleation and growth of mineral phase.

There are two different bone tissue types:

The *cortical bone* (or compact bone) is the hard-outer layer of bones, a dense bone that surround the marrow space. The fundamental structure of compact bones are the osteons, they are generally several mm long and about 0.2mm of diameter. Each osteon is composed of numerous concentric layers (5-20), called also lamellae, of bone tissue that surround the haversian canal, a central canal that contains the bone's blood supplies. In the osteons are present oblique channels, called Volkmann's canals, that interconnect the haversian canal, in order to allow the branching to the blood vessels (Fig. 1.3).[5]

The *trabecular bone* (or cancellous/spongy bone) is the tissue inside the bones, a honeycombed trabecular plates and rods dispersed in the bone marrow compartment.

The lamellae, inside the cancellous bone, are not organized concentrically but in a disordered manner that leaves communicating cavity in bone matrix, that are occupied by nerves, bone marrow and blood vessels (Fig. 1.3). The distribution of the lamellae in cancellous bone is not casually but it depends from mechanical solicitation of bone, indeed the lamellae are aligned in direction of the mechanical solicitation.[6]

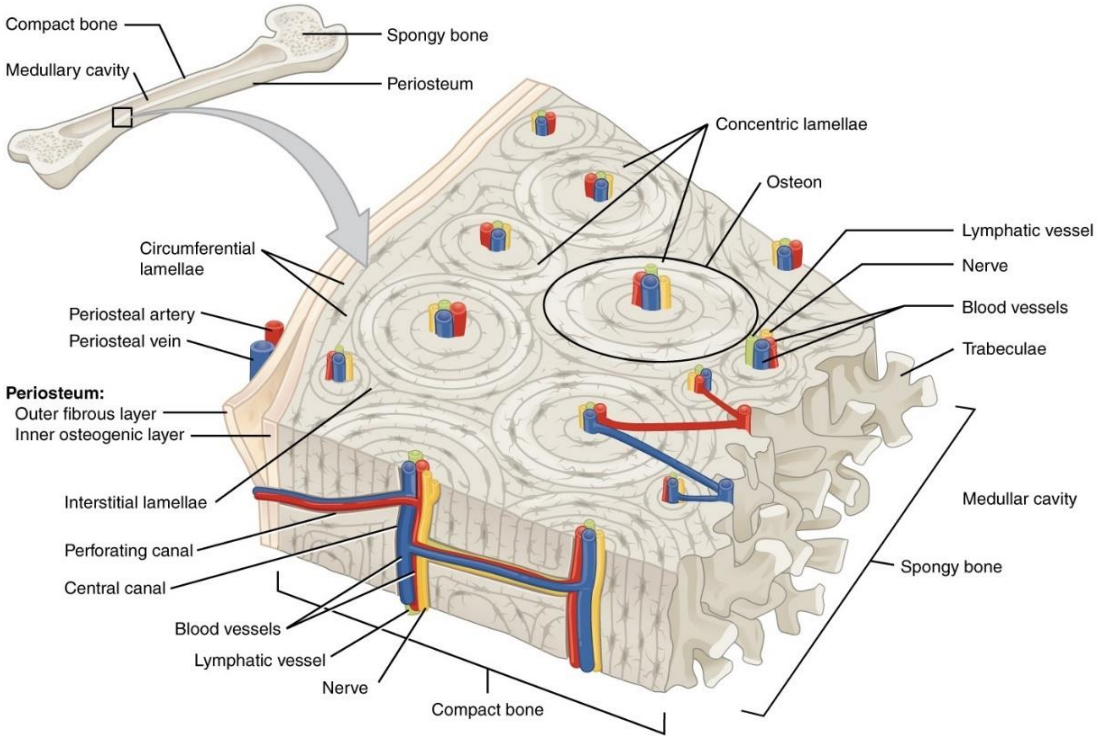

Fig. 1.3 – Internal structure of a bone (openstax.org)

The ratio between cortical and trabecular bones varies depending on types of bone (vertebrae, femoral heads) or human age. Generally, an adult human skeleton is made of 80% cortical bone and 20% trabecular bone.[7]

Bone tissue is organized in a complex and hierarchic way from molecular to the macroscopic scale. At molecular level, ECM made of type I collagen fibrils surrounds cells (≈300 nm long, ≈1.5 nm in diameter) and along collagen fibrils nano-apatitic crystals are present (plate-shaped, 50 nm × 25 nm in size, 1.5–4 nm thick). The nano-apatitic crystals are preferentially oriented along c axis of the collagen fibrils and arranged in a periodic staggered array along the fibrils (Figure 1.3).[8, 9] The material produced is firm but light and flexible, self-healing and multifunctional; it has a high fracture resistance thanks to a multitude of deformations and reinforcement mechanisms happening at many size scales, varying from the nano-structural level to the macroscopic physiological level.[9, 10]

1.2.2 Bone Cells

Bone tissue is continuously remodeled through the concerted actions of bone cells, which include *osteogenic cells*, *osteoblasts*, *osteoclasts, osteocytes*.[11] Bone cells are divided in osteoblasts, osteocytes and osteoclasts, differentiating for the specific functions of bone formation, conservation and removal respectively (Fig 1.4). Osteoblasts and osteocytes are derived from osteogenic cells, but osteoclasts are derived from the same stem cells that differentiate to form macrophages and monocytes.[12] Within the marrow of the bone there are also hematopoietic stem cells. These cells give rise to other cells, including white blood cells, red blood cells, and platelets.[13, 14]

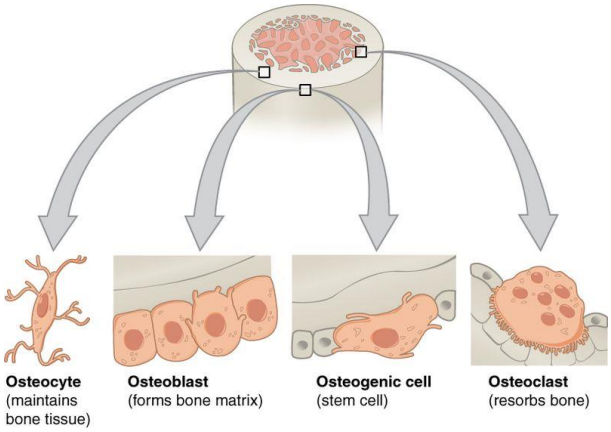

Fig 1.4 – Bone cells (openstax.org)

Osteoblasts: their roles are to synthesize new bone matrix and regulate the osteoclasts. Osteoblasts form a framework of collagen fibres around it, that gives a tight connection with the adjacent osteoblast cells. Then attached to the collagen matrix, the osteoblast release calcium and phosphate ions which naturally precipitate forming hydroxyapatite (mineral phase of bones), so a matrix called osteoid is formed. The osteoblast could be inside or outside the osteon. When the osteoblast becomes trapped inside the osteon, it becomes an osteocyte. Other osteoblasts remaining outside the osteon are called lining cells and are used to protect the underlying bone.

Osteoclasts: they are large and moving cells, endowed with more nuclei formed in bone marrow. They can degrade the mineralized bone tissue, isolating it in microenvironments and acidifying it until bone tissue is dissolved in the organic and inorganic matrices. Their activity is regulated by chemical signals (hormones, low

calcium levels) or mechanical signals that promote the osteoclasts activity to destroy some lamellae to deposit new differently oriented lamellae to stabilize the applied stress.

Osteocytes: they are the most common cells in a bone, with a star-like shape. The main body of these cells reside inside lacuna, small holes inside the osteons. They communicate each other thanks to their extension located inside the canaliculi, small channels. Therefore, osteocytes are thought to act as mechanosensors, instructing osteoclasts where and when to resorb bone and osteoblasts where and when to form it. In case of trauma or fracture, the osteocytes could become osteoblasts once again.[15]

1.2.3 Bone Modeling and Remodeling

The bone is a living tissue that constantly undergoes processes of modeling and remodeling, adapting to metabolic and structural demands. Modeling and remodeling are two different processes that occurs in different moments. In case of mechanical overload, trauma or fracture, the modeling changes the shape and size of bones. The bones in order to ensure a proper function, needs a constant turnover. Remodelling is the responsible of that turnover (Fig 1.5).

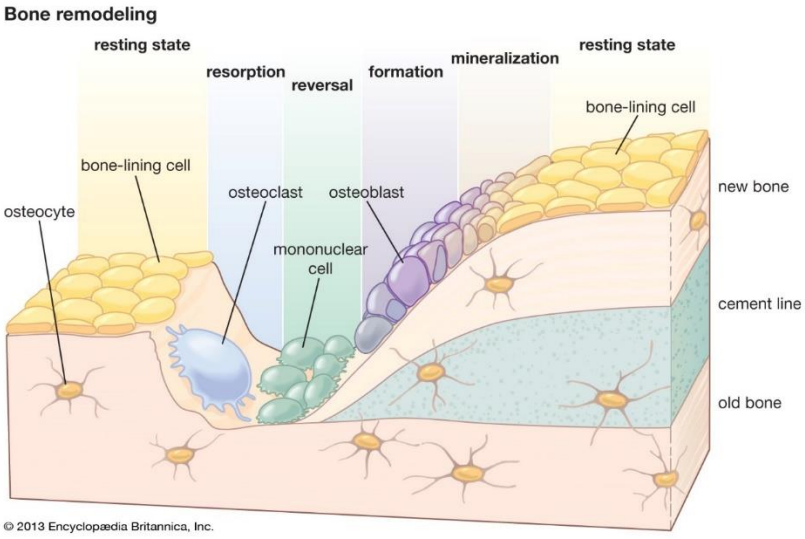

Fig 1.5 – Bone remodeling process (© 2013 Encyclopaedia Britanica, Inc.)

The first phase of the remodeling process is resorption phase, in which osteoclast, after differentiation, start their activity of bone resorption, forming an Howship lacuna (resorption phase). When osteoclasts finish their works, in the reversal

phase, some mononuclear cells are attached to the lacuna surface. The function of these cells is not completely clear, but it helps the activity of the following phases, formation and mineralization. In the final phases osteoblast fill the lacuna, depositing layers of osteoid. Finally, the osteocytes cells could differentiate in osteoclast or lining cells, depending from the position. [16]

The self-repair ability of bone is related to its hierarchical structure and there is increasing evidence that such structure is relevant for activation of mechano-transduction phenomena at the basis of bone remodeling. It is evident that mechanical loading at physiological strain magnitudes results in an increase of the metabolic activity of osteocytes and provides evidence for their involvement in bone mechano-transduction. Unfortunately, it is not clear how osteocytes actually sense mechanical loading and transduce it into cellular signal. Forces applied on bone during movement result in changes of the hydrostatic pressure, direct cell strain, fluid-flow-induced shear stress, and electric fields (as a result of fluid flow). A number of researchers hypothesize that flow of interstitial fluid is the most probable way of informing bone cells about mechanical loading. Flow of interstitial fluid occurs because the application of mechanical strain causes the volume of some pores to decrease slightly and the volume of other pores to increase slightly, creating differences in bone fluid pressure, which results in fluid flow. If this theory is correct, then the osteocytes with their canaliculi network are the mechano-sensor cells of bone.[17]

1.2.4 Mechanical Properties of Bone

The hierarchical architecture of bones, especially that of the cortical bone is the most responsible of the mechanical properties of Bones. The mechanical forces acting on the bones is distributed on all the elements of the structure, thanks to the osteons. The mechanical forces influence the structural arrangement of osteons that are aligned to the direction of the mechanical strength. For this reason, cortical bone is an anisotropic material, varying its properties when loaded in different directions.

For long bones stiffness is maximal for axial loads and minimal for perpendicular loads. Typically, for cortical bone the axial compressive strength value is about 190MPa while for transverse loading the typical value decreases to 130MPa.[18]

In case of small load, there is a small deformation that vanish after the load is removed, so bone goes back to its original shape (elastic response). When the load is bigger than yield strength, the behaviour become plastic and the deformation is permanent also after load removal. At the failure point we have the fracture of the bones.[19]

Bone is a composite material, in which collagen is weak and ductile while the hydroxyapatite is strong and brittle, so that the bones can exhibit a viscoelastic behavior. Viscoelasticity in bone arises from a variety of mechanisms. Since bone is a hierarchical composite, which contains structure at multiple length scales, viscoelasticity can arise from multiple processes at the different scales. On the molecular scale, collagen as a proteinaceous phase can give rise to significant viscoelasticity. At a grosser scale, there are also many interfaces such as the cement lines between osteons (which are large, 200-µm-dia, hollow fibers), and the boundaries between lamellae within osteons, in bone. A thin layer of a protein-polysaccharide substance occurs at cement line interfaces. Cement lines are compliant. Viscous-like cement line motion gives rise to a portion of the viscoelasticity in bone, particularly at long times. The mineral phase of bone is crystalline hydroxyapatite, which is virtually elastic; it provides the stiffness of bone.[20]

1.3 Bone Disease

In case of a simple fracture, the typical therapy is based on the reduction of the fracture to realign the two stumps of the bone and the immobilization of them, and the healing of the bones starts spontaneously and in an autonomous way, thanks to the ability of bone cells to repair bone damage.

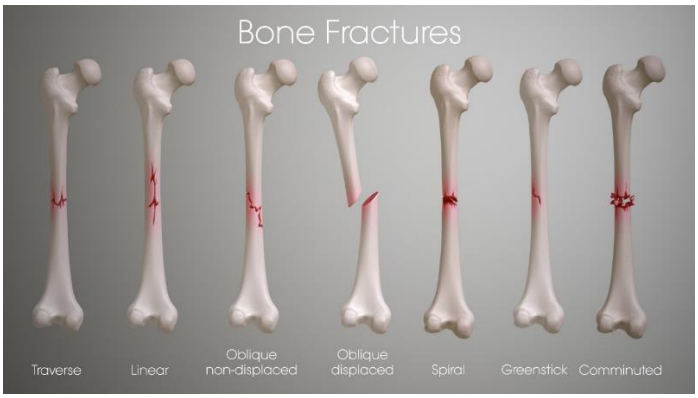

Fig 1.6 – Bone fractures (scientificanimations.com)

In the cases of more serious fractures, complicated by significant bone loss or fragmentation, spontaneous healing is no more possible (Fig 1.6). In some fractures called displaced fractures, the pieces of fractured bone are not in their original place, so an operation is required to put the pieces of bone in axis to ensure healing. In case of a bone broken into several pieces, metallic screws have to be inserted to hold together the different pieces, but in the case of significant bone lack above a critical dimension (which in human is about 2 cm) the implantation of a bone substitute is required.

Besides fractures, several degenerative diseases can impair the bone functionality with serious impact on the life quality and wellbeing. Also in these cases significant bone loss can occur and in such cases the use of bone substitutes is mandatory. In this respect, given the metabolic impairment related to such diseases, great scientific activity is today dedicated to the development of bone substitutes able to give enhanced support to bone regeneration.[21-24]

Osteoporosis is one of the most common diseases that affects the bones. Osteoporosis commonly affects people over 50 but also a significant number of younger patients and, considering the increasing of the average life expectancy, the incidence of the disease is expected to raise steadily in the incoming years. Osteoporosis is characterized by deterioration of the bone tissue microarchitecture and decreased bone mass. What causes osteoporosis is an imbalance between the activity of osteoclasts, which resorb bone, and the osteoblasts, which deposit new tissue. That imbalance leads to a progressive reduction of the bone mass and to an increase in bone fragility and consequent increased risk of fractures. To restore the physiological bone turnover, several drugs have been developed, such as vitamin D, hormones, bisphosphonates. The use of strontium ranelate has been the most relevant antiosteoporotic therapy but it was withdrawn due to the numerous secondary effects and drawbacks at a systemic level. In spite the systemic administration of drugs is still a very common procedure, it can yield problems like sensitization to drugs or drug resistance. Therefore, the investigation of new biomaterials able to release therapeutic factors is today a hot research topic. A good solution to prevent systemic administration could be the use of biomaterials able to release in situ therapeutically active molecules in controlled profiles, suitable for sustained and more effective bone therapies.[25, 26] Strontium doped

biomaterials could provoke an in situ release of Sr ions that inhibits bone resorption, acting as anti-osteoporotic agent, without the side effect related to a systemic administration. [27]

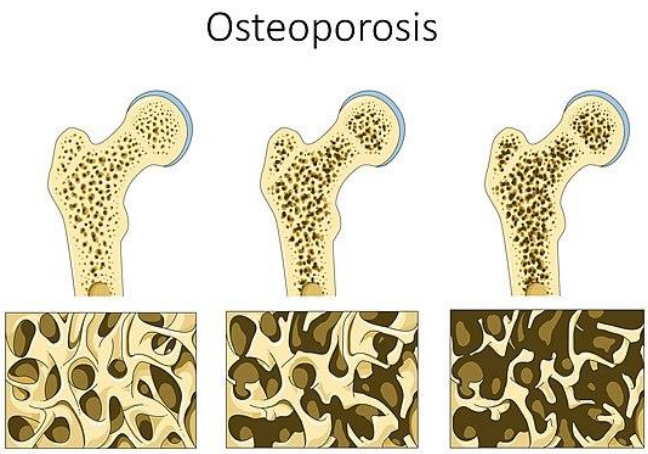

Fig 1.7 - The left bone is a healthy bone while the right bone is affected by osteoporosis

(smart.servier.com)

Remaining on disease affecting bone metabolism, another serious disease is Paget's disease of bone that affect the 3% of the population approximately.[28] The disease caused by a virus, paramyxoviridae, but also favoured by genetic and environmental factors, causes an excessive turnover of bone, that leads to a disorganization in bone remodeling. That disorganization can cause misshapen bones, arthritis, fractures with the consequent pain. Often Paget's disease commonly affected only a few bones in the body, the femur, the pelvis and lower lumbar vertebrae. In rare occasion, it can develop into a bone tumour known as Paget's sarcoma.[29] The more commonly used drugs to treat Paget's disease are calcitonin and bisphosphonates. In the worst cases a surgical operation is needed for the reduction of the fracture caused by this disease or remodeling the bone deformity.

Cancer is a major disease involving bone tissue, in particular there are 4 types of cancers that can affect the skeletal system, chondrosarcoma that originates from cartilage,[30] osteosarcoma that develops inside the bones,[29] metastatic tumours, due to metastases in the bones resulting from tumours in other parts of the body and Ewing's sarcoma, which develops from immature nerve terminations of the bone marrow.[31] For all 4 cases, the treatments are the same, chemotherapy, radiotherapy, generally not very effective, and surgical intervention, for physically removing the bone portion containing the

cancerous cells. Treatments are often performed simultaneously to treat the same tumour. However, the lack of bone substitutes effective with large bone defects is still a concern and hampers the development of new anticancer therapies.

1.4 Bone Scaffolds

1.4.1 Ideal Bone Scaffolds

When a bone fracture occurs, our body works to heal the fracture and create new bone. In the zone of the fracture, the blood vessels, that also damage, starts bleeding and there is the formation of a hematoma. Then our cells work to create cartilage and we have the formation of a soft callus, where there is the creation of new blood vessels. In this situation osteoblast starts to create new bone tissue and the soft callus become a hard callus. Finally, the osteoblast works to consolidate the bone and the osteoclast works to remodelling it (Fig. 1.8). That is the bone healing procedure that occurs when the two-piece bone, after a fracture or after a surgery, are not so much distant and the cartilage could fill that gap the time necessary to a new bone formation.

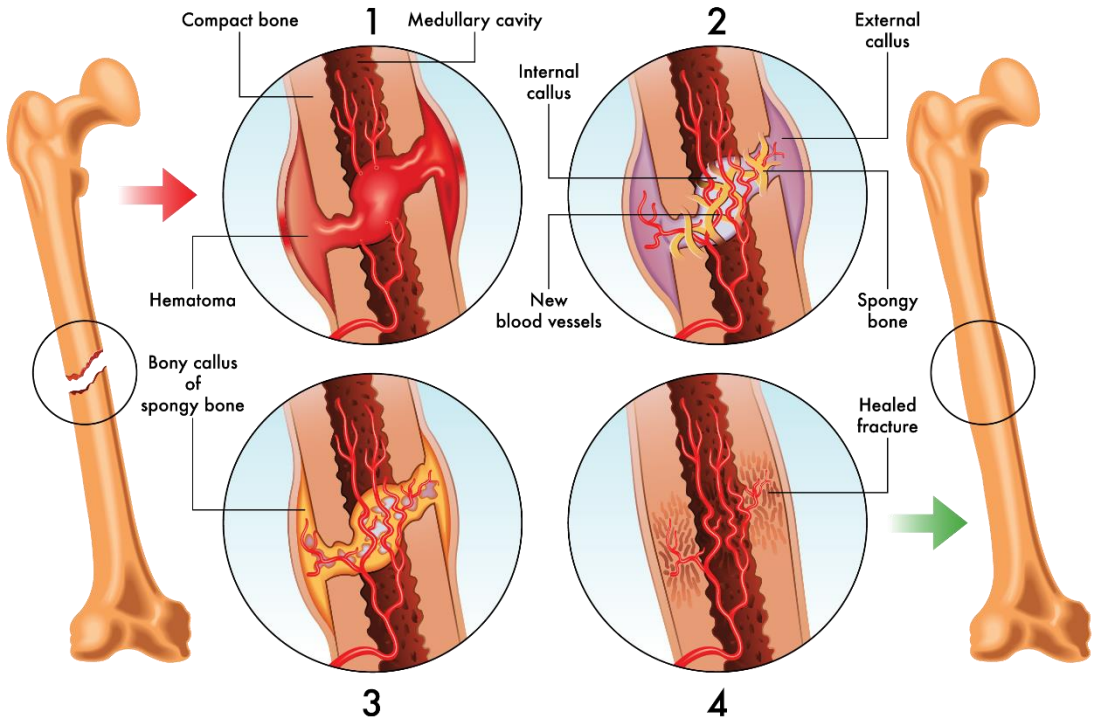

Fig 1.8 – Bone regeneration (burstbiologics.com)

There is some case where it's impossible for our body to regenerate the bone by itself, that occurs when the two pieces of bone are too much distant. In that case the use of device that fill that gap could be useful for the bone healing process. So that should be the function of bone graft, help our body in the regeneration of new bone (fig 1.9).

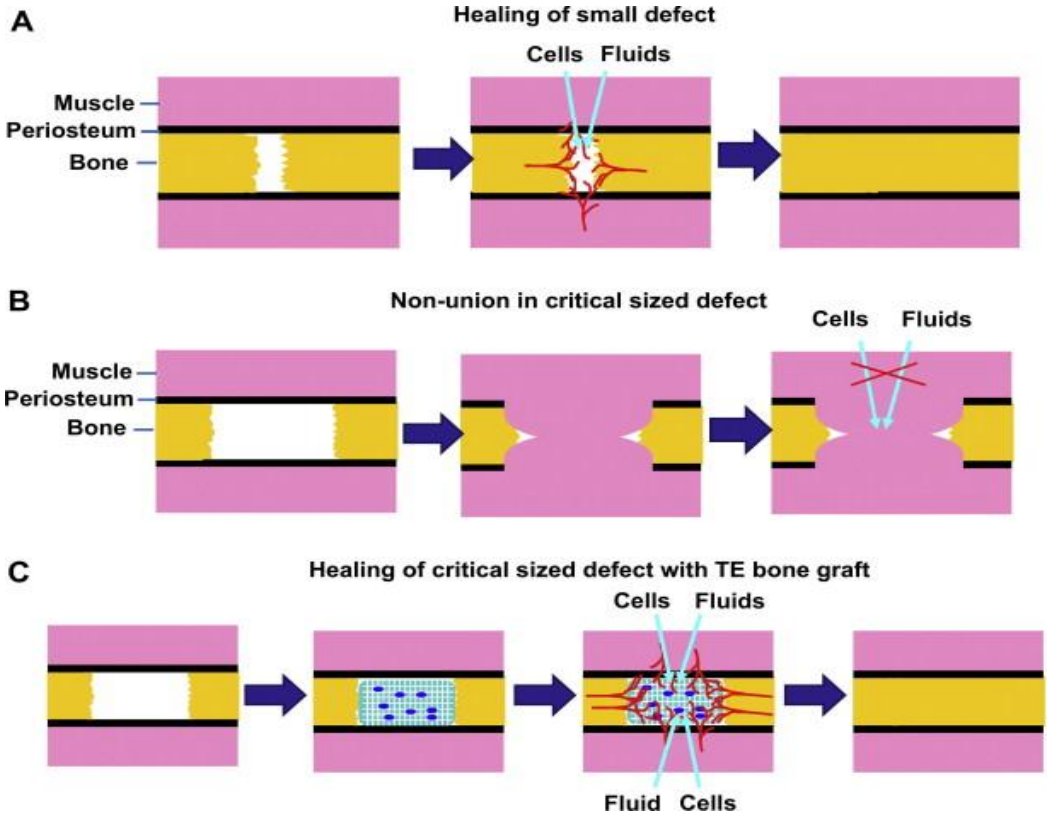

Fig 1.9 – A) Healing of small defects; B) Critical sized defects; C) Healing of a critical sized defects with bone scaffolds (sciencedirect.com)

The most common scaffolds used for bone regeneration are natural bones, there are three different sources for these bones: autograft, allograft and xenograft. Autograft transplant consists in the removal of part of one bone of the patient, usually iliac crest, and its insertion in the damaged site.[32] It is usually considered as the gold standard for its regenerative properties and safety. However, the quantity of bone that can be withdrawn is limited and it can cause morbidity in the site from which the bone is taken. Allograft implant consists in the use of bones taken from human cadaver.[32] However, before the use of the implants, the bones must be sterilized and stored in special bone banks, with a very expensive procedure. Moreover, the purification treatment destroys the original bioactivity of the bone, thus reducing its regenerative ability to a mere

physical sustain. With respect to autografts, allograft implants are less safe and do not lead to a total regeneration but guarantee a larger quantity of material without secondary damages for the patient. Xenograft implants consist in the use of bone materials from a different species, commonly bovine or porcine, freeze dried and deproteinized.[33] Xenografts allow for a greater availability of the material at the expense of a lesser biocompatibility.

Considering the poor regenerative ability of implants made of natural bone, the development of synthetic bone grafts is intensively pursued since decades. Connective tissues can be regenerated only in the presence of scaffolds able to direct cell activity toward suitable phenotypes and to chemically and structurally assist the regeneration process. In the case of hard tissues such as bone, this requires the synthesis of three-dimensional (3D) constructs that are able to exchange chemical signals promoting osteogenesis and can then be progressively resorbed during the formation and remodeling of new tissue. Moreover, particularly when the regeneration of extensive portions of bone is involved, morphological and mechanical biomimetics is also strictly required, in order to allow cell colonization and the formation of a proper vascularization network. In addition, the healing of load-bearing bones also needs scaffolds with complex and organized morphology, so as to provide improved biomechanical behavior and to allow proper mechanotransduction of the mechanical stimuli down to the cell level.[34]

Composition. The composition of the scaffold is a fundamental aspect to elicit a positive reply by cells. Suitable chemical signals from the scaffold can help cells to attach to its surface, proliferate and finally, differentiate into opportune phenotypes. The scaffold composition can be also tailored to enhance bio-resorption which is a very relevant phenomenon to allow digestion of the scaffold by osteoclasts and new bone formation by osteoblasts.

Porosity. For bone regeneration the colonization of the whole scaffold by the bone cells is required, therefore a high porosity extent with a good interconnection level is required, also to achieve effective exchange of nutrients and permitting the development of a vascular network. For this reason, the pores size is an important aspect, so that a macro porosity in the order of 100-300 micron allowing cells inflow,

associated with a micro porosity (i.e. few microns) allowing the interchange of liquids and signals between cells and blood flow, is considered as an effective configuration.[35]

Surface properties. The roughness of the material favours the attachment of the cells and their proliferation.[36, 37] Depending on the material composing the implant there are different methods to improve the roughness of the surface. For plastic and metallic prostheses, the roughness of the material is improved by chemical reaction or by coating with a rough material. For ceramic materials the roughness of the surface relates to the crystallinity of the material. A low crystallinity relates to high surface area and roughness of the material.

Mechanical properties. The mechanical properties of the scaffold must be similar to the one of natural bones. This would give to the scaffolds the function of support the bone in the initial phase of regeneration. An important aspect to take in account is stress shielding or stress protection, that occurs when metal implants, such as bone plates and screws, are used to repair fractures or in joint replacement surgery. Although rigid metal plates stabilize the fracture site, help maintain contact between bone fragments, and allow early weight bearing and patient mobility, the higher stiffness of the implant results in bone loss as a result of decreased physiologic loading of the bone.

The above physical and chemical features determine key properties of a biomaterial, regulating its biologic behaviour in vivo:

Osteoconduction. An osteoconductive scaffolds allows and helps bone with its chemical-physical properties, to grow and proliferate on its surface.[38]

Osteoinduction. An osteoinductive scaffolds has the capacity to recruit immature cells and stimulate them to differentiate in preosteoblasts.[39] It is the same process involved naturally in bone healing from fracture.

Osseointegration. After surgery, if there is a connection between the scaffold's surface and the living bone, that is called osseointegration.[40]

Angiogenesis. Means the capacity of the prostheses of promoting the formation of new blood vessels and their penetration into the prostheses. Blood vessels are fundamental for making all the prostheses habitable to the cells, not only the surface, providing the correct provision of nutrients.[41]

Resorbability. The prostheses could be dissolved or not. In the case of polymeric scaffolds, there could be a chemical dissolution that could produce acidic chemical

species, that jeopardize the regeneration process. If the materials take parts in the metabolic processes, we have not a real dissolution but a resorption of the materialThe properties is called bioresorbability.[42]

Antibacterial effects. Implantation of medical devices is a frequent surgical practice which, however, is a gateway for pathogen contamination and infections that are often at the basis of the implant failure. Nowadays, this problem raises great concern, mostly due to the bacterial resistance to antibiotic drugs, which is increasing at an alarming rate. In this scenario, the development of drug-free solutions as an alternative to systemic and intensive administration of antibiotics and associated with therapeutically effective biomaterials is increasingly demanded.

In case of bone, this requires the synthesis of three-dimensional constructs able to exchange chemical signals promoting osteogenesis and to progressively be resorbed during the formation and remodelling of new bone. Besides, particularly for the regeneration of extensive portion of bone, a morphological and mechanical biomimesis is also required, to allow cell colonization and formation of a proper vascularization tree. The healing of load-bearing bones also requires scaffolds with a hierarchically organized morphology, to provide improved biomechanical behaviour and allow a proper mechano-transduction of the mechanical stimuli down to the cell level.

1.4.2 Current Solutions

The first bone implants are traceable to early Egyptians, South-Central American and China cultures, using ivory or stone to replace teeth.[43] In the last century, biological and material science made huge step forward, contributing to the development of increasingly performing biomaterials. Nowadays, the materials used for bone grafting are divided into three main different groups: polymeric, metallic and ceramics.

1.4.2.1 Polymeric implants

A lot of different natural or synthetic polymers are widely used for bone grafting. Depending on the polymer used, the scaffold can have different properties. According to the use, their composition can be changed easily, in order to change the physical characteristics of the polymers. Polymers can be changed in to more porous or softer

form. Polymers can be manipulated easily and allow better reproduction. They show fibrous connective tissue attachment. It is also possibly to prepare resorbable scaffolds in different ways. They are plastic and easily mouldable, also in 3D printing. However, polymers present several disadvantages. They have poor mechanical properties, not adequate for function of support. There is no adhesion between living tissues and polymer scaffolds, and they can generate adverse immunologic reactions.

One of the most polymers used is Polyether ether ketone (PEEK) that is not resorbable, indeed several resorbable polymers are used: collagen, chitosan, silk, polylysine (PLL), poly-L-lactic acid (PLLA) and acid poly-lactic-co-glycolic acid (PLGA). [44]

However, there are several concerns related to the use of polymeric absorbable implants. One of the major concerns is the potential for adverse reactions due to accumulated degradation products. These degradation products create a micro-environment at low pH, that cause interaction problems between the implants and the cells.[45]

1.4.2.2 Metallic implants

The biomechanical properties of metals which made them suitable as an implant material. Besides these properties, metals are also easy to process, and it is possible to product them in every shape. Metallic implants can be sterilized by the common sterilization procedure which makes them easy to use. The first metals used were stainless steel, gold and cobalt-chromium but, but these materials presented low success rates, so they have now become obsolete and, thanks to the technological process, are now replaced by newer ones.

Nowadays, the most common metals for implants is Titanium (Ti) and its alloys (mainly Ti6Al4V and Ti6Al7Nb). Titanium shows excellent mechanical properties and biocompatibility due to the formation of stable oxide layer, thanks to these properties, titanium has a good record of being used successfully as an implant material. [29a]. Titanium reacts with several other elements for e.g.: aluminium, copper, silver, iron, zinc, niobium and vanadium to form alloys. Titanium alloys exists in three forms alpha (α), beta (β) and alpha-beta (α-β). The alloys most commonly used for implants are of the alpha-beta variety. The most common are Ti6Al4V that contains 6wt% of aluminium

and 4wt% of Vanadium (a.k.a. titanium grade 5) and Ti6Al7Nb containing 6wt% of aluminium and 7wt% of Niobium (UNS designation R56700).[43]

Despite their great biocompatibility, their excellent mechanical properties and their workability, metallic implants are not resorbable and after a period requires surgical intervention for substitution of the implant because of the corrosion. The problem of resorbability and corrosion is overcome by magnesium, resorbable in the body. This means that the corrosion by-products are excreted or integrated through natural metabolic processes.[46]

To conclude, metals are excellent materials for prosthesis, thanks to their biocompatibility, mechanical properties but they have some drawbacks: they can cause infection more easily than bioceramics and they disperse debris by erosion in the physiological environment and so their role as bone graft is limited but it's being explored thanks to their unique properties.[47]

1.4.2.3 Bioceramics

Bioceramics are widely considered as the elective materials for bone grafting. They are anticorrosive, resistant, biocompatible and in certain cases show osteointegrative properties. Usually, the main disadvantages of bioceramics are rigidity, brittleness and they do not show resorbability. The bioceramics commonly used are calcium phosphates (in particular hydroxyapatite and tricalcium phosphate) or metal oxides, like titanium oxide (TiO_2), aluminium oxide (Al_2O_3) and zirconium oxide (ZrO_2). Bio-glasses represent a wide range of biomaterials, developed with the purpose to obtain a composition rich of bioactive ions whereas retaining an amorphous structure that can favour biologic performance. Bioglasses contain variable amounts of SiO_2 (30-60wt%), CaO and/or CaF_2 (20-40wt%), Na_2O (5-25wt%) and P_2O_5 (2-15wt%) or aluminosilicates. Bio-glasses can be obtained in a wide variety of formulations, enabling a tailoring of their applications. A significant drawback is that bio-glasses cannot be easily obtained as a 3-D mechanically performing structure because of the impossibility to apply high sintering temperatures (which would provoke the crystallization of various phases, and the loss of many bioactive properties related to the crystal disorder).

Among bioceramic materials of particular importance are the calcium phosphates. These are composed of calcium, phosphorus and oxygen as fundamental elements. Calcium is an essential ion in the human body that, in an adult, contains approximately 1100g of calcium. Normally 99% of calcium present in the body is contained in bones but could also be complexed with proteins, like albumin or globulin, with anions, like bicarbonate, lactate or sulphate, or in the free ionized form. In combination with phosphate calcium is the main component of bones and teeth. Phosphorus is an essential element in the body, that mass about 1% of the total weight of the body. It is used in a large number of molecules like DNA and ATP and, in combination with calcium is the main component of human bone and teeth. All these phases are characterized by a specific calcium: phosphorus (Ca/P) ratio; in the case of hydroxyapatite, however, this value can vary significantly

The most common calcium phosphates are:

Monocalcium phosphate (MCP), ($Ca(H_2PO_4)_2$, Ca/P=0.5. It is the most acidic and soluble (K_s=1.14) among all calcium phosphates. It can be obtained as a monohydrated or anhydrous phase. It is not biocompatible, and it is widely used as fertilizer.

Dicalcium phosphate dehydrate (DCPD), ($CaHPO_4*2H_2O$), Ca/P=1. It is soluble (K_s=6.59) and for this reason it is used as a bone cement. It has the mineralogic name of brushite. It can be also as anhydrous form and is called dicalcium phosphate dehydrate or with the mineralogic name of monetite (DCPA, $CaHPO_4$)

Octacalcium phosphate (OCP), ($Ca_8(HPO_4)_2(PO_4)_4*5H_2O$), Ca/P=1.33. It is an insoluble form of calcium phosphate (K_s=96,6) that is considered the promotor of calcium phosphates precipitation.

Tricalcium phosphate (TCP), ($Ca_3(PO_4)_2$, Ca/P=1.5. It is one of the most important calcium phosphates. It exists in two main different polymorphs, α and β, where the α is stable only at high temperatures. The solubility differs significantly from α to β and the α polymorph results much more soluble.

Amorphous calcium phosphate (ACP), Ca/P=1.2-2.2. It has not a crystalline structure or a well-defined formula. It is more soluble than α-TCP.

Tetracalcium phosphate (TTCP), ($Ca_4(PO_4)_2O$, Ca/P=2. It is the most basic of all the calcium phosphates and the one with the highest Ca/P ratio. It is stable at high temperature (≥1300°C) and is partially soluble (K_s=42).

Hydroxyapatite (HA), ($Ca_{10}(PO_4)_6(OH)_2$), Ca/P=1.67. It is one of the most insoluble form of calcium phosphates (K_s=58) but it is the most studied compound because it closely resembles the main component of the mineral part of human bone. In its stoichiometric form it is not resorbable, but it is widely studied in the form of an ion doped phase where doping ions strongly affect the physico-chemical properties and confer enhanced biological ability.

In the next paragraphs we will more deeply describe the most important calcium phosphates for medicine: TCP and HA.

1.5 Hydroxyapatite

The hydroxyapatite (HA) is a naturally occurring mineral with the formula $Ca_5(PO_4)_3(OH)$ but is usually written $Ca_{10}(PO_4)_6(OH)_2$ to denote that the crystal unit cell comprises two entities (Fig 1.10). It is also the main inorganic component of biological hard tissues such as bones and teeth of vertebrates.

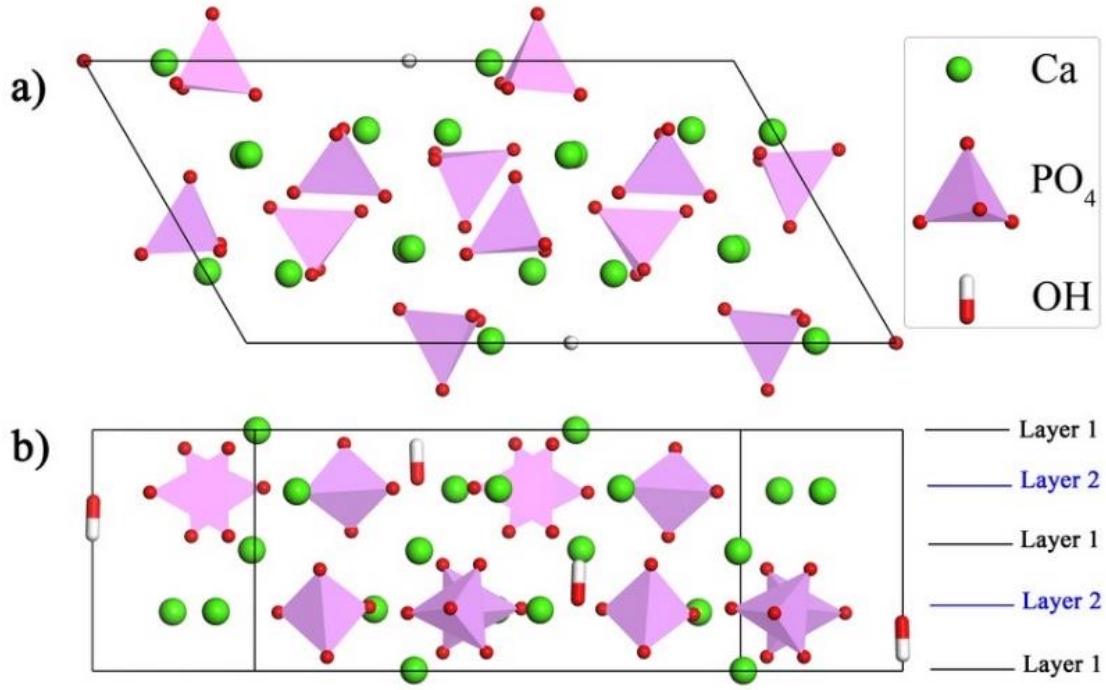

Fig 1.10 – Hydroxyapatite crystal structure a) top view b) side view[48]

The formation of new bone tissue is promoted by the exchange of chemical signals between the bone scaffolds and the surrounding environment. A good bone

scaffolds could generate a chemical signal, that induce osteoblast cells to synthesize new bone tissue whereas, osteoclast cells carry out a process that leading to the remodelling of the newly formed bone tissue in a morphologically well-organized bone. The mineral part of bone is made up of hydroxyapatite crystal nano-structured, in a nearly amorphous form. The hydroxyapatite (HA) of the mineral part of bone is not the stoichiometric one ($Ca_{10}(PO_4)_6(OH)_2$) but it contains also several doping ions, such as CO_3^{2-}, Mg^{2+}, Na^+, K^+, Cl^-, F^- and many others. The presence of these ions inside the HA lattice, induce a crystallographic disorder of the apatite structure itself. That disorder causes an increase in solubility of HA, making more bio-available the ions inside the HA lattice, not only the doping ones but also Ca^{2+}, HPO_4^{2-}, OH^-. The bioavailability of all these ions induces the chemical signal that lead to the adhesion of cells on the HA and the subsequent activity of bone formation and remodelling.[49, 50]

Carbonate ions can occupy two different sites in the HA crystal lattice, the site of hydroxyl (A-type carbonation) or phosphate site (B-type carbonation). The carbonate in the B-type position is the major source of the structural disorder in bone mineral, enhancing the apatite solubility and the chemical reactivity. The content of carbonate and its position inside the bone mineral, change depending on the age of the individual. Furthermore, in young bone carbonate ions are also presents in a hydrated layer that surround the HA crystals (an amorphous domain), thus representing a reservoir of ions that promote the remodeling processes.[51] Tests of ion release carried out in a simulated body fluid at 37°C show the increase in solubility due to the carbonate presence.[52, 53] The increase of solubility is not the only effect of the presence of carbonate inside mineral bone, but in vitro studies evidenced that the carbonate content influences osteoclastogenesis and substrate resorption, so to favour osteoblast proliferation and osteogenesis.[54, 55]

Magnesium is a doping ion that replace calcium in HA crystals of the bone mineral. Mg^{2+} is particularly important in the regenerative and remodeling processes, indeed it was found that is concentration in bone mineral is about 5mol% during bone formation and it decreases with calcification and the ageing of the individual.[56, 57] Magnesium affect the size and shape of mineral nuclei, increasing the kinetic of HA nucleation on collagen fibres and contemporary retards its crystallization. The presence of magnesium in the mineral bone causes a structural disorder, that induce a continuous

exchange of ions between the outer amorphous hydrated layer to the crystalline core. The replacement of calcium by magnesium in surface crystal sites favours protein adsorption and cells adhesion to the scaffold because Mg^{2+} is able to increase the number of molecular layers of coordinated water.[58, 59] On the contrary, the lack or the low content of magnesium inside the HA crystal lattice can cause the cessation of bone growth, the decreasing of osteoblast and osteoblast activities, inducing osteopenia and bone fragility.[57] In vivo studies of granulated Mg-HA, implanted in rabbit femur, evidenced a greater osteoconductivity over the time and higher material resorption of the Mg-HA respect the stoichiometric HA;[52] moreover, studies of osteoblast gene expression profiles from Mg-HA scaffolds revealed higher expression of specific markers of osteoblast differentiation and bone formation, associated with a lower osteoclastogenic potential.[60]

Another doping ion that replace calcium inside the HA crystal lattice is strontium. In vivo studies showed that the presence of strontium inside the bone enhance the osteogenesis and reduce the bone resorption, that leads to a gain in bone mass and improvement in mechanical properties.[61, 62] In some cases the effect of osteoporosis is reduced by an oral administration of strontium ranelate, chloride and lactate, there also evidence of stimulatory effects on bone collagen synthesis.[62, 63] Thanks to its anti-osteoporotic properties, able to induce biomineralization process, the incorporation of strontium ions was widely performed in recent years.[61, 64]

In natural bones, it is possible to find another doping ion, that replace calcium, in smaller amount (about 0,1mol%), the zinc ion. Zn^{2+} could inhibits osteoclasts activity, which cause bone resorption and to stimulate the proliferation of osteoblasts, increasing bone regeneration. The zinc has also an antibacterial ability, exploitable in the scaffold designing to contrast the post-surgical infections caused by vary bacteria, in particular the staphylococcus aureus, a possible initiator of osteomylits.[65, 66]

In the present work, new hydroxyapatite nanophases presenting multiple ion substitutions were synthesized with the purpose to confer both enhanced osteogenic ability and antibacterial effect. More specifically, the wet synthesis of low-crystallinity hydroxyapatite was carried out in the presence of magnesium and carbonate ions, as well as of zinc or strontium to obtain a (Mg, CO_3, Zn/Sr)-substituted hydroxyapatite. Furthermore, the influence of doping ions on mechanical properties were investigated,

indeed the presence of doping ions leads to small grain size, that result in better mechanical properties.

1.5.1 Synthesis

For its biological relevance, a great number of studies are performed on hydroxyapatite and a number of synthetic routes have been described.[67-74] The most used are precipitation technique, sol-gel approach, biomimetic deposition technique, multiple emulsion technique, hydrothermal technique and electrodeposition technique.

The *sol-gel approach* guarantees, respect to the precipitation technique, a better control of the parameter of process and a major homogeneity of the mixing. Also, in this case two different precursors are used, one containing calcium and the other the phosphate, setting the Ca/P molar ratio equal to 1.67. As calcium precursor are widely used calcium nitrate ($Ca(NO_3)_2$) and calcium acetate ($Ca(CH_3COO)_2$) and as phosphate reagents are commonly used organic compounds containing phosphorous, such as dichlorophenylphosphine ($C_6H_5PCl_2$), phosphonoacetic acid ($C_2H_5O_5P$) or triethyl phosphate ($(C_2H_5)_3PO_4$). The reagents were mixed and heated at high temperature (500-900°C).[69]

The *biomimetic deposition technique*, differently from the precipitation technique, uses metastable synthetic body fluid to facilitate the spontaneous nucleation and growth of biomimetic hydroxyapatite. The obtained HA is more like biological one respect to the one obtained with a typical precipitation technique but could produce smaller amount of powder for each synthesis. This synthesis was developed for the creation of coating directly on the surface of the implant.[70]

The *multiple emulsion technique* is an innovative route for the synthesis of HA that uses a water/oil/water (w/o/w) emulsion made of dipotassium hydrogen phosphate as inner aqueous phase, benzene as oil phase and calcium nitrate as outer aqueous phase. This technique has the advantages of using a simple apparatus and can be carried out at room temperature.[71]

Hydrothermal synthesis is a process that utilizes single or heterogeneous phase reactions in aqueous solvent at elevated temperature (T > 50°C) and pressure (P > 100 kPa) to crystallize ceramic materials directly from solutions. It is particularly useful to

convert scaffolds made of calcium carbonate, derived from corals[72] or wood[73], into HA. In this case as source of phosphate are used different phosphate salts, such as ammonium phosphates or potassium phosphates. Phosphoric acid could not be used in this case because is not possible to adjust the pH during the synthesis.

$$10\ CaCO_3 + 6\ (NH_4)_2HPO_4 \rightarrow Ca_{10}(PO_4)_6(OH)_2$$

The *electrodeposition technique* is used to synthesize coatings of ultrafine-grained nanocrystalline HA using dilute solutions of calcium and phosphate and an electric field.[74]

The *precipitation technique* is the most popular and widely used approach for synthesis of HA. This technique is also called as wet precipitation or aqueous precipitation or chemical precipitation.[68] This technique is commonly chosen to synthesize HA because relatively large amounts of HA can be produced in absence of any organic solvents at a reasonable cost. Furthermore size, crystallinity, shape and surface area of the obtained crystals can be modulated modifying the parameters of the synthesis, such as temperature (0-100°C). The precipitation technique involved the reaction in aqueous solution or suspension of two different salt, one containing calcium ions (Ca) and the other containing phosphate ions (PO_4^{3-}) by ensuring that the final Ca/P ratio is 1.67. The pH during the reaction must be controlled and maintained in basic condition, to avoid the formation of other phases, like brushite. The more used reagents containing calcium are calcium hydroxide ($Ca(OH)_2$) and calcium nitrate ($Ca(NO_3)_2$). The more common reagents containing phosphate are phosphoric acid (H_3PO_4) and ammonium phosphates ($(NH_4)_2HPO_4$ or $(NH_4)H_2PO_4$). In case of reaction of calcium hydroxide and phosphoric acid the involved reaction is a neutralization and no other reagents for ensure that the pH is basic are required.[67] This synthetic route is frequently used also for its possibility to insert doping ions in the lattice during the precipitation.[52, 53, 64, 75-78]

$$10\ Ca(OH)_2 + 6\ H_3PO_4 \rightarrow Ca_{10}(PO_4)_6(OH)_2 + 18\ H_2O$$

In the other cases it is necessary to adjust pH to maintain basic, using compounds such as NH_4OH or urea.

1.5.2 Ionic substitutions

Hydroxyapatite has a crystalline structure that can easily accept ionic substitution, particularly when ions are introduced during the synthesis at low temperature. It is also possible to introduce ions in a HA already synthesized for ion exchange with an ion-rich solution.[79]

When an ion substituted HA is sintered, ions can be retained in the HA lattice, giving distortion of the crystal parameter, or remain as intercalating ions or be segregated in a side phase, usually whitlockite or the corresponding oxide. Recently, it has been shown that the ion doping can favour enhanced biologic properties, such as antiosteoporotic effect, or enhanced resistance to bacterial proliferation.[64, 76, 78, 80, 81]

Magnesium and strontium are cations of the same group of calcium in the periodic table of the elements, the second, alkaline earth metals. They have the same charge (2+) and a similar ionic radius (Ca^{2+} 114 pm, Mg^{2+} 86pm, Sr^{2+} 132pm) of calcium. For this reason, they are obvious candidates to be used to substitute calcium in HA, as in the natural bone tissue.

Magnesium can be inserted in HA during a low-temperature synthesis of the phase but create a β-TCP phase (β-tricalcium phosphate, a secondary phase) when is sintered. The effect of Mg on HA is a decrease of the crystallinity, a decrease in crystallite dimension and an improvement in its solubility.[82]

Strontium doped HA can be easily synthesized and sintered without the formation of any secondary phase. The doping with Sr is useful because it could provoke an in-situ release of Sr ions that inhibits bone resorption, acting as anti-osteoporotic agent, without the side effects related to a systemic administration.

Many other cations have been inserted, with different ionic radius and charge, like Zn,[83] Ga[80], Mn,[84] Fe,[75] Na[85], Ag[86] or Cu[87]. When an ion with a different charge is introduced in the crystal, the restoring of the neutrality could involve the exchange of other ions such as hydroxyl (OH^-) or their migration from the lattice to more disordered regions. For the same reason, it is also possible to create atomic vacancies in the HA lattice with the removal of an ion without inducing HA phase degeneration.

Another important ion that is commonly found also in synthetic HA is carbonate. A spontaneous carbonation always occurs when the synthesis is conducted in water

without controlled azote/argon atmosphere. The carbon dioxide present in the air spontaneously dissolves into water, generating carbonate ions, that precipitate inside the apatite lattice. The carbonate ions can enter in the apatite lattice in two different position, A and B. In the A position the carbonate ion substitute the hydroxyl group while in the B position substitute the phosphate group. In biological hydroxyapatite the B substitution is prevalent and biological in vitro tests reveals that the substitution in the B position favours HA solubility and cells vitality and differentiation. The insertion of a carbonate ion in the place of a phosphate ion generate an unbalance of a negative charge. A proposed mechanism to balance the charge is the simultaneous loss of a calcium ion and of a hydroxyl group, recovering neutrality. In this case the obtained HA is carbonate substituted and calcium deficient, further increasing its solubility.

Another proposed mechanism for charge balance is the simultaneous substitution of one calcium ion with a monovalent cation, like Na^+, K^+ or $NH4^+$.[77, 88] Other anions can be substituted to phosphate like silicate, sulphate or selenium.[89]

1.5.3 Porous Hydroxyapatite Scaffolds

Materials containing tailored porosity exhibit special properties and features that usually cannot be achieved by their conventional dense counterparts. In this respect, in the last decades the porous ceramics have been extensively studied for a wide range of applications and several processing methods were proposed for their preparation.[90, 91]

The development of artificial bone substitutes with effective regenerative ability represents one of the most serious challenges for material scientists, especially due to the difficulty of mimicking the properties of the natural bone. Hydroxyapatite (HA) is widely recognized as the golden material for bone and teeth regeneration, due to its close similarity with the inorganic part of bone, which confer excellent biocompatibility and ability to permit new bone formation and adhesion.[92-94]

The traditional processes reported in literature for the production of macroporous ceramics are partial sintering, sacrificial fugitives, replica templates and direct foaming (Fig 1.11).

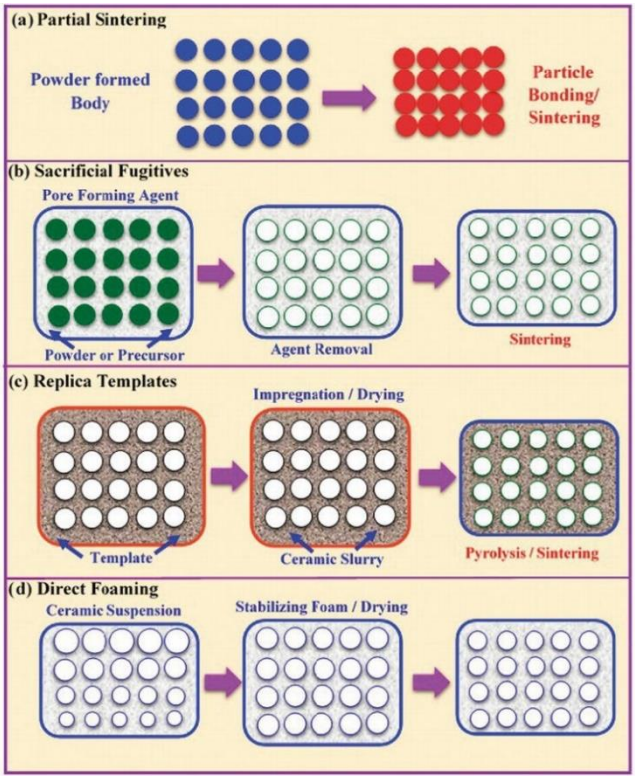

Fig 1.11 – Fabrication processes of macroporous ceramic scaffolds[90]

The *partial sintering* of powder: the high temperature thermal treatment induces surface diffusion or evaporation-condensation phenomena (see paragraph 1.5.4), but the process is carried out at a lower temperature so that the limited grain growth reflects in an incomplete densification and the presence of a residual porosity. Pore size and porosity can be controlled by the size of starting powders and degree of partial sintering, respectively.[95]

The *sacrificial template technique* usually foresees to prepare a biphasic composite, consisting of a continuous matrix of ceramic powders and a dispersed sacrificial phase, that is initially homogeneously distributed throughout the matrix and finally extracted to generate pores inside the microstructure. Porosity is controlled by the amount of the agents. This approach is useful particularly for obtaining high open porosity.[96]

The *replica method* is considered as the first method used to produce macroporous ceramics. It involves the impregnation of a polymeric cellular structure with a ceramic suspension in order to produce a macroporous ceramic exhibiting the same morphology as the original template. The success of this method is attributed to its simplicity and flexibility. However, some critical aspects have to be strictly controlled

and optimized, such as the rheological behaviour of the ceramic suspensions (shear-thinning), the presence of binders or plasticizers in the initial suspension to avoid the strut cracking during pyrolysis and the final thermal treatment parameters (heating rate, high temperature). In this respect, a disadvantage of this method is the cracking of the struts after thermal treatment, leading to a severe degradation of the mechanical performance of the structure.[97]

The *direct foaming method* was stated to be a low-cost and easy process that can provide pore volumes in the range 40-97% by incorporating a gas (e.g. air) into a ceramic suspension, that is subsequently dried and sintered. In comparison with the previous methods it is very interesting because it does not make use of a solid template to be eliminated upon sintering and this improves the microstructural stability and the formation of rounded pores which can offer increased resistance to fracture. Furthermore, cellular structures prepared by direct foaming usually exhibit considerably higher mechanical strength than those obtained by other template-based techniques, mainly due to the strongly reduced occurrence of flaws in the cell struts[91]. The total porosity of directly foamed ceramics is proportional to the amount of gas incorporated into the suspension or liquid medium during the foaming process. The pore size, on the other hand, is determined by the stability of the wet foam before setting takes place. Liquid foams are thermodynamically unstable systems due to their high gas-liquid interfacial area. Several physical processes take place in wet foams to decrease the overall system free energy, leading to foam destabilization. The main destabilization mechanisms are drainage, coalescence, Ostwald ripening[98]. Drainage is the physical separation between the gaseous and liquid phases of the foam because of the effect of gravity: light gas bubbles move upwards forming a denser foam layer on the top, while the heavier liquid phase is concentrated on the bottom. Coalescence takes place when the thin films formed after drainage are not stable enough to keep the touching cells apart, resulting in the association of neighbouring bubbles: the stability of the thin films is determined by the attractive and repulsive interactions between bubbles. Coalescence is favoured by attractive van der Waals forces and can only be hindered by providing steric and/or electrostatic repulsion among the interacting bubbles. Foams can be tailored to efficiently prevent drainage and coalescence processes, but in long-term the Ostwald ripening phenomenon can occur, leading to the destabilization of the

system due to the difference in Laplace pressure between bubbles of different sizes. Surfactants and biomolecules adsorbed at the gas–liquid interface can slow down this coarsening process by decreasing the interfacial energy[91].

1.5.4 Sintering

Ceramic processes consist of three main successive steps: powder synthesis, shaping and sintering. This last step consists of high-temperature thermal treatment of a porous powder compact, but at a temperature lower than the melting point. It leads to the final ceramic part by elimination of pores contained in the shaped body. During this treatment, several phenomena induce consolidation and densification of the shaped part. At the same time, particle size and shape may change in a wide range. Reactions may also occur and change the chemical composition and/or the phase composition of the fired product. Therefore, the sintering is of prime importance, because the final properties of the ceramic parts strongly depend on it.

Sintering will occur only when the driving force is sufficiently high. It is possible if the total Gibbs free energy (G) of the system is minimized ($dG < 0$) by decreasing the solid-gas surface area A_{sg} ($dA_{sg} < 0$) of high energy (γ_{sg}), which is replaced by a solid-solid surface area Ass ($dA_{ss} > 0$) of lower energy (γ_{ss}):

$$dG = dA_{ss}\gamma ss + dA_{sg}\gamma_{sg}$$

The driving force for sintering is the reduction in surface free energy of the consolidated mass of particles. This reduction in energy can be accomplished by atom diffusion processes that lead to either densification of the body (by transport matter from inside the grains into the pores) or coarsening of the microstructure (by rearrangement of matter between different parts of the pore surfaces without actually leading to a decrease in the pore volume).

Physical parameters, such as powder grain size distribution, specific surface area of powder or compacity of shaped body, may change sintering ability and kinetics. The sintering of a powder compact is generally divided in three sequential stages.

I. In the initial stage the interparticle neck forms and grows (Fig. 1.12). This stage can occur with a light or without densification, and it lasts up to a relative density of ~65% of the ‘‘theoretical’’ (i.e. the value of fully dense material). A simple

model of spherical particles can be used to schematize the initial powder compact and the changes that occur at the microscopic scale during this stage (Fig. 1.12 stage II).

II. In the intermediate stage, densification is generally assumed to occur by the shrinking of the pores. Pores remain open and constitute a continuous phase. This stage covers the major part of sintering, and it ends when the pores pinch off to become isolated, which corresponds to an increase in relative density to ~90%. It is characterized by two temperatures: T_B, temperature at which the shrinkage begins; T_M, temperature at which the sintering rate is maximum. The main values of T_B and T_M for HA are ~750°C and 1050°C, respectively (Fig. 1.12 stage III).

III. In the final stage of sintering (from a relative density of ~90%), the isolated pores may disappear altogether, leaving a fully or nearly fully dense ceramic (Fig. 1.12 stage IV).

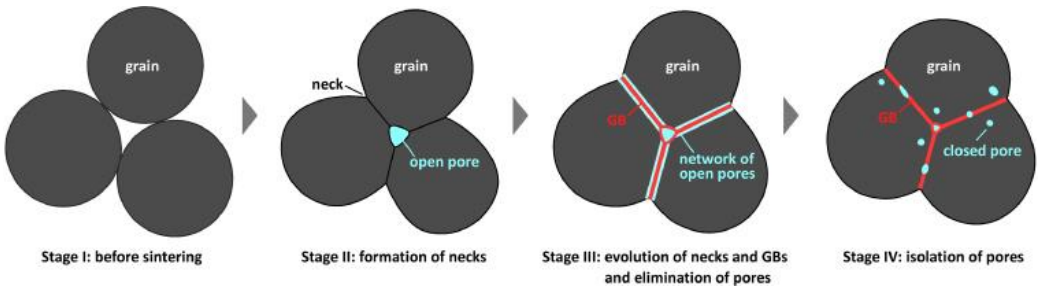

Fig. 1.12 – Schematic diagrams of stages in solid-state self-sintering

Then, during cooling to room temperature, the sample retracts in accordance with the expansion coefficient of the sintered ceramic.

The sintering behaviour is strongly affected by the chemical composition. Calcium-deficient hydroxyapatite powders are characterized by a calcium-to-phosphorus molar ratio Ca/P < 1.667, and they decompose into β-TCP above 700°C, that is also the case of doped HA where cations like Mg^{2+},Sr^{2+}, Zn^{2+} takes the place of calcium decreasing the Ca/p molar ratio.[99, 100]

References

1. Birbrair, A.; Frenette, P. S., Niche heterogeneity in the bone marrow. *Ann N Y Acad Sci* **2016,** *1370* (1), 82-96.
2. Lee, N. K.; Sowa, H.; Hinoi, E.; Ferron, M.; Ahn, J. D.; Confavreux, C.; Dacquin, R.; Mee, P. J.; McKee, M. D.; Jung, D. Y.; Zhang, Z.; Kim, J. K.; Mauvais-Jarvis, F.; Ducy, P.; Karsenty, G., Endocrine regulation of energy metabolism by the skeleton. *Cell* **2007,** *130* (3), 456-69.
3. Saladin, K.; Miller, L., *Anatomy & physiology*. WCB/McGraw-Hill: 1998.
4. Wingender, B.; Bradley, P.; Saxena, N.; Ruberti, J. W.; Gower, L., Biomimetic organization of collagen matrices to template bone-like microstructures. *Matrix Biol* **2016,** *52-54*, 384-396.
5. Cooper, R. R.; Milgram, J. W.; Robinson, R. A., Morphology of the osteon. An electron microscopic study. *J Bone Joint Surg Am* **1966,** *48* (7), 1239-71.
6. Gdyczynski, C. M.; Manbachi, A.; Hashemi, S.; Lashkari, B.; Cobbold, R. S., On estimating the directionality distribution in pedicle trabecular bone from micro-CT images. *Physiol Meas* **2014,** *35* (12), 2415-28.
7. Stegen, S.; Carmeliet, G., The skeletal vascular system - Breathing life into bone tissue. *Bone* **2018,** *115*, 50-58.
8. Bose, S.; Tarafder, S.; Bandyopadhyay, A., Effect of Chemistry on Osteogenesis and Angiogenesis Towards Bone Tissue Engineering Using 3D Printed Scaffolds. *Ann Biomed Eng* **2017,** *45* (1), 261-272.
9. Thula, T. T.; Rodriguez, D. E.; Lee, M. H.; Pendi, L.; Podschun, J.; Gower, L. B., In Vitro Mineralization of Dense Collagen Substrates: A Biomimetic Approach Toward the Development of Bone-Graft Materials. *Acta Biomater* **2011,** *7* (8), 3158-69.
10. Palmer, L. C.; Newcomb, C. J.; Kaltz, S. R.; Spoerke, E. D.; Stupp, S. I., Biomimetic Systems for Hydroxyapatite Mineralization Inspired By Bone and Enamel. *Chem Rev* **2008,** *108* (11), 4754-83.
11. Katsimbri, P., The biology of normal bone remodelling. *Eur J Cancer Care (Engl)* **2017,** *26* (6).
12. Pacifici, R., T cells, osteoblasts, and osteocytes: interacting lineages key for the bone anabolic and catabolic activities of parathyroid hormone. *Ann N Y Acad Sci* **2016,** *1364*, 11-24.
13. Florencio-Silva, R.; Sasso, G. R.; Sasso-Cerri, E.; Simoes, M. J.; Cerri, P. S., Biology of Bone Tissue: Structure, Function, and Factors That Influence Bone Cells. *Biomed Res Int* **2015,** *2015*, 421746.
14. Mizuno, H.; Kikuta, J.; Ishii, M., In vivo live imaging of bone cells. *Histochem Cell Biol* **2018,** *149* (4), 417-422.
15. Chen, J. H.; Liu, C.; You, L.; Simmons, C. A., Boning up on Wolff's Law: mechanical regulation of the cells that make and maintain bone. *J Biomech* **2010,** *43* (1), 108-18.
16. Robling, A. G.; Turner, C. H., Mechanical Signaling for Bone Modeling and Remodeling. *Crit Rev Eukaryot Gene Expr* **2009,** *19* (4), 319-38.
17. Sikavitsas, V. I.; Temenoff, J. S.; Mikos, A. G., Biomaterials and bone mechanotransduction. *Biomaterials* **2001,** *22* (19), 2581-93.
18. Reilly, D. T.; Burstein, A. H., The elastic and ultimate properties of compact bone tissue. *J Biomech* **1975,** *8* (6), 393-405.
19. Bankoff, A., *Biomechanical Characteristics of the Bone*. INTECH Open Access: 2012; Vol. Human Musculoskeletal Biomechanics.
20. Garner, E.; Lakes, R.; Lee, T.; Swan, C.; Brand, R., Viscoelastic Dissipation in Compact Bone: Implications for Stress-Induced Fluid Flow in Bone. *Journal of Biomechanical Engineering* **2000,** *122* (2), 166-172.

21. Kim, H.-W.; Knowles, J. C.; Kim, H.-E., Porous scaffolds of gelatin–hydroxyapatite nanocomposites obtained by biomimetic approach: Characterization and antibiotic drug release. *Journal of Biomedical Materials Research* **2005,** *74B* (2), 686-698.
22. Wang, G.; Babadağli, M. E.; Uludağ, H., Bisphosphonate-Derivatized Liposomes to Control Drug Release from Collagen/Hydroxyapatite Scaffolds. *Mol. Pharmaceutics* **2011,** *8* (4), 1025-1034.
23. Kim, H.-W.; Knowles, J. C.; Kim, H.-E., Hydroxyapatite/poly(ε-caprolactone) composite coatings on hydroxyapatite porous bone scaffold for drug delivery. *Biomaterials* **2004,** *25* (7), 1279-1287.
24. Son, J. S.; Appleford, M.; Ong, J. L.; Wenke, J. C.; Kim, J. M.; Choi, S. H.; Oh, D. S., Porous hydroxyapatite scaffold with three-dimensional localized drug delivery system using biodegradable microspheres. *Journal of Controlled Release* **2011,** *153* (2), 133-140.
25. Zhang, Y.; Cheng, N.; Miron, R.; Shi, B.; Cheng, X., Delivery of PDGF-B and BMP-7 by mesoporous bioglass/silk fibrin scaffolds for the repair of osteoporotic defects. *Biomaterials* **2012,** *33* (28), 6698-6708.
26. Sterling, J. A.; Guelcher, S. A., Biomaterial Scaffolds for Treating Osteoporotic Bone. *Current Osteoporosis Reports* **2014,** *12* (1), 48-54.
27. Hamdy, N. A., Strontium ranelate improves bone microarchitecture in osteoporosis. *Rheumatology (Oxford)* **2009,** *48 Suppl 4*, iv9-13.
28. Fauci, A., *Harrison's Internal Medicine, 17th edition.* McGraw-Hill: 1998.
29. Tamparo, C., *Diseases of the Human Body, 6th edition*. F.A. Davis Company: 2016.
30. Gelderblom, H.; Hogendoorn, P. C.; Dijkstra, S. D.; van Rijswijk, C. S.; Krol, A. D.; Taminiau, A. H.; Bovee, J. V., The clinical approach towards chondrosarcoma. *Oncologist* **2008,** *13* (3), 320-9.
31. Iwamoto, Y., Diagnosis and treatment of Ewing's sarcoma. *Jpn J Clin Oncol* **2007,** *37* (2), 79-89.
32. Goldberg, V. M.; Stevenson, S., Natural history of autografts and allografts. *Clin Orthop Relat Res* **1987,** (225), 7-16.
33. Sachs, D.; FH, B., Human Immunology. *Human Immunology* **1990,** *28* (2), 7.
34. Tampieri, A.; Iafisco, M.; Sprio, S.; Ruffini, A.; Panseri, S.; Montesi, M.; Adamiano, A.; Sandri, M., Hydroxyapatite: From Nanocrystals to Hybrid Nanocomposites for Regenerative Medicine. In *Handbook of Bioceramics and Biocomposites*, Springer: 2015.
35. Murphy, C. M.; Haugh, M. G.; O'Brien, F. J., The effect of mean pore size on cell attachment, proliferation and migration in collagen-glycosaminoglycan scaffolds for bone tissue engineering. *Biomaterials* **2010,** *31* (3), 461-6.
36. Shalabi, M. M.; Gortemaker, A.; Van't Hof, M. A.; Jansen, J. A.; Creugers, N. H., Implant surface roughness and bone healing: a systematic review. *J Dent Res* **2006,** *85* (6), 496-500.
37. Alla, R. K.; University, A.-F.; Ginjupalli, K.; Department of Dental Materials, M. C. o. D. S., Manipal; Upadhya, N.; Department of Dental Materials, M. C. o. D. S., Manipal; Shammas, M.; University, A.-F.; Ravi, R. K.; College, S. P. D.; Sekhar, R.; College, S. J. D., Surface roughness of implants: A review. *Trends in Biomaterials and Artificial Organs* **2011,** *25* (3), 112-118.
38. Vaccaro, A. R., The role of the osteoconductive scaffold in synthetic bone graft. *Orthopedics* **2002,** *25* (5 Suppl), s571-8.
39. Polini, A.; Pisignano, D.; Parodi, M.; Quarto, R.; Scaglione, S., Osteoinduction of human mesenchymal stem cells by bioactive composite scaffolds without supplemental osteogenic growth factors. *PLoS One* **2011,** *6* (10), e26211.
40. Albrektsson, T.; Johansson, C., Osteoinduction, osteoconduction and osseointegration. *Eur Spine J* **2001,** *10 Suppl 2*, S96-101.
41. Kanczler, J. M.; Oreffo, R. O., Osteogenesis and angiogenesis: the potential for engineering bone. *Eur Cell Mater* **2008,** *15*, 100-14.

42. Kellomaki, M.; Niiranen, H.; Puumanen, K.; Ashammakhi, N.; Waris, T.; Tormala, P., Bioabsorbable scaffolds for guided bone regeneration and generation. *Biomaterials* **2000,** *21* (24), 2495-505.
43. Saini, M.; Singh, Y.; Arora, P.; Arora, V.; Jain, K., Implant biomaterials: A comprehensive review. *World J Clin Cases* **2015,** *3* (1), 52-7.
44. Stratton, S.; Shelke, N. B.; Hoshino, K.; Rudraiah, S.; Kumbar, S. G., Bioactive polymeric scaffolds for tissue engineering. *Bioact Mater* **2016,** *1* (2), 93-108.
45. Taylor, M. S.; Daniels, A. U.; Andriano, K. P.; Heller, J., Six bioabsorbable polymers: In vitro acute toxicity of accumulated degradation products. *Journal of Applied Biomaterials* **1994,** *5* (2), 151-157.
46. Ibrahim, H.; Esfahani, S. N.; Poorganji, B.; Dean, D.; Elahinia, M., Resorbable bone fixation alloys, forming, and post-fabrication treatments. *Materials Science and Engineering: C* **2017,** *70*, 870-888.
47. Case, C. P.; Langkamer, V. G.; James, C.; Palmer, M. R.; Kemp, A. J.; Heap, P. F.; Solomon, L., Widespread dissemination of metal debris from implants. *J Bone Joint Surg Br* **1994,** *76* (5), 701-12.
48. Ri, M.-H.; Jang, Y.-M.; Ri, U.-S.; Yu, C.-J.; Kim, K.-I.; Kim, S.-U., Ab initio Investigation of Adsorption Characteristics of Bisphosphonates on Hydroxyapatite (001) Surface. *Journal of Materials Science* **2017,** *53* (6), 4252-4261.
49. LeGeros, R. Z.; J.P., L., Phosphate Minerals in Human Tissues. In *Nriagu, J.O. Moore, P.B.*, Nriagu, J. O.; Moore, P. B., Eds. Springer: 1984; Vol. Phosphate Minerals.
50. LeGeros, R., Apatites in Biological Systems. *Progress in Crystal Growth and Characterization of Materials* **1981,** *4* (1-2), 1-45.
51. Boskey, A. L., Mineralization, structure and function of bone. In *Dynamics of Bone and Cartilage Metabolism*, Seibel, M. J.; Robins, S. P.; Bilezikian, J. P., Eds. Academic Press: 2006.
52. Landi, E.; Logroscino, G.; Proietti, L.; Tampieri, A.; Sandri, M.; Sprio, S., Biomimetic Mg-substituted hydroxyapatite: from synthesis to in vivo behaviour. *J Mater Sci Mater Med* **2008,** *19* (1), 239-47.
53. Sprio, S.; Tampieri, A.; Landi, E.; Sandri, M.; Martorana, S.; Celotti, G.; Logroscino, G., Physico-chemical properties and solubility behaviour of multi-substituted hydroxyapatite powders containing silicon. *Materials Science and Engineering: C* **2008,** *28* (1), 179-187.
54. Spence, G.; Patel, N.; Brooks, R.; Rushton, N., Carbonate substituted hydroxyapatite: resorption by osteoclasts modifies the osteoblastic response. *J Biomed Mater Res A* **2009,** *90* (1), 217-24.
55. Spence, G.; Patel, N.; Brooks, R.; Bonfield, W.; Rushton, N., Osteoclastogenesis on hydroxyapatite ceramics: the effect of carbonate substitution. *J Biomed Mater Res A* **2010,** *92* (4), 1292-300.
56. Bigi, A.; Foresti, E.; Gregorini, R.; Ripamonti, A.; Roveri, N.; Shah, J. S., The role of magnesium on the structure of biological apatites. *Calcif Tissue Int* **1992,** *50* (5), 439-44.
57. Bigi, A.; Falini, G.; Foresti, E.; Ripamonti, A.; Gazzano, M.; Roveri, N., Magnesium influence on hydroxyapatite crystallization. *Journal of Inorganic Biochemistry* **1993,** *49* (1), 69-78.
58. Cazalbou, S.; Combes, C.; Eichert, D.; Rey, C.; Glimcher, M. J., Poorly crystalline apatites: evolution and maturation in vitro and in vivo. *J Bone Miner Metab* **2004,** *22* (4), 310-7.
59. Bertinetti, L.; Tampieri, A.; Landi, E.; Martra, G.; , C., S., Punctual investigation of surface sites of HA and magnesium-HA. *Journal of the European Ceramic Society* **2006,** *26* (6), 987-997.
60. Crespi, R.; Mariani, E.; Benasciutti, E.; Cappare, P.; Cenci, S.; Gherlone, E., Magnesium-enriched hydroxyapatite versus autologous bone in maxillary sinus grafting: combining histomorphometry with osteoblast gene expression profiles ex vivo. *J Periodontol* **2009,** *80* (4), 586-593.

61. Dahl, S. G.; Allain, P.; Marie, P. J.; Mauras, Y.; Boivin, G.; Ammann, P.; Tsouderos, Y.; Delmas, P. D.; Christiansen, C., Incorporation and distribution of strontium in bone. *Bone* **2001,** *28* (4), 446-53.
62. Marie, P. J.; Ammann, P.; Boivin, G.; Rey, C., Mechanisms of action and therapeutic potential of strontium in bone. *Calcif Tissue Int* **2001,** *69* (3), 121-129.
63. Pors Nielsen, S., The biological role of strontium. *Bone* **2004,** *35* (3), 583-8.
64. Landi, E.; Tampieri, A.; Celotti, G.; Sprio, S.; Sandri, M.; Logroscino, G., Sr-substituted hydroxyapatites for osteoporotic bone replacement. *Acta Biomater* **2007,** *3* (6), 961-9.
65. Ito, A.; Ojima, K.; Naito, H.; Ichinose, N.; Tateishi, T., Preparation, solubility, and cytocompatibility of zinc-releasing calcium phosphate ceramics. *J Biomed Mater Res* **2000,** *50* (2), 178-83.
66. Thian, E. S.; Konishi, T.; Kawanobe, Y.; Lim, P. N.; Choong, C.; Ho, B.; Aizawa, M., Zinc-substituted hydroxyapatite: a biomaterial with enhanced bioactivity and antibacterial properties. *J Mater Sci Mater Med* **2013,** *24* (2), 437-45.
67. Smičiklas, I.; Onjia, A.; Raičević, S., Experimental design approach in the synthesis of hydroxyapatite by neutralization method. *Separation and Purification Technology* **2005,** *44* (2), 97-102.
68. Mobasherpour, I., Synthesis of Nanocrystalline Hydroxyapatite by Using Precipitation Method | Request PDF. *Journal of Alloys and Compounds* **2007,** *430* (1), 330-333.
69. Chai, C. S.; Ben-Nissan, B., Bioactive nanocrystalline sol-gel hydroxyapatite coatings. *Journal of Materials Science: Materials in Medicine* **1999,** *10* (8), 465-469.
70. Zhang, Q.; Leng, Y.; Xin, R., A comparative study of electrochemical deposition and biomimetic deposition of calcium phosphate on porous titanium. *Biomaterials* **2005,** *26* (16), 2857-65.
71. Kimura, I., Synthesis of Hydroxyapatite by Interfacial Reaction in a Multiple Emulsion. *Research Letters in Materials Science* **2007,** *1*.
72. Damien, E.; Revell, P. A., Coralline hydroxyapatite bone graft substitute: A review of experimental studies and biomedical applications. *J Appl Biomater Biomech* **2004,** *2* (2), 65-73.
73. Andrea, R.; Simone, S.; Lorenzo, P.; Anna, T., Synthesis of Nanostructured Hydroxyapatite via Controlled Hydrothermal Route, Biomaterial-supported Tissue Reconstruction or Regeneration. In *Biomaterial-supported Tissue Reconstruction or Regeneration*, Mike, B.; Ole, J.; Ralf, S.; Tadas, K., Eds. IntechOpen: 2019.
74. Jamesh, M.; Kumar, S.; Sankara Narayanan, T. S. N., Electrodeposition of hydroxyapatite coating on magnesium for biomedical applications. *Journal of Coatings Technology and Research* **2012,** *9* (4), 495-502.
75. Tampieri, A.; D'Alessandro, T.; Sandri, M.; Sprio, S.; Landi, E.; Bertinetti, L.; Panseri, S.; Pepponi, G.; Goettlicher, J.; Banobre-Lopez, M.; Rivas, J., Intrinsic magnetism and hyperthermia in bioactive Fe-doped hydroxyapatite. *Acta Biomater* **2012,** *8* (2), 843-51.
76. Tampieri, A.; Celotti, G.; Landi, E.; Sandri, M., Magnesium Doped Hydroxyapatite: Synthesis and Characterization. *Key Engineering Materials* **2004,** *264* (3), 2051-2054.
77. Landi, E.; Sprio, S.; Sandri, M.; Celotti, G.; Tampieri, A., Development of Sr and CO3 co-substituted hydroxyapatites for biomedical applications. *Acta Biomater* **2008,** *4* (3), 656-63.
78. E., L.; A., T.; M., M.-B.; G., C.; M., S.; A., G.; P., F.; G., B., Biomimetic Mg- and Mg,CO3-substituted hydroxyapatites: synthesis characterization and in vitro behaviour. *J. Eur. Ceram. Soc.* **2006,** *26* (13), 2593-2601.
79. Tampieri, A.; Ruffini, A.; Ballardini, A.; Montesi, M.; Panseri, S.; Salamanna, F.; Fini, M.; Sprio, S., Heterogeneous chemistry in the 3-D state: an original approach to generate bioactive, mechanically-competent bone scaffolds. *Biomater Sci* **2018,** *7* (1), 307-321.
80. Ballardini, A.; Montesi, M.; Panseri, S.; Vandini, A.; Balboni, P. G.; Tampieri, A.; Sprio, S., New hydroxyapatite nanophases with enhanced osteogenic and anti-bacterial activity. *J Biomed Mater Res A* **2018,** *106* (2), 521-530.

81. Sprio, S.; Preti, L.; Montesi, M.; Panseri, S.; Adamiano, A.; Vandini, A.; Pugno, N. M.; Tampieri, A., Surface Phenomena Enhancing the Antibacterial and Osteogenic Ability of Nanocrystalline Hydroxyapatite, Activated by Multiple-Ion Doping. *ACS Biomater. Sci. Eng* **2019,** *5* (11), 5947-5959.
82. Cacciotti, I.; Bianco, A.; Lombardi, M.; Montanaro, L., Mg-substituted hydroxyapatite nanopowders: Synthesis, thermal stability and sintering behaviour | Request PDF. *Journal of the European Ceramic Society* **2009,** *29* (14), 2969.
83. F., M.; Y., K.; Y., S., Formation and structure of zinc-substituted calcium hydroxyapatite. *Mater. Res.Bull.* **2005,** *40* (2), 209-220.
84. Li, Y.; Widodo, J.; Lim, S.; Ooi, C., Synthesis and cytocompatibility of manganese (II) and iron (III) substituted hydroxyapatite nanoparticles. *Journal of Materials Science* **2012,** (2).
85. Kannan, S.; Ferreira, J. M. F., Synthesis and Thermal Stability of Hydroxyapatite−β-Tricalcium Phosphate Composites with Cosubstituted Sodium, Magnesium, and Fluorine. *Chemistry of Materials* **2006,** *18* (1), 198-203.
86. Rameshbabu, N.; Sampath Kumar, T. S.; Prabhakar, T. G.; Sastry, V. S.; Murty, K. V.; Prasad Rao, K., Antibacterial nanosized silver substituted hydroxyapatite: synthesis and characterization. *J Biomed Mater Res A* **2007,** *80* (3), 581-91.
87. V., S.; S., D.; J., A.-S.; M., M.; B., J.; B., P. I.; S., R., Synthesis, characterization and antimicrobial activity of copper and zinc-doped hydroxyapatite nanopowders. **2010,** *256* (20), 6083-6089.
88. Gibson, I.; W, B., Novel synthesis and characterization of an AB-type carbonate-substituted hydroxyapatite. *Journal of Biomedical Materials Research* **2001,** *59* (4), 697-708.
89. Kannan, S.; Rebero, A.; Lemos, A.; Barba, A.; Ferreira, J., Synthesis and mechanical behaviour of chlorapatite and chlorapatite/β-TCP composites. *Journal of the European Ceramic Society* **2007,** *27* (5), 2287-2294.
90. Ohji, T.; Fukushima, M., Macro-Porous Ceramics: Processing and Properties. *International Materials Reviews* **2012,** *57* (2), 115-131.
91. Studart, A. R.; Gonzenbach, U. T.; Tervoort, E.; Gauckler, L. J., Processing Routes to Macroporous Ceramics: A Review. *J Am Ceram Soc* **2006,** *89* (6), 1771-1789.
92. Venkatesan, J.; Kim, S.-K., Nano-Hydroxyapatite Composite Biomaterials for Bone Tissue Engineering—A Review. **2014**.
93. Pepla, E.; Besharat, L. K.; Palaia, G.; Tenore, G.; Migliau, G., Nano-hydroxyapatite and its applications in preventive, restorative and regenerative dentistry: a review of literature. In *Ann Stomatol (Roma)*, 2014; Vol. 5, pp 108-14.
94. Dutta, S. R.; Passi, D.; Singh, P.; Bhuibhar, A., Ceramic and non-ceramic hydroxyapatite as a bone graft material: a brief review. *Irish Journal of Medical Science (1971 -)* **2014,** *184* (1), 101-106.
95. Mohamad Yunos, D.; Bretcanu, O.; Boccaccini, A. R., Polymer-bioceramic composites for tissue engineering scaffolds. *Journal of Materials Science* **2008,** *43* (13), 4433-4442.
96. Bose, S.; Roy, M.; Bandyopadhyay, A., Recent advances in bone tissue engineering scaffolds. *Trends Biotechnol* **2012,** *30* (10), 546-54.
97. Scarano, A.; Lorusso, F.; Santos de Oliveira, P.; Kunjalukkal Padmanabhan, S.; Licciulli, A., Hydroxyapatite Block Produced by Sponge Replica Method: Mechanical, Clinical and Histologic Observations. *Materials (Basel)* **2019,** *12* (19).
98. Studart, A. R.; Gonzenbach, U. T.; Tervoort, E.; Gauckler, L. J., Processing Routes to Macroporous Ceramics: A Review. *J Am Ceram Soc* **2020,** *89* (6), 1771-1789.
99. Champion, E., Sintering of calcium phosphate bioceramics. *Acta Biomater* **2013,** *9* (4), 5855-75.
100. Suk-Joong, L. K., *Sintering, Densification, Grain Growth and Microstructure*. Elsevier: 2005.

Chapter 2
Characterization Methods

2.1 X-Ray Diffraction (XRD)

X-ray diffraction (XRD) is a non-destructive analytical technique primarily used for phase identification of a crystalline material. The material is finely ground, homogenized and the average bulk phase composition is analysed.[1]

Crystals are solids in which the atoms are regularly arranged, that can be described in terms of symmetry elements, reflecting the symmetry of the physical properties of a crystal. The crystal structure of a material is identified by its unit cell and its lattice parameters, the length of the cell edges and the angles between them. Inside the unit cell the atomic position is described by the position on the three spatial axis, x_i, y_i, z_i, measured from a given lattice point. There are different structures with different geometrical entities (points, axes or planes) with a different lattice symmetry that occurs and are defined symmetry elements. The geometrical entities (points, axes or planes) with respect to which a lattice symmetry occurs are defined symmetry elements.

By using the symmetry elements, it is possible to define the symmetry operations. Complex symmetry operations lead to space groups, the most detailed level to describe the symmetry properties of the crystal, such as cleavage, electronic band structure and optical properties. Although there are an infinite number of ways to specify a unit cell, for each crystal structure there is a conventional unit cell, which is chosen to display the full symmetry of the crystal.

However, the conventional unit cell is not always the smallest possible choice. The smallest structure filled by stacked atoms is called primitive unit cell and each atom has an identical arrangement of the neighbouring atoms.[2]

The crystal structure consists of the same group of atoms, the basis, positioned around each lattice point. This group of atoms therefore repeats indefinitely in three dimensions according to the arrangement of one of the 14 Bravais lattices. (Fig. 2.1.)

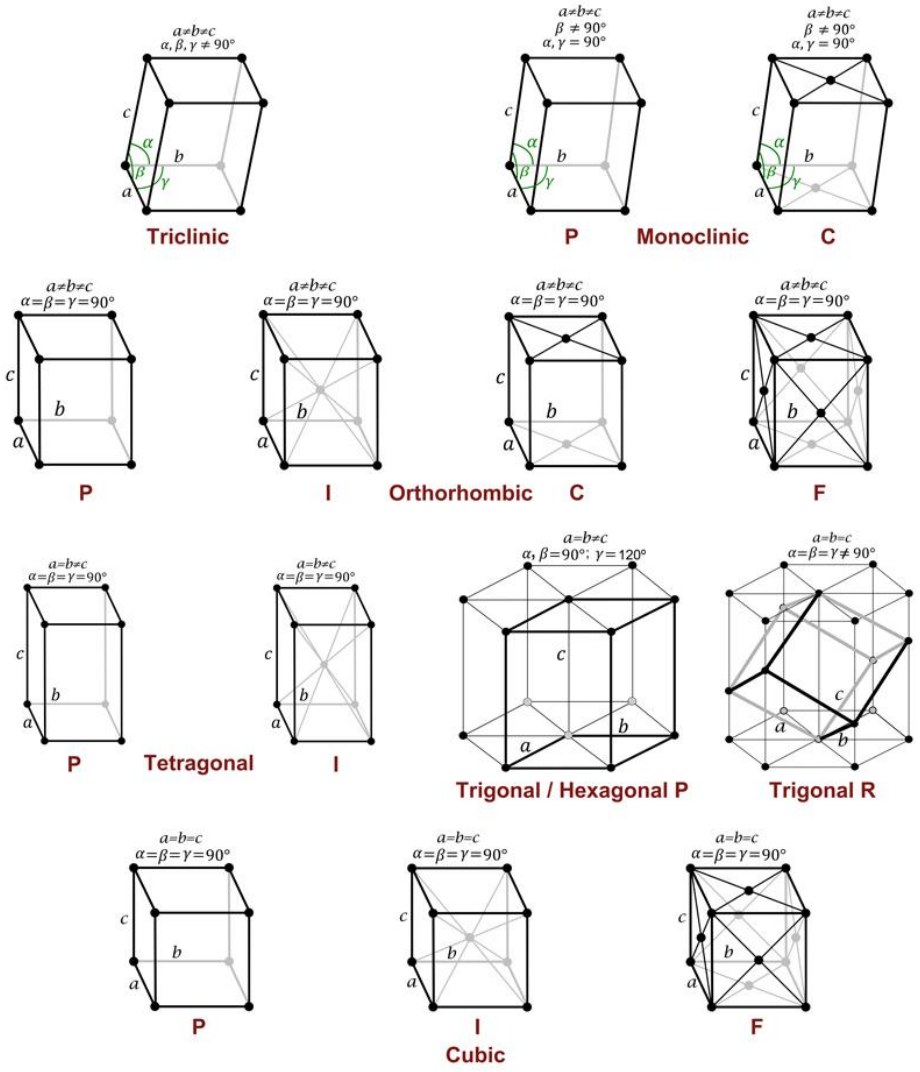

Fig 2.1 – the 14 Bravais lattices (xtal.iqfr.csic.es)

The possible lattice centrings are:

- P: Simple or Primitive centring, lattice points on the cell corners only;
- I: Body centred, one additional lattice point at the centre of the cell;
- F: Face centred, one additional lattice point at centre of each of the faces of the cell;
- C: Centred on a single face, one additional lattice point at the centre of one of the cell faces.

A useful notation tools to identify the different planes and directions of a Bravais lattice are the Miller indices. With the Miller indices is possible to identify a reticular plane with three integers h, k, l, reported as (hkl). These indices are vectors reciprocals of the intercepts of the plane on the axes x, y and z.

XRD is based on the constructive interference of monochromatic X-rays, generated by a cathode ray tube, filtered to produce monochromatic radiation with the crystalline material, finely ground to guarantee homogenization of the phase composition. Incident X-ray interacts with the sample, producing constructive interference if the Bragg's law is satisfied. (Fig. 2.2).

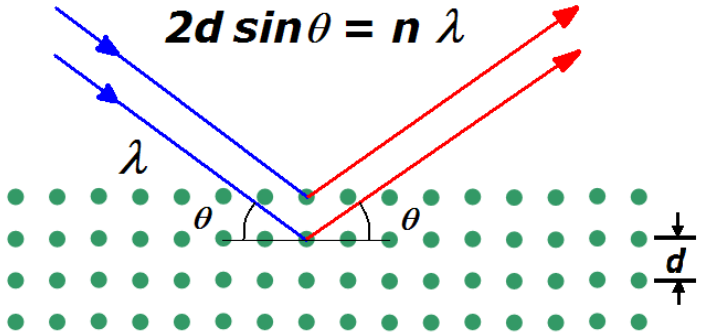

Fig 2.1 - Bragg's law and constructive interference

Where λ is the wavelength of the radiation, d is the distance between the layers of atoms and θ is the angle of incidence. If n is a whole number the radiation will be constructive, otherwise it will be destructive.

The interaction of X-rays with atoms leads to the movement of the electronic cloud, with subsequent re-radiation waves with the same frequency, a phenomenon known as elastic scattering or Rayleigh scattering (Fig. 2.3).

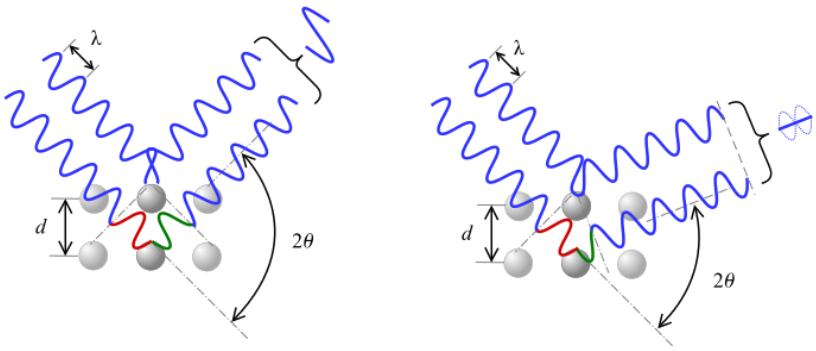

Fig. 2.3 – Constructive (left fig) or destructive (right fig) interference in Rayleigh scattering of X-rays

The results are usually presented in diffractograms, plots that reports peaks as function of the scattering angle 2θ. Peaks appears when a constructive interference occurs between X-rays and the crystalline matrix.

In diffractograms where analysed position and relative intensity of the peaks, used as fingerprints for the material composition, compared with the powder diffraction files of the international centre for diffraction data (ICDD). Diffractograms could be refined with Rietveld techniques, providing structural information, such as crystallite dimension, unit cell and axis dimension.

Another useful information in diffractograms is the width of diffraction peak. It is related to several factors, including instrumental factors, the presence of lattice defects, strain dishomogeneity among the grains and the size of the crystallites.

Usually for in a peak is analysed the full-width at half-maximum (FWHM) that is related with the variation in microstructure and the presence of stress-strain accumulation in the material, that causes an increase of FWHM.

X-ray diffractometers consist of three basic elements: an x-ray tube, a sample holder, and an x-ray detector. X-rays are generated in a cathode ray tube by heating a filament to produce electrons, accelerating the electrons toward a target by applying a voltage, and bombarding the target material with electrons (Fig. 2.4).[1]

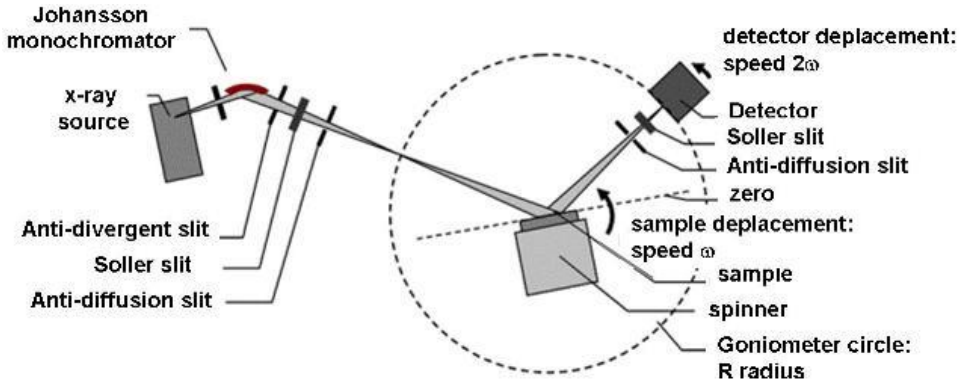

Fig 2.4 – Typical scheme of a Bragg-Brentano type diffractometer (crismat.ensicaen.fr)

The model of diffractometer employed in this activity is a D8 Advance diffractometer (CuKα radiation) (λ = 1.54178Å) generated at 40kV and 40mA equipped with LINXEYE detector (Bruker, Karlsruhe, Germany) working with Bragg-Brentano configuration. XRD spectra were recorded in the 2θ range from 20 to 60° 2θ with a counting time of 0.5s and a step size of 0.02° The lattice parameters refinement was performed according to the Rietveld method (TOPAS 4.2 software).

2.2 Inductively Coupled Plasma Optical Emission Spectroscopy (ICP-OES)

The inductively coupled plasma optical emission spectroscopy (ICP-OES) is the most popular and precise analytical technique for the determination of the elemental composition and for the determination of trace elements (Fig. 2.5)

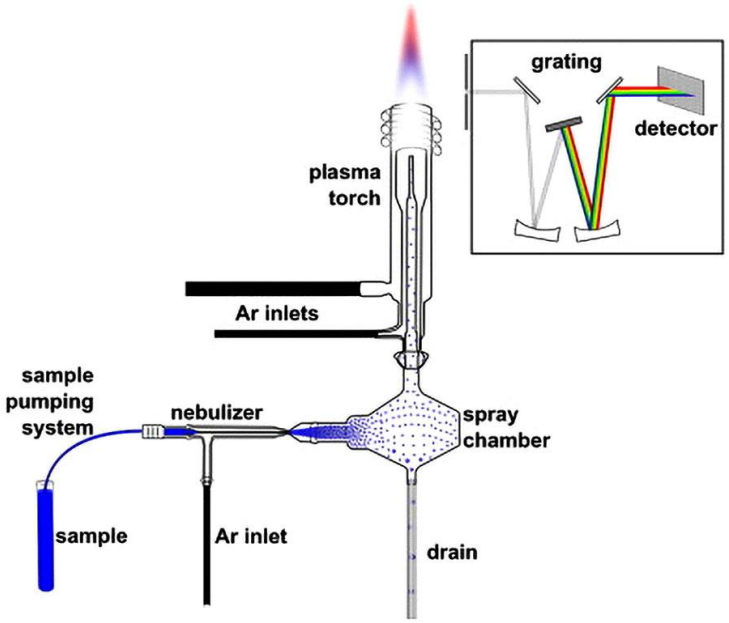

Fig. 2.5 – Schematic view of an ICP-OES instrument (nanoceramiran.com)

The technique is based upon the spontaneous emission of photons from atoms and ions that have been excited by a radiofrequency (RF) discharge. Atoms and ions were analysed in plasma. Plasma can simply be considered as a gaseous mixture of negatively charged electrons and highly charged positive ions, being created by heating a gas or by subjecting gas to a strong electromagnetic field. In this case an inductively coupled plasma is created in a torch, that consists of three concentric tubes, usually made of quartz. The end of this torch is placed inside an induction coil supplied with a radio-frequency electric current. A flow of argon gas is introduced between the two outermost tubes of the torch and an electrical spark is applied for a short time to introduce free electrons into the gas stream.

The sample, that has to be in liquid phase, is converted to an aerosol and conveyed into the central channel of the plasma. The maximum temperature that can be reached by the inductively coupled plasma (ICP) is 10000K, so that the aerosol is

quickly vaporized. Analyte elements are liberated as free atoms in the gaseous state. Further collisional excitation within the plasma imparts additional energy to the atoms, promoting them to excited states. Sufficient energy is often available to convert the atoms to ions and subsequently promote the ions to excited states. Both the atomic and ionic excited species may then relax to the ground state via the emission of photons. The wavelength of the emitted photons is characteristic of the quantized energy level structure of the atoms and can be used to identify the elements from which they were originated.[3] In addition, the total number of photons is directly proportional to the concentration of the originating element in the sample and could be correlated using a previous calibration obtained with opportune standard solutions.

2.3 Thermo-Gravimetric Analysis (TGA)

The Thermogravimetric analysis is a useful test to determine changes in weight in relation to change in temperature. Such analysis relies on a high degree of precision in three measurements: weight, temperature, and temperature change. As many weight loss curves look similar, the weight loss curve may require transformation before results may be interpreted. A derivative weight loss curve can be used to tell the point at which weight loss is most apparent.

The analyser usually consists of a high-precision balance with a pan loaded with the sample. The sample is placed in a small electrically heated oven with a thermocouple to accurately measure the temperature. The atmosphere may be purged with an inert gas to prevent oxidation or other undesired reactions. A computer is used to control the instrument. Analysis is carried out by raising the temperature gradually and plotting weight against temperature. After the data is obtained, curve smoothing and other operations may be done such as to find the exact points of inflection.[5]

In this activity, the Simultaneous Thermal Analyser (STA 449 Jupiter Netzsch Geratebau, Selb, Germany) was used.

2.4 Scanning Electron Microscopy (SEM)

A scanning electron microscope (SEM) is a type of electron microscope that produces high magnification images of a sample (up to 200000x), with both resolution

and field depth higher than the conventional optical microscope, by scanning it with a focused beam of electrons. The electrons interact with atoms in the sample and, after focusing the high-energy beam of electrons onto the surface of a sample, produces various signals that contain information about the sample's surface topography and composition (Fig. 2.6).

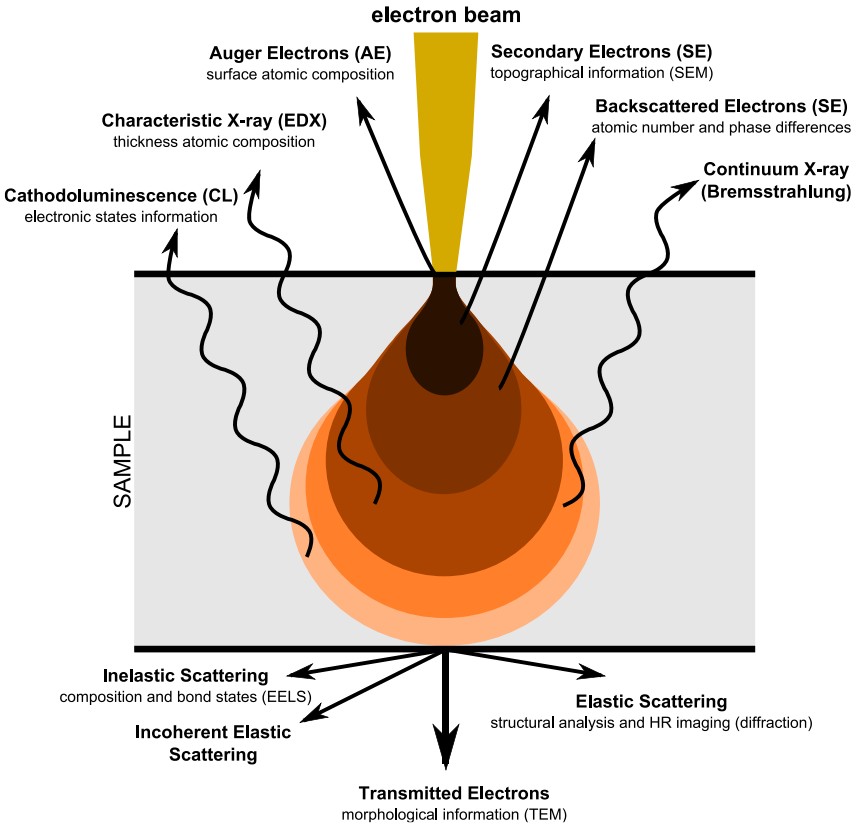

Fig 2.6 - Electron-mater interaction

The primary electrons which are not reflected transfer their energy to some of the electrons of the samples, making them able to diffuse towards the surface and escape outside of the sample with a low energy (energy < 50eV), the so-called secondary electrons. Furthermore, characteristic x-ray photons are emitted when the primary beam causes the ejection of inner shell electrons from the sample and are used to investigate the elemental composition of the sample. The back- scattered electrons emitted from the sample may be used alone to form an image or in conjunction with the characteristic x-rays as atomic number contrast clues to the elemental composition of the sample.

In a typical SEM, an electron beam is thermionically emitted from an electron gun fitted with a tungsten filament cathode. Tungsten is normally used in thermionic

electron guns because it has the highest melting point and lowest vapor pressure of all metals, thereby allowing it to be electrically heated for electron emission, and because of its low cost. The electron beam, which typically has an energy ranging from 0.2keV to 40keV, is focused by one or two condenser lenses to a spot about 0.4nm to 5nm in diameter. The beam passes through pairs of scanning coils or pairs of deflector plates in the electron column, typically in the final lens, which deflect the beam in the x and y axes so that it scans in a raster fashion over a rectangular area of the sample surface (Fig. 2.7). The interaction volume depends on the electron beam energy, the atomic number of the specimen and the specimen's density.

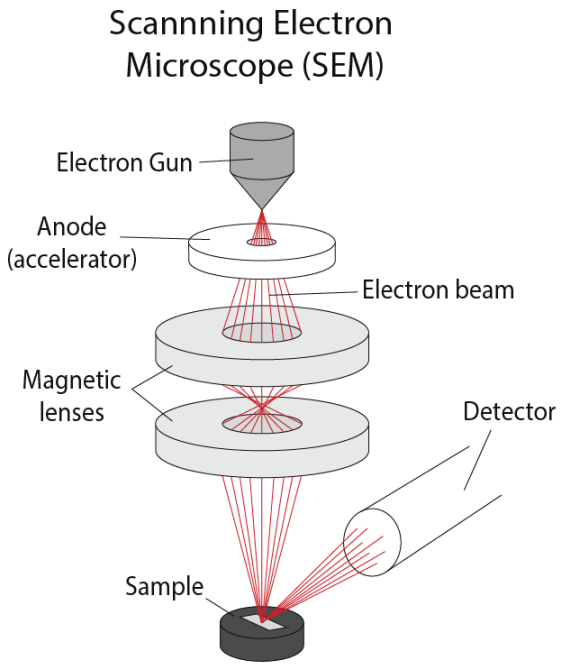

Fig 2.7 – Structure of a SEM (rrutc.msm.cam.ac.uk)

The secondary electrons, due to their low energy, are detected by a scintillator-photomultiplier device and the resulting signal is rendered into a two-dimensional intensity distribution that can be viewed and saved as a digital image. The brightness of the signal depends on the number of secondary electrons reaching the detector. The spatial resolution of the SEM depends on the size of the electron spot, which in turn depends on both the wavelength of the electrons and the magnetic electron-optical system which produces the scanning beam.[6]

The equipment employed in the present work is a Sigma NTS GmbH, Carl Zeiss, Oberkochen, Germany.

2.5 Specific Surface Area (SSA-BET)

Of enormous importance in the materials chemistry, particularly in ceramic processing, is reserved to size, shape and specific surface area (SSA) of the powders. For the calculation of specific surface area is assumed that a powder is composed by small spherical particles with the same diameter. The specific surface area (m^2/g) of the powder, S, can be calculated by multiplying the surface area of each particle and n, the number of the particles per weight unit ($S = 4\pi r^2 n$).

Indeed, the size and shape of the powder particles are usually irregular and unexpected, so that it is not possible to define a simple model of the surface area. In this case, the SSA is indirectly measured by the adsorption of a gas on the outer surface of the particles.

When a gas is adsorbed on the surface of a material, two different adsorption processes can occur: a physical and a chemical adsorption. The main difference relates to the interaction forces involved in the adsorption of the gas: the first one is characterized by weak Van der Waals and electrostatic forces, while the latter includes also stronger chemical bonds. For that reason, a physical adsorption is considered the easier way to determine SSA, with the quantification of the reversible process (desorption) can be adopted to quantify the adsorbed gas.

The scientists Stephen Brunauer, Paul Hugh Emmett and Edward Teller published in 1938 a theory to describe the multilayer adsorption phenomena as an extension of the Langmuir theory. Three main postulates were proposed:

1. gas molecules physically adsorb on a solid in layers infinitely
2. there is no interaction between each adsorption layer 60
3. the Langmuir theory can be applied to each layer

The resulting BET equation, simplified using the parameters of a single gas, is:

$$\frac{p}{V_{ads}(p^0 - p)} = \alpha \frac{p}{p^0} + \beta$$

$$\alpha \frac{C-1}{V_m C} \qquad \beta = \frac{1}{V_m C}$$

where V_{ads} is the adsorbed gas quantity, V_m is the monolayer adsorbed gas quantity, p is the equilibrium pressure of the adsorbates at the temperature of adsorption, p^0 is the saturation pressure of the adsorbates at the temperature of adsorption and C is the BET constant, related to the net adsorption energy.

This equation can be parameterized, resulting in the equation of a line, $y=\alpha x+\beta$, especially in a low-pressure range 0.05-0.30. Once derived the α and β coefficients, V_m is determined as $1/(\alpha+\beta)$.

The total surface area of the adsorbed gas, S, is determined by multiplying V_m and S0, the area correspondent to 1 cm3 of an adsorbed gas monolayer ($S = V_m S0$). Finally, SSA is determined by dividing S and W, the sample weight.

Returning to the assumption that all the particles were spherical and equal, the specific surface area measurement can also be used to evaluate the size of the particles according to the formula:

$$S = \frac{6}{d \cdot l}$$

where S is the specific surface area, d is the density of the material and l is the dimension of the particle.

To perform an SSA-BET analysis the sample holder is immersed in liquid nitrogen to enable the adsorption process. After few minutes, the gas stabilization occurs, and the adsorption process is quantified. Then, the desorption process is forced by substituting the liquid nitrogen with a room temperature water bath; in this condition, the previously adsorbed nitrogen is released. Ideally, the gas adsorption is completely reversible and the desorption is equivalent to the adsorption.[7, 8]

In this activity, the Micrometrics FlowSorb II 2300 instrument was used.

2.6 Mercury Porosimetry

In the creation of 3D object, a property of great interest to control is the porosity, that affect physical properties of the materials. The term porosimetry refers to an analytical technique used to measure the distribution of pore in function of their dimension.

Mercury intrusion porosimetry is based on the premise that a nonwetting liquid (contact angle > 90°), in this case Hg, will intrude capillaries only under pressure (Fig. 2.8).

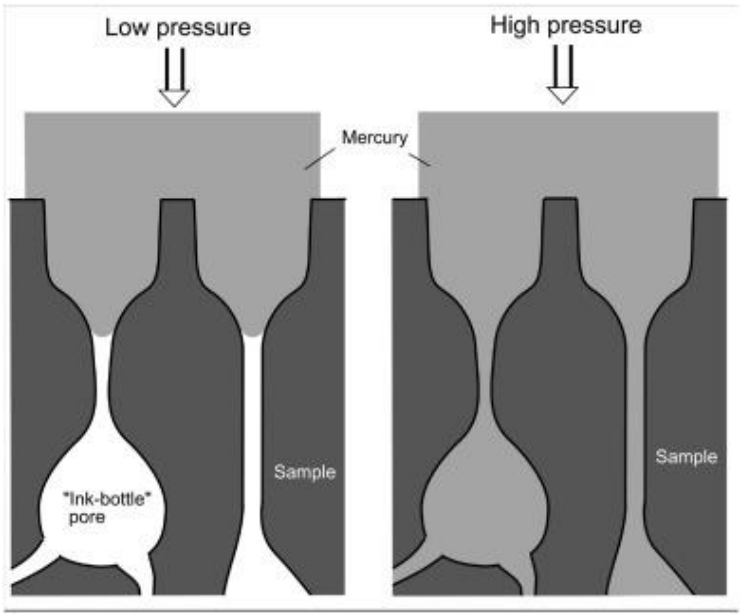

Fig 2.8 Mercury Intrusion inside the pore of the sample (ars.els-cdn.com)

The relationship between the pressure and capillary diameter was described by Washburn as:

$$p = \frac{-4 \cdot \gamma \cdot \cos\theta}{d}$$

where P is the pressure, γ is the surface tension of the liquid, θ is the contact angle of the liquid and d is the diameter of the capillary.

The pressure required for the infiltration of Hg is inversely proportional to the size of the pores, so that a low pressure is required to intrude mercury into large macropores, whereas a greater pressure is required to force mercury into small pores.

The pore size distribution is determined from the volume intruded at each pressure increment, while the total porosity is determined from the total volume intruded.[9]

In this work, the pore volume and pore size distributions were evaluated by mercury intrusion porosimetry (surface tension = 0.48N/m and contact angle = 140°, Hg pressure in the range 0-200Pa, Thermo Scientific Surfer). The measurement error is related to the accuracy of Hg intrusion porosimetry (<4%).

2.7 Mechanical Characterization

2.7.1 Compression

The strength of ceramics materials is mainly characterized by compressive tests, because of the intrinsic micron-size defects that can be easily extended during a tensile stress, affecting the measurement. For that reason, the compressive strength of ceramics is generally higher than their tensile strength. A compressive test of a specimen involves a system of converging forces which tends to reduce its size (Fig. 2.9).

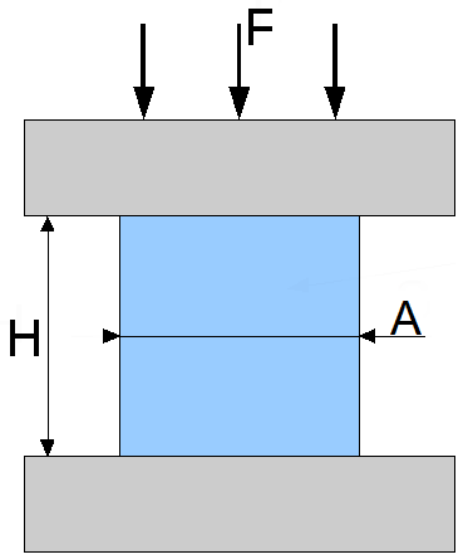

Fig. 2.9 – Simple Scheme of Compression Test

Ideally, the force is homogeneously distributed on the whole surface of the specimen sections, so that dividing the force, F, by the cross-sectional area, A, the average value of the compressive stress, σ, can be obtained. A uniform distribution of the normal stress can be assumed in axially loaded specimens, except for the local areas of application of the loads.

The compressive strength of scaffolds is an important bio-engineering consideration. When using porous structures for tissue engineering scaffolds, the structure must retain sufficient mechanical properties to fulfil the requirements of structural integrity once implanted in host tissue.[10]

The tests were performed in displacement control at 0.5 mm/min, by collecting data at 20 Hz with a universal testing machine (MTS Insight 5, Minnesota, USA).

2.7.2 Flexure (4-point bending)

The flexural strength is a material property defined as the stress in a material just before it yields in a flexure test. The flexural strength would be the same as the tensile strength if the material were homogeneous; in fact, most materials have small or large defects which act as local stress concentrators, effectively causing a localized weakness.

Ceramics are usually very brittle, and their flexural strength depends on both their inherent toughness and the size and severity of flaws.

In this activity, the flexural strength was calculated by 4-point bending tests: a loading force is applied by means of two loading pins with a distance between them equal to a half of the distance between the supporting pins (Fig 2.10).[10]

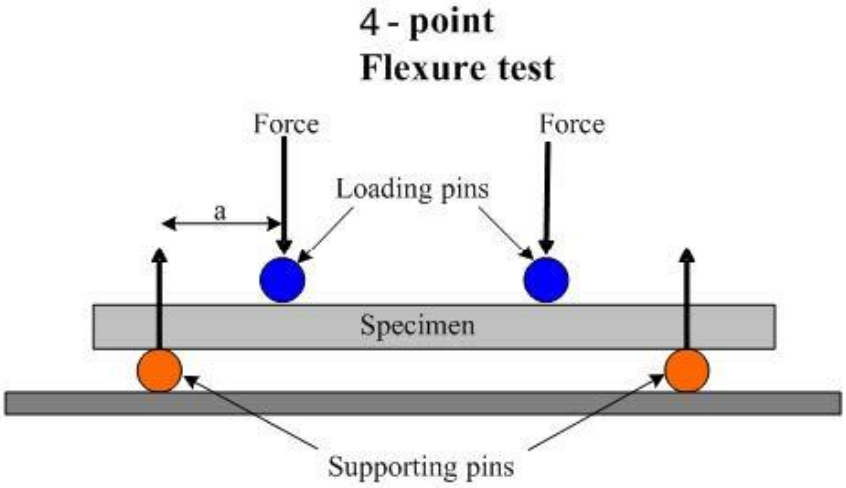

Fig 2.10 – scheme of the 4-point flexural test (touchstonetesting.com)

It should be noted that no specific reference standards are given for 4-point bending tests of macroporous ceramic materials, so that only some indications were adopted (ASTM C1341-00: Standard Test Method for Flexural Properties of Continuous Fiber Reinforced Advanced Ceramic Composites).

The flexural strength was determined by testing parallelepiped specimens. The tests were performed in displacement control at 0.5 mm/min, by collecting data at 20 Hz with a universal testing machine (MTS Insight 5, Minnesota, USA).

The resultant state of stress in flexural testing is reported in Fig 2.11.

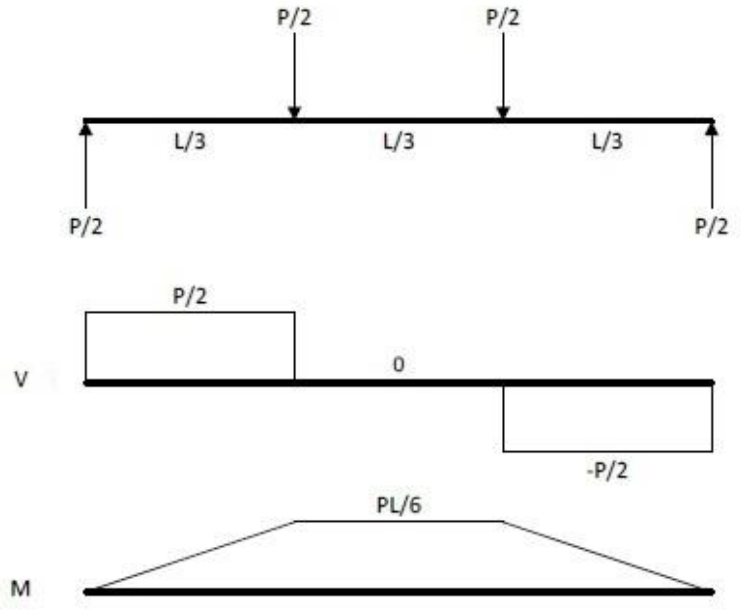

Fig 2.11 - Shear force and bending moment distribution during a 4-point bending test (scielo.org.za)

Despite a stress concentration is assumed to be locally present at the loading points, the region of the specimen between the upper pins is characterized by a uniform bending moment and null shear stress, leading to pure bending loading (PL/6) in the central part of the specimen. Once derived the fracture load, PN, the flexural strength is given by:

$$\sigma = \frac{3 \cdot P_N \cdot a}{b \cdot d^2}$$

where b and d represent the weight and the height of the specimens, respectively.
For each test, the deformation ε has been evaluated on displacement control, δ, according to:

$$\varepsilon = \frac{6 \cdot \delta \cdot d}{L^2}$$

2.7.3 Nanoindentation

In indentation, a tip (or indenter) with known geometry (the most common is Berkovich tip that has a three-sided pyramid geometry) is pressed, with known load, against the samples, leaving an impression on the surface. From the shape, dimension and depth of the impression it's possible to calculate several mechanical properties like

modulus of elasticity, hardness and others. In nanoindentation small loads and various tip sizes are used, so that the indentation area can be only a few μm^2 or even nm^2.

In nanoindentation a recording of the penetration depth is made and therefore the area of the impression is determined using the known geometry of the indentation tip, while the various indenting parameters, such as the load and the depth of penetration, can be measured. A record of these values can be shown on a graph to create a load-displacement curve (Fig. 2.12). These curves can be used to extract the mechanical properties of the material.

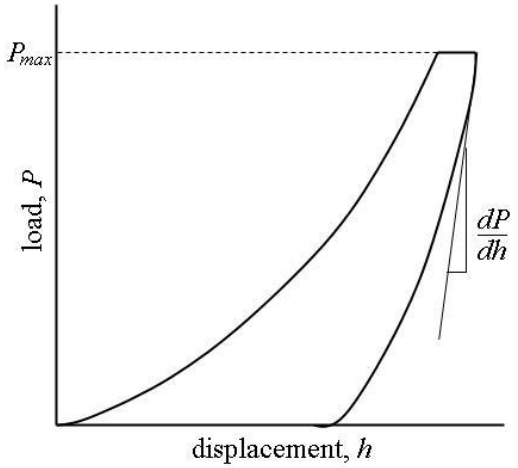

Fig 2.12 – Load-displacement curve of a nanoindentation test

The slope of the curve, dP/dH, upon unloading is indicative of the stiffness S of the contact. The stiffness of the contact can be used to calculate the reduced Young's modulus E_r.

$$E_r = \frac{1}{\beta}\frac{\sqrt{\pi}}{2}\frac{S}{\sqrt{A_p(h_c)}}$$

Where $A_p(h_c)$ is the projected area of the indentation at the contact depth h_c, and β is a geometrical constant on the order of unity. $A_p(h_c)$ is often approximated by a fitting polynomial that depends on the tip used.

The reduced modulus E_r is related to Young's modulus E_s of the test specimen through the following relationship from contact mechanics:

$$\frac{1}{E_r} = \frac{1-\nu_i^2}{E_i} + \frac{1-\nu_s^2}{E_s}$$

v_i indicates the Poisson's ratio of the indenter material while v_s indicates the Poisson's ratio of the specimen, that generally varies between 0 and 0.5 for most materials (though it can be negative) and is typically around 0.3.

To gain nanohardness values, some nanoindenters use an area function based on the geometry of the tip, compensating for elastic load during the test, this area function provides a load-displacement graph from which is possible gaining real-time nanohardness values.[11]

References

1. Cullity, B., *Elements Of X Ray Diffraction*. Addison-Wesley Pubblishing Company: 1956.
2. Wondratschek, H.; Muller, U., *International Table for Crystallography*. Springer: 2005; Vol. Volume A1: Symmetry Relations between Space Groups.
3. Hou, X.; Amais, R.; Jones, B.; Donati, G., *Inductively Coupled Plasma Optical Emission Spectrometry*. John Wiley & Sons: 2016.
4. Griffiths, P.; De Haseth, J.; JD, W., *Fourier Transform Infrared Spectrometry, 2nd Edition*. Wiley: 2007.
5. Coats, A.; Redfern, J., Thermogravimetric analysis. A review. *Analyst* **1963,** *88* (906-924).
6. McMullan, D., Scanning electron microscopy 1928–1965. *The Journal of Scanning Microsocopies* **2019,** *17* (3), 175-185.
7. Brunauer, S.; Emmett, P. H.; Teller, E., Adsorption of Gases in Multimolecular Layers. *Journal of the American Chemical Society* **1938,** *60* (2), 309-319.
8. Langmuir, I., The adsorption of gases on plane surfaces of glass, mica and platinum. *Journal of the American Chemical Society* **1918,** *40* (9), 1361-1403.
9. Washburn, E. W., Note on a Method of Determining the Distribution of Pore Sizes in a Porous Material. *Proc Natl Acad Sci U S A* **1921,** *7* (4), 115-6.
10. Kokubo, T., *Bioceramics and their Clinical Applications*. Woodhead Publishing Limited: 2008.
11. Chowdhury, S.; Thomas, V.; Dean, D.; Catledge, S. A.; Vohra, Y. K., Nanoindentation on Porous Bioceramic Scaffolds for Bone Tissue Engineering. *Journal of Nanoscience and Nanotechnology* **2005,** *5* (11), 1816-1820.

Chapter 3
Development of Multi-doped Hydroxyapatites with Multifunctional Abilities

The inorganic component of the bone tissue is a poorly crystalline calcium phosphate with the structure of hydroxyapatite (HA) and characterized by atomic vacancies (particularly Ca^{2+}) and multiple ion substitutions, thus having a composition far from the typical HA stoichiometry $Ca_{10}(PO_4)_6(OH)_2$. This evidence stimulated the design and development of a new generation of synthetic apatite bone substitutes which, simulating bio-relevant physicochemical features of the biological phase, can stimulate and sustain the bone regeneration process, thus overcoming the relatively poor bioactivity of currently used HA implants. Biological apatites contain cationic and anionic substitutions at the atomic sites of the hydroxyapatite crystal structure and, also, in a more disordered surface layer surrounding the more crystalline core.[1]

Mg^{2+} is a major divalent ion associated with new bone formation. It has been verified that in calcified tissues, the amount of magnesium associated with the apatitic phase is higher at the beginning of the calcification process and decreases with increasing calcification.[2] The development of synthetic Mg-substituted hydroxyapatite was extensively investigated[3, 4] and its improved effect on early formation of new bone tissue *in vivo* and *in vitro*, compared to stoichiometric HA, was reported.[5, 6]

Sr^{2+}-substituted apatite powders have been prepared by ion exchange of Sr^{2+} for Ca^{2+} using wet chemical synthesis approaches.[7, 8] The good interfacial bonding of Sr-containing HA with cancellous and cortical bone has been recently reported in a rabbit hip replacement model, pointing out the good affinity of an apatite cement with both types of bone, and remarkable integration with the cancellous bone.[9-11]

The doping of HA with Zn^{2+} ions, present in the natural bone as a trace element, -∼0.2 wt %,[12]- was previously studied, reporting ability to substitute Ca^{2+} ions in the HA structure and to confer improved biological and antibacterial properties.[13, 14] Zinc is of

great importance for many metabolic processes and is at the same time a relatively harmless element;[15] thus, many studies on Zn doped HA concerned Zn doping in much higher amounts with respect to the physiological levels.[13, 16, 17]

The doping of synthetic HA with carbonate ions, to mimic biologic HA (which contains ~4-8%wt of CO_3^{2-} ions) is reported in previous studies.[18, 19] The presence of B-carbonation (i.e. substituting the PO_4^{3-} group in the HA lattice) was shown to cause a destabilization of the apatite lattice resulting in decreased crystal ordering, with reduced domain size and increased solubility in both *in vitro* and *in vivo* tests.[3]

Previous results regarding in vitro and in vivo studies of multi-doped apatites clearly show that they are elective materials for bone regeneration; however, in spite of the many studies carried out so far on the use of apatite particles, very few works report on studies carried out on consolidated materials. Bone regeneration requires the use of 3-D scaffolds with mechanical properties enabling application in critical size bone defects and, possible, in load-bearing site. Otherwise, the use of apatite powders is limited to the development of granules which are however suitable to treat small, confined bone defects.

With the purpose to develop new biomaterials potentially applicable in bone regeneration, which today lack of satisfactory solutions, in the present work I attempted to develop consolidated calcium phosphate scaffolds with enhanced mechanical performance, starting from new HA nanophases presenting multiple ion substitutions in both cationic and anionic sites. I carried out wet neutralization processes to synthesize the starting apatite powders as raw materials for the scaffold production. That technique was chosen for the possibility to control the crystallinity of the hydroxyapatite varying the temperature (low temperature lead to HA with low crystallinity, more similar to the HA crystal of our bones) and the possibility to introduce foreign ions inside the HA lattice. The obtained raw materials were thoroughly characterized and sintered to develop dense sample characterized in terms of composition, crystallinity, ability of ion release and exchange in physiological fluids. Specifically, the influence of the doping ions on the crystal stability of HA was investigated and related to the phase composition of sintered solids. Furthermore, the influence of doping ions on the microstructure development and mechanical properties was investigated, to evaluate starting compositions promising to give enhanced mechanical strength in the final scaffolds.

3.1 Synthesis of materials

A precipitation method was used for the preparation of the new hydroxyapatite phase, particularly a neutralization reaction, between an aqueous suspension of calcium hydroxide ($Ca(OH)_2$, Sigma Aldrich, 95% purity), and a solution of phosphoric acid (H_3PO_4, Fluka, 85% purity). The synthesis technique was chosen for its repeatability and for the possibility of introducing foreign ions during the formation of the HA crystals. To introduce foreign ions in the final product, zinc, strontium and magnesium cations were added by dissolving suitable reactants in the aqueous calcium suspension, namely zinc chloride ($ZnCl_2$, Sigma Aldrich), strontium chloride ($SrCl_2$, Sigma Aldrich) and magnesium chloride ($MgCl_2$, Sigma Aldrich). To introduce carbonate anions in the reaction vessel, a solution of calcium bicarbonate ($NaHCO_3$, Sigma Aldrich) was dropped in the basic suspension simultaneously with the phosphoric acid solution. The initial Ca/P ratio was set to 1.67, i.e. equal to that of stoichiometric hydroxyapatite.

The reaction is conducted in a round-bottomed flask, filled with an aqueous suspension of calcium hydroxide, where the chloride salts of the doping cations were dissolved (Fig. 3.1). The suspension is mechanically stirred. The alkaline suspension was slowly added with the H_3PO_4 and $NaHCO_3$ solutions (dripping rate = 1 drop/s). The entire reaction is conducted at 37°C, in order to simulate the temperature at which bone formation occurs in vivo; these conditions limit the growth of the HA crystals to the nanosize, similarly as the biologic apatite. In conclusion, the suspension is left in agitation at 37°C for 2 hours, then the suspension is left to mature after-night at room temperature. Then, the suspension is washed with bi-distilled water for 3 times, in order to eliminate ions simply adsorbed on the HA surface (such as HPO_4^{2-} which can create undesired pyrophosphate phases upon thermal treatment) and then dried at 40°C in oven. Finally, the obtained powder is sieved at 150µm.

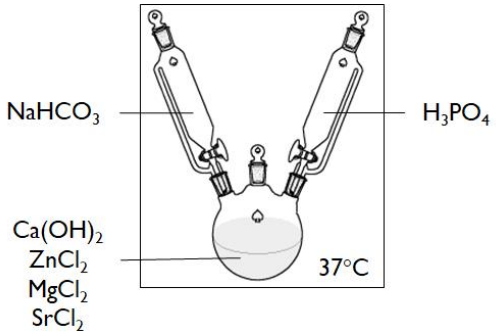

Fig. 3.1 – Schematic setting for the synthesis of multidoped hydroxyapatite

In the present work, two different sets of hydroxyapatite powders were synthesized, the first set includes simple HA (as reference material), HA doped with magnesium (MgHA), HA doped with magnesium and strontium (MgSrHA) and HA doped with magnesium and zinc (MgZnHA), the second set includes the same HAs of the first set but doped also with carbonate: carbonated HA (CHA), carbonated HA doped with magnesium (MgCHA) carbonated HA doped with magnesium and strontium (MgSrCHA) and carbonated HA doped with magnesium and zinc (MgZnCHA). The study of the sintering behaviour of carbonated HA is relevant because, even though CO_3 is unfortunately eliminated during sintering (as gaseous CO_2) and cannot be retained in the final scaffold when sintering is carried out well above 1000 °C, as typical of HA, the crystal structure of carbonated apatites is affected by ionic vacancies in the phosphate site, in turn possibly influencing the sintering behaviour and thus the composition and microstructure of the final sintered phases. The list of synthesized hydroxyapatites is shown in Table 3.1. The symbols X_{Mg}, X_{Sr} and X_{Zn} indicates the initial molar fraction, respectively, of Mg^{2+}, Sr^{2+} and Zn^{2+}, calculated as $\frac{mole\ of\ XX}{mole\ of\ Ca} \cdot 100$, where XX could be Mg, Sr or Zn.

Samples	Initial X_{Mg} **(mol%)**	Initial X_{Sr} **(mol%)**	Initial X_{Zn} **(mol%)**	Carbonate **(wt%)**
HA	-	-	-	-
CHA	-	-	-	6
MgHA	15	-	-	-
MgCHA	15	-	-	6
MgSrHA	15	1.5	-	-
MgSrCHA	15	1.5	-	6
MgZnHA	15	-	5	-
MgZnCHA	15	-	5	6

Table 3.1 – List of synthesized hydroxyapatites

The amount of CO_3^{2-} introduced in the HA structure was limited to 6%wt, a value in the range of the carbonate content in healthy bones[20], because with higher amounts supersaturation of CO_3^{2-} ions in the reaction vessel occurred and thus it was not possible to avoid the formation of secondary phases such as calcium carbonate ($CaCO_3$) in the final powder.

3.2 Physicochemical Characterization of Hydroxyapatites Powders

The phase composition of the as-obtained materials was obtained by X-ray diffraction (XRD) with a D8 ADVANCE (Bruker, Karlsruhe, Germany) diffractometer using Cu Kα radiation (λ = 1.54178 Å) generated at 40 kV and 40 mA, a counting time of 0.5 s, and a step size of 0.02° 2θ. Cell parameters and crystallite size were assessed by the full profile analysis of the XRD spectra (TOPAS 5, Bruker, Karlsruhe, Germany).

XRD analysis (Fig. 3.2) confirms that the HA phase is the only crystalline component (PDF card #09-0432) of all the as-obtained materials. The XRD spectra of the ion-doped materials are characterized by broader patterns as compared with the undoped HA. This effect can be ascribed to a reduction of the crystalline domain size because of the presence of doping Mg^{2+}, Sr^{2+} and Zn^{2+} ions as substitutes for Ca^{2+} and of CO_3^{2-} ions for PO_4^{3-}, as also observed in previous works.[8, 16, 21-23]

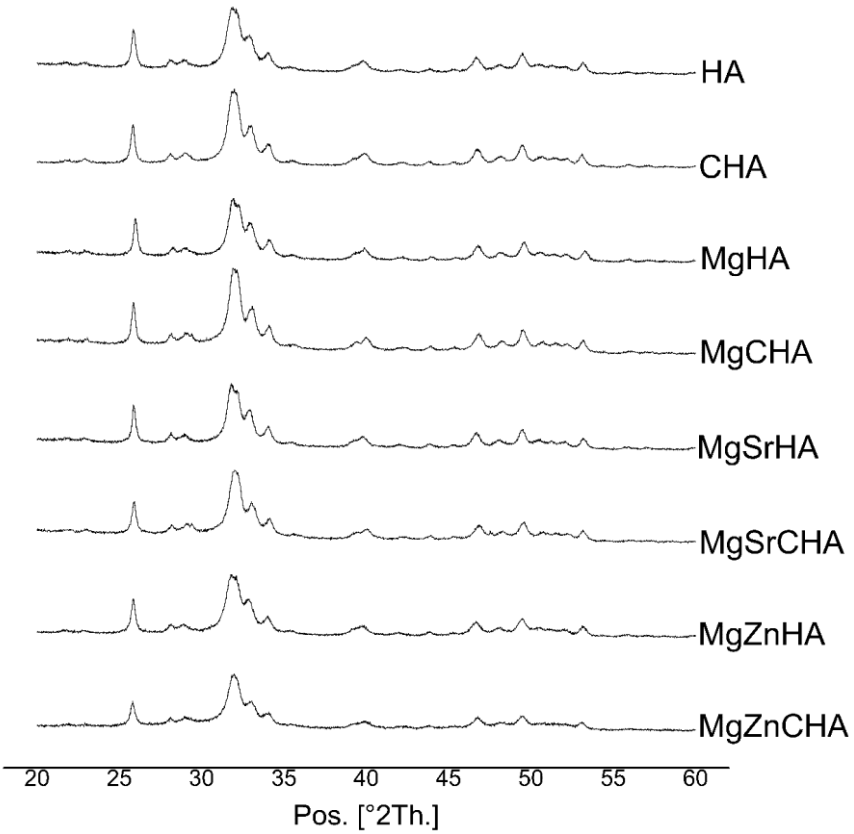

Fig. 3.2 – XRD patterns of the hydroxyapatite powders

Crystallographic data obtained by the full profile analysis of the XRD patterns in Fig. 3.2 are reported in Table 3.2. The ion-doped HA powders show lattice deformation. The presence of carbonate cause a decrease in *a* and *c* parameters, confirming the

trends shows in other works[19, 24], also Mg^{2+} and Zn^{2+} decrease the *a, c* parameters and the average crystallite size in the multi-doped HAs, the cause is related to alteration of the interatomic distances, which can be ascribed to the smaller atomic radius of the doping ions with respect to calcium (i.e., Zn^{2+} = 88pm and Mg^{2+} = 86pm compared with Ca^{2+} = 114pm) and phosphate ions (i.e., CO_3^{2-} = 178 pm compared withPO_4^{3-} = 238 pm). In contrast, the presence of Sr^{2+} seems to increase the cell parameters due to the bigger atomic radius of Sr^{2+} respect to calcium (i.e., Sr^{2+} = 132 pm). There are not substantial differences in parameters of HA and MgHA, so it's possible to assume that magnesium does not enter in structure.

Samples	*a* **(Å)**	*c* **(Å)**	*Cell Vol.* **(Å3)**	D_{av} **(nm)**
HA	9.4328	6.8935	531.19	25.7
CHA	9.4034	6.8954	528.03	27.7
Mg-HA	9.4385	6.8882	531.42	35.1
Mg-CHA	9.3946	6.8936	526.9	40.1
MgSr-HA	9.4411	6.8924	532.04	33.5
MgSr-CHA	9.4013	6.8984	528.03	34.6
MgZnHA	9.4351	6.8862	530.89	29.0

Table 3.2 – Crystallographic analysis of the as-obtained HAs powder

The carbonate content was evaluated by thermo-gravimetric analysis (TGA) of dried samples (10 mg) in the range 600-1100 °C[19], using a Stanton STA 1500 (Stanton, London, UK), with heating rate of 10 °C/min.

The chemical analysis was performed on dried samples (20mg) using ICP-OES spectrometer (Agilent 5100, United States) and primary standards (1000 ppm, Fluka). The samples were dissolved into 2 ml of nitric acid then diluted in 100 ml of milliQ water.

The chemical analysis and the carbonate content, reported in Table 3.3, shown that Mg^{2+}, Sr^{2+}, Zn^{2+} and CO_3^{2-} are found in the final apatite powder. Not all magnesium nominally introduced in the round-bottomed flask remained incorporated in the apatite structure. Considering the yield of Mg^{2+} incorporation, similar in all the apatite samples (see Table 3.1) it seems that the co-doping with other ions such as Sr^{2+} and Zn^{2+} did not drastically affect the Mg^{2+} entering. This is interesting, as all these cations are expected to occupy the Ca^{2+} sites if the HA lattice. Similar observation can be made considering

the yield of incorporation of Sr^{2+} and Zn^{2+} cations which is almost 100% either with or without carbonate ions added. This confirms that, at least with the amounts of doping considered, ions substitution is not affected by the competition between multiple divalent ions. In this respect, particularly in case of simultaneous presence of various divalent ions, it is possible that part of the doping ions have instead occupied the amorphous hydrated layer typical of nanocrystalline apatites, rather than the HA lattice, particularly Mg^{2+} which is quite smaller than Ca^{2+} [6, 8, 25], whereas strontium and zinc are more likely to enter in the HA lattice.

In the multi-doped carbonated HA powders, the presence of CO_3^{2-} decreases with the increase of substitution, even though carbonate and cations, theoretically, do not compete for the same crystal site. This finding suggests that the alteration of the overall HA structure induced by cations doping could have limited CO_3 substitution. To be noted that in the not-carbonated HA, some CO_3^{2-} was found to enter as a dopant; this phenomenon is due to the dissolution of the carbon dioxide present in the air atmosphere in the alkaline calcium suspension contained in the reaction vessel, until a equilibrium between ionic species dissolved in water such as HCO_3^- and atmospheric CO_2 is reached.

Samples	Initial X_{Mg} **(mol%)**	Actual X_{Mg} **(mol%)**	Mg Yield **(%)**	Initial X_{Sr} **(mol%)**	Actual X_{Sr} **(mol%)**	Initial X_{Zn} **(mol%)**	Actual X_{Zn} **(mol%)**	Initial CO_3^{2-} **(wt%)**	Actual CO_3^{2-} **(wt%)**
HA	-	-	-	-	-	-	-	-	1.83
CHA	-	-	-	-	-	-	-	6	5.69
MgHA	15	6.11	40.7	-	-	-	-	-	1.79
MgCHA	15	6.07	40.5	-	-	-	-	6	5.20
MgSrHA	15	6.21	41.4	1.5	1.47	-	-	-	1.76
MgSrCHA	15	6.11	40.7	1.5	1.43	-	-	6	4.62
MgZnHA	15	5.82	38.8	-	-	5	4.99	-	1.78
MgZnCHA	15	5.63	37.5	-	-	5	4.97	6	4.91

Table 3.3 – Chemical analysis and carbonate content of the as-obtained HA powders

3.3 Sintering

To obtain a 3D solid scaffolds with appropriate mechanical properties, starting from a ceramic powder there is the need of a consolidation process; the typical process

of consolidation for ceramics is sintering, which is a treatment at high temperature activating physico-chemical reactions in the particle surface and bulk yielding their coalescence, reduction of inter-particle porosity and achievement of mechanical strength. The sintering was performed on pellets produced by pressing 1,5g of HA powders in a steel mould (20mm in diameter) by uniaxial press at 700bar, then further consolidation of the green bodies was obtained by cold isostatic pressing at 2500bar. This further treatment allowed to obtain green bodies with relative density of 55-60 %wt, which is considered as acceptable to obtain high density in the final sintered bodies.

The optimal sintering temperature for HA is widely considered as 1250°C.[26-28] However, at that temperature, there is the complete loss of carbonate content, indeed thermogravimetric analysis reveals that above 600°C HA starts to release CO_2, resulting from the decomposition of CO_3 therein contained. A previous study by Landi et al attempted to retain carbonation in sintered HA bodies by sintering in CO_2 atmospheres.[24] In this work porous hydroxyapatite scaffolds with good mechanical properties were obtained by sintering at 900°C with CO_2 flux. At those conditions some residual carbonate ions could be retained in the HA structure. With the purpose to investigate for the first time the thermal behaviour of multi-doped hydroxyapatite powders, in my work the sintering process was carried out under conventional air atmosphere and also under CO_2 flux in a range of temperatures from 900°C to 1250°C (Table 3.4). The heating rate was 150°C/h for all the sintering process with a final dwell time of 1 hour. The obtained materials were investigated in terms of phase composition, carbonate content and mechanical properties.

	Temperature	**Environment**
1	900 °C	Air
2	900 °C	CO_2
3	1000°C	Air
4	1000°C	CO_2
5	1100°C	Air
6	1100°C	CO_2
7	1250 °C	Air
8	1250 °C	CO_2

Table 3.4 – List of tested sintering

The carbonate content of the hydroxyapatites after sintering was evaluated by thermo-gravimetric analysis (TGA) of dried samples (10 mg) in the range 600-1100 °C[19], using a Stanton STA 1500 (Stanton, London, UK), with heating rate of 10 °C/min. (Fig. 3.3 & 3.4).

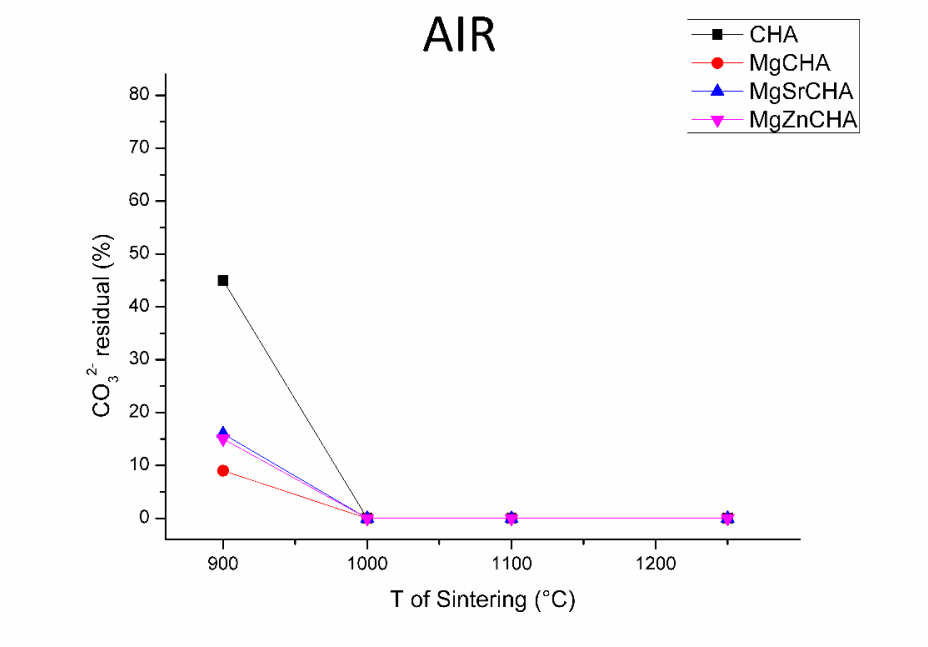

Fig. 3.3 – Carbonate residual in HA after sintering in air

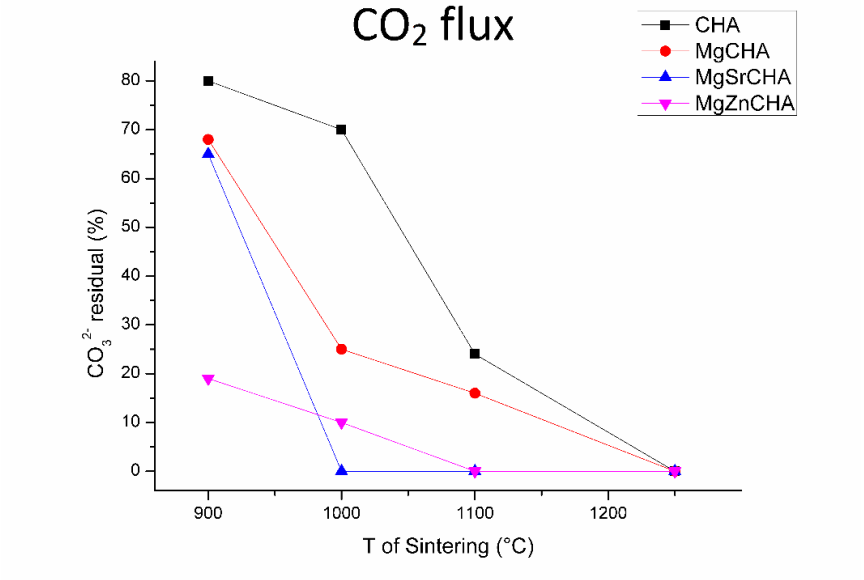

Fig. 3.4 – Carbonate residual in HA after sintering in CO_2 flux

For the HA green bodies sintered in a static air environment total loss of carbonate over 1000°C is detected for all the samples and at 900°C, the residual

carbonate in doped HA is below 20% respect the initial content. Only simple carbonated HA (i.e. without any other doping ions) shows a residual carbonate content over 40%. The results suggest that the presence of doping ions destabilized the crystal structure of HA, with a lower binding energy of CO_3^{2-} ions in the HA lattice, thus promoting the loss of carbonate at lower temperatures. Moreover, the data shown that is not possible to obtain a doped HA with relevant content of carbonate, with the typical sintering in air at 1250°C, indeed taking as example the MgZnCHA, there is an initial carbonate content of 4.91%wt, after sintering at 900°C the residual carbonate is 15% respect the initial content, so the final content of carbonate is 0.74%wt, not comparable with the content of carbonate in a human bone, between 4%wt and 8%wt[24].

The HA sintered under CO_2 flux presents smaller loss of carbonate after sintering above 1000°C. It is possible to have higher amount of carbonate for multi-doped HA phases like MgCHA and MgSrCHA (3.54%wt and 3,00%wt respectively), only at 900°C, while even at this temperature MgZnCHA lose more than 80% of his initial carbonate content. Comparing the amount of carbonate inside the multi-doped HA (MgCHA, MgSrCHA, MgZnCHA) and simple carbonated HA (CHA), after sintering, it is possible to notice that the presence of ions increases the loss of carbonate in thermal treatment, especially when zinc ions are present.

XRD analysis made on 2 sets of dense hydroxyapatite bodies, the first set sintered with CO_2 flux at 900°C while the second sintered in air at 1250°C, reveals that at 1250°C there is the formation of a secondary phase (beta-tricalcium phosphate: β-TCP, $Ca_3(PO_4)_2$) in the doped HAs (Fig. 3.5). β-TCP is a compound with formula $Ca_3(PO_4)_2$ and Ca/P molar ratio of 1,5. The formation of a crystalline phase with Ca/P<1.67, such as TCP, is due to calcium deficiency in the starting material. During the thermal treatment, the lattice of the Ca-deficient HA stabilizes to recover its stoichiometry, so that stoichiometric HA and TCP result after sintering. This effect is more marked in the ion-doped HAs, due to the substitution of Mg^{2+}, Sr^{2+} or Zn^{2+} that reduce the Ca^{2+} content in HA. Different amounts of β-TCP are formed in all the doped hydroxyapatite dense scaffolds, also traces of magnesium oxide (MgO) have been detected, while HA and CHA show only some traces of calcium oxide (CaO, see Table 3.4). β-TCP is widely studied because of its use as material for bone substitution. β-TCP can be used to create composite bone substitutes with hydroxyapatite. Such a biphasic bone substitutes was

previously studied to combine the different properties of the two materials. β-TCP is more soluble than HA ($Ks_{B\text{-}TCP}$=28.9; Ks_{HA}=58), so its presence could be helpful, improving the release of elements like calcium and other ions to give a chemical signal to the cells relevant for the bone regeneration process.

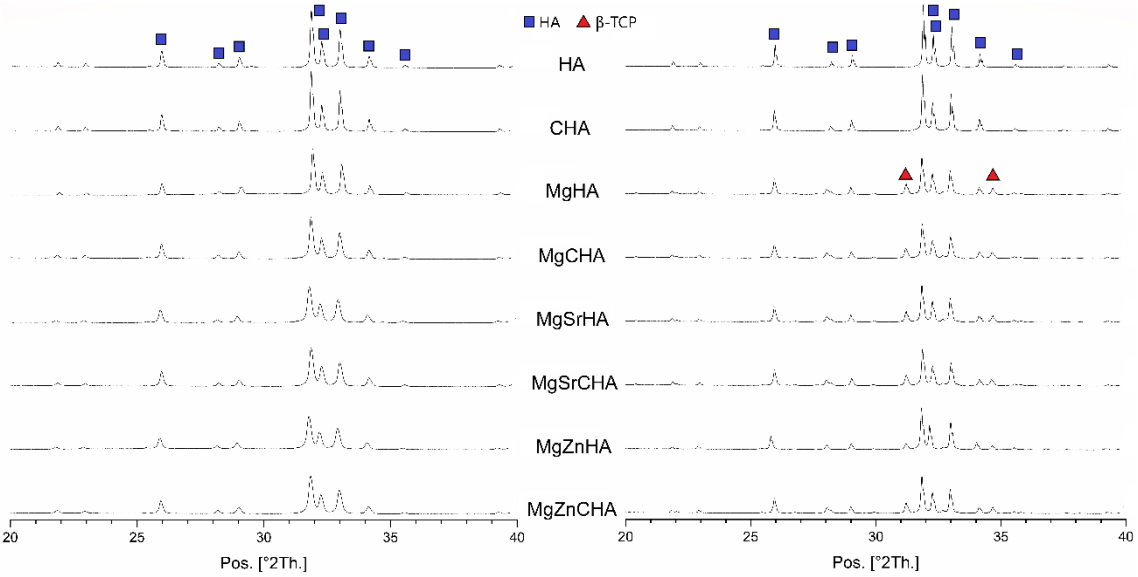

Fig. 3.5 – XRD Pattern of sintered HA dense bodies. Left) Sintered with CO_2@900°C Right) Sintered in air@1250°C

Samples	*a (Å)*	*c (Å)*	*Cell Vol. (Å³)*	*D_{av} (nm)*	Sec. Phase (%vol)	*a (Å)*	*c (Å)*	*Cell Vol. (Å3)*	*D_{av} (nm)*
HA	9.4196	6.8865	529.17	504.7	CaO	0.7	4.806		488.8
CHA	9.4205	6.8872	529.33	254.8	CaO	0.7	4.807		249.8
MgHA	9.4287	6.8835	529.96	551.5	b-TCP MgO	25 1	10.3637 4.2104	37.3561	139.4 142.5
MgCHA	9.4282	6.8834	529.89	373.4	b-TCP MgO	25 1	10.3649 4.2107	37.3487	123.1 153.6
MgSrHA	9.4125	6.9100	530.17	447.4	b-TCP MgO	33 1	10.3618 4.23	37.3169	126.5 140.5
MgSrCHA	9.4274	6.8903	530.33	509.5	b-TCP MgO	27 1	10.3827 4.2110	37.3510	122.6 131.6
MgZnHA	9.4255	6.8937	530.39	221.9	b-TCP MgO	8 2	10.3856 4.2117	37.3079	83.3 118.8
MgZnCHA	9.4117	6.9074	529.88	100.6	b-TCP MgO	13 3	10.3571 4.2355	37.2923	83.5 106.8

Table 3.5 – Crystallographic analysis of the HA dense bodies sintered in air@1250°C

The presence of carbonate does not influence the formation of secondary phase, indeed the not carbonated HAs present similar amounts of secondary phase as their carbonated counterparts. As an example, MgSrHA presents a composition made by 33%vol of β-TCP and 1%vol of MgO similar to the composition of MgSrCHA made by 27%vol of β-TCP and 1%vol of MgO. The full profile analysis of the XRD spectra (Table 3.5) reported an increase of the *c* parameter of the HA lattice in the MgSrHA sample compared to the non-doped HA, thus suggesting that Sr^{2+} ions could enter into the apatite lattice in substitutional position. In contrast, considering the low changes in the lattice parameters in the case of Mg^{2+} and Zn^{2+} doping, we can suppose that these ions were segregated away by the HA lattice during sintering and were incorporated in the β-TCP structure.

Samples	Pre-Sintering X_{Mg} **(mol%)**	Post-Sintering X_{Mg} **(mol%)**	Pre-Sintering X_{Sr} **(mol%)**	Post-Sintering X_{Sr} **(mol%)**	Pre-Sintering X_{Zn} **(mol%)**	Post-Sintering X_{Zn} **(mol%)**
HA	-	-	-	-	-	-
CHA	-	-	-	-	-	-
MgHA	6.11±0.02	6.12±0.05	-	-	-	-
MgCHA	6.07±0.03	6.08±0.04	-	-	-	-
MgSrHA	6.21±0.04	6.18±0.02	1.47±0.03	1.44±0.02	-	-
MgSrCHA	6.11±0.03	6.05±0.04	1.43±0.05	1.43±0.04	-	-
MgZnHA	5.82±0.02	5.85±0.06	-	-	4.99±0.05	5.02±0.03
MgZnCHA	5.63±0.03	5.64±0.02	-	-	4.97±0.04	4.94±0.06

Table 3.6 – Chemical analysis of the dense HA bodies pre and post sintering

The chemical analysis reveals that the content of ions doesn't change after sintering (Table 3.6), like it was expected.

3.4 Mechanical and Morphological Characterization of Sintered Hydroxyapatites

The aim of this work is to develop a multi-doped hydroxyapatite scaffold with adequate properties for substituting a load-bearing bone, so the function of sintering with CO_2 flux at 900°C is not only to prevent the total loss of initial carbonate content, but also to obtain a scaffold with good mechanical properties, at least comparable with that of classic sintering in air at 1250°C or in the range of natural bone tissue.

To test the mechanical properties of the sintered HA, the powders were compacted in dense scaffolds, firstly with an uniaxial press and then with a cold isostatic press at 2500bar to increase the green density at levels suitable to achieve full densification in the sintered bodies; finally the scaffolds were sintered, as above described.

In order to test the mechanical properties of the multi-doped HA sintered with CO_2 flux, 5 dense scaffolds, for each sample, in form of cylinders with diameter of 10mm and height of 15mm were tested with a universal testing machine (MTS Insight 5, Minnesota, USA) in a compression test with the crosshead speed was 2mm/min (Fig. 3.7).

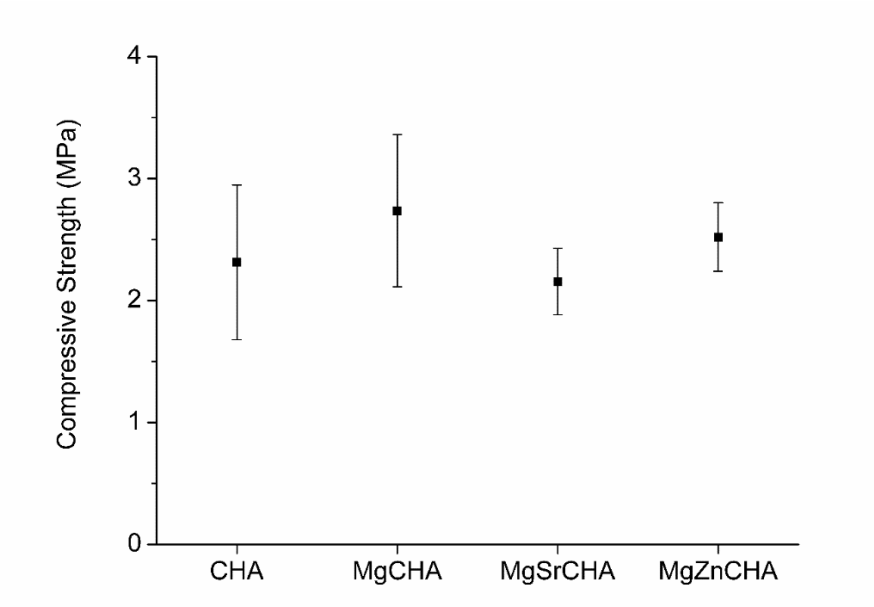

Fig. 3.7 – Compressive strength of HA dense bodies sintered at 900°C with CO_2 flux

The compressive strength of carbonated HAs sintered with CO_2 flux are not comparable with that of a HA dense scaffolds sintered at 1250°C in air, indeed the fracture load at compression of HA sintered at 1250°C is ~200MPa[29]. A simple but efficient way to evaluate the products of the sintering process is by evaluation of the relative density. This can be obtained by dividing the density of the scaffolds (weight:volume) by the nominal density of HA (3,16g/cm^3). Comparing the relative density of HAs sintered at 1250°C in air (~95%), and the relative density of HAs sintered with CO_2 flux at 900°C (~65%), it is possible to assume that effective consolidation could not be obtained with such sintering process. Therefore, from now on the sintering

process is carried out at 1250°C in air, unfortunately losing the whole carbonate during the sintering.

To understand how doping ions could influence the mechanical properties of hydroxyapatite, compression tests, 4-point bending tests and nanoindentation tests were carried out on multi-doped hydroxyapatites sintered samples.

For the compression test, 5 dense scaffolds, for each sample, in form of cylinders with diameter of 10mm and height of 15mm were tested with a universal testing machine (MTS Insight 5, Minnesota, USA), after sintering at 1250°C in air. The crosshead speed was 2mm/min (Fig. 3.8).

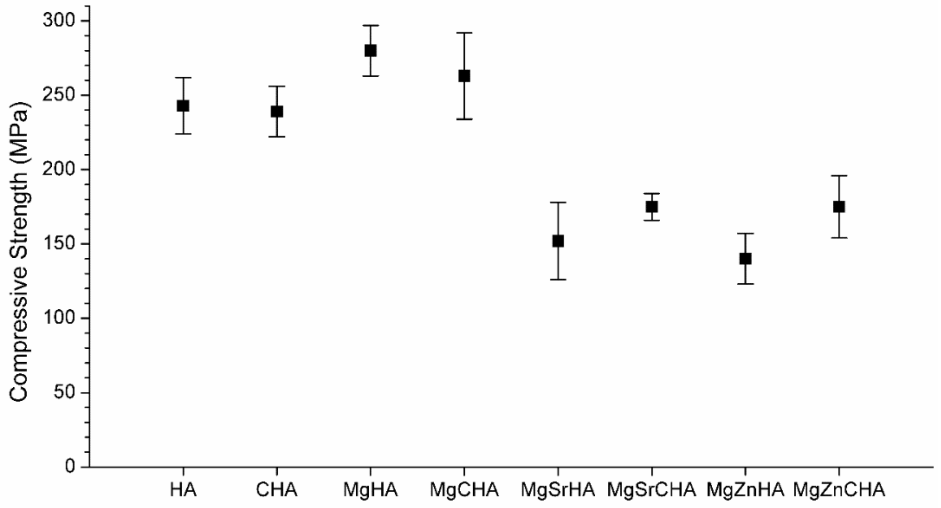

Fig. 3.8 - Compressive strength of HA dense bodies sintered at 1250°C in air

The multi-doped hydroxyapatites (MgSrHA, MgZnHA) result less resistant to compression in respect to the undoped HA and the single doped MgHA. HA co-doped with Mg^{2+}, Zn^{2+} and Sr^{2+} ions resulted in the lowest value of compression strength. The initial content of carbonate did not seem to affect the mechanical properties of the final dense bodies, indeed there are no differences in compressive strength of HAs with or without carbonate. That was predictable, because after sintering at 1250°C there is the complete loss of carbonate and no differences in phase composition between HAs carbonated or not were detected.

For 4-point bending test, 5 dense scaffolds, for each sample, in form of parallelepipeds, with 25.0*2.5*2.0mm dimension, were tested with a universal testing

machine (MTS Insight 5, Minnesota, USA), after sintering at 1250°C in air. The crosshead speed was 2mm/min (Fig. 3.9).

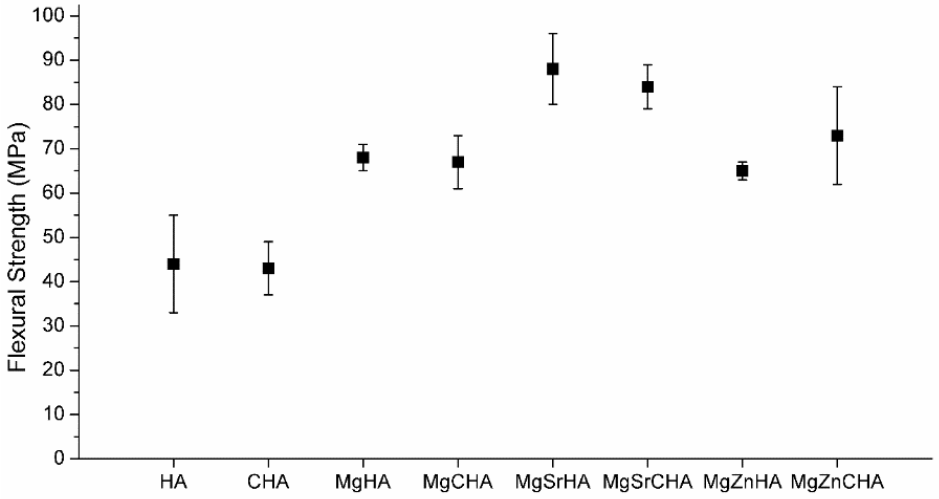

Fig. 3.9 - Flexural strength of HA dense bodies sintered at 1250°C in air

In that case, contrary to the compression test, the Mg^{2+}-doped hydroxyapatite and multi-doped hydroxyapatites result more resistant to flexural strength than the undoped, stoichiometric HA. The hydroxyapatite doped with Mg^{2+} and Sr^{2+} ions shows the highest bending strength in respect to the other doped hydroxyapatites, so the presence of strontium could be ascribed as a main cause for that difference. Also, in that case the initial content of carbonate (that is completely lost after sintering at 1250°C), did not influence the flexural strength, so it is possible to assume that after sintering at 1250°C there is no difference in mechanical properties between the not carbonated hydroxyapatites and their respective carbonated one.

Considering that the carbonation of the initial hydroxyapatite powders does not seem to give relevant differences in the mechanical properties of the sintered final scaffolds, so from now on the tests have been conducted on only one material between the carbonated and the not carbonated. So, the following tests have been conducted on simple HA, as control, and on MgHA, MgSrHA and MgZnCHA; the selection of these materials is made because they show the most similar phase compositions and better mechanical properties respect their counterpart (i.e, in respect to MgCHA, MgSRCHA, and MgZnHA, respectively).

For the nanoindentation test, sintered samples were mirror polished. In the nanoindentation experiments (using iNano, Nanomechanics, Inc., USA), Berkovich indenter was used to perform indentations up to a maximum load of 45mN. With that type of experiment, it is possible to obtain two different types of information on hardness (Fig. 3.10) and Young's modulus (Fig. 311).

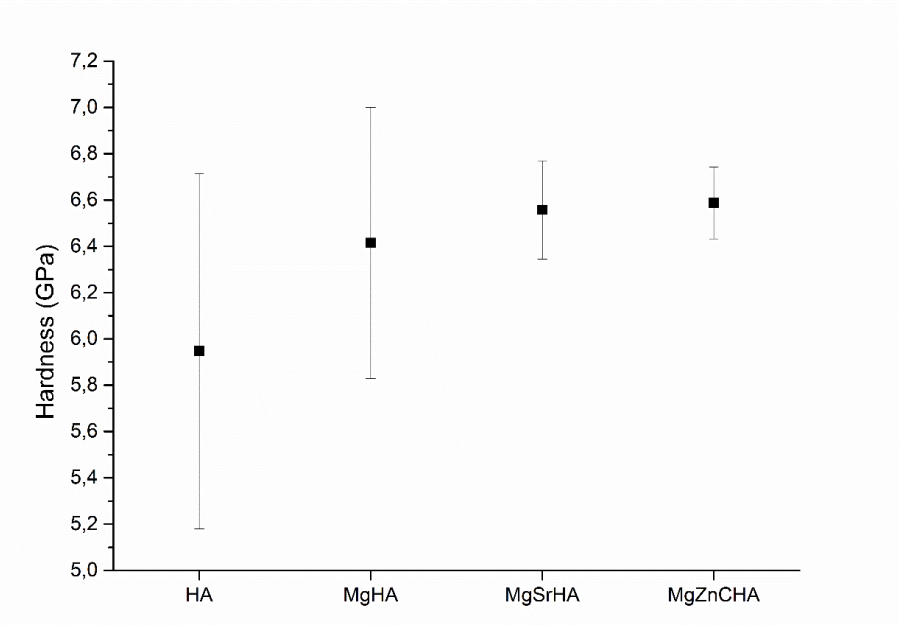

Fig. 3.10 – Hardness values of HA, MgHA, MgSrHA and MgZnCHA

There is no big difference in the hardness showed by HA, MgHA and multi-doped HAs. There is a light increase in the hardness value of doped hydroxyapatites but the differences are not statistically significant.

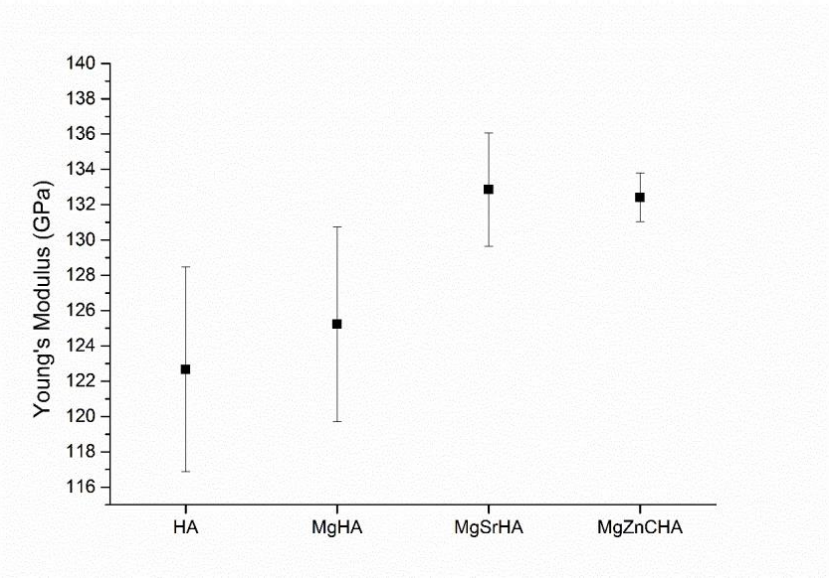

Fig. 3.11 – Young's modulus values of HA, MgHA, MgSrHA and MgZnCHA

Also, the Young's modulus presents a modest increase (about 8%) in the multi-doped HAs compared with HA and MgHA.

One of the most important parameters that influence the mechanical properties is the grain size; indeed, smaller grain size in ceramics is a feature pursued to reduce the size of critical defects and thus enhance the mechanical properties. Therefore, in order to evaluate the grain size of the four different hydroxyapatites, micrographs of the dense scaffolds sintered in air@1250°C were taken by SEM (Fig. 3.12). The grains were put in evidence by mirror-polishing and a subsequent acid attack with HCl 1M for 5s. The equipment used is Sigma NTS GmbH (Carl Zeiss, Oberkochen, Germany).

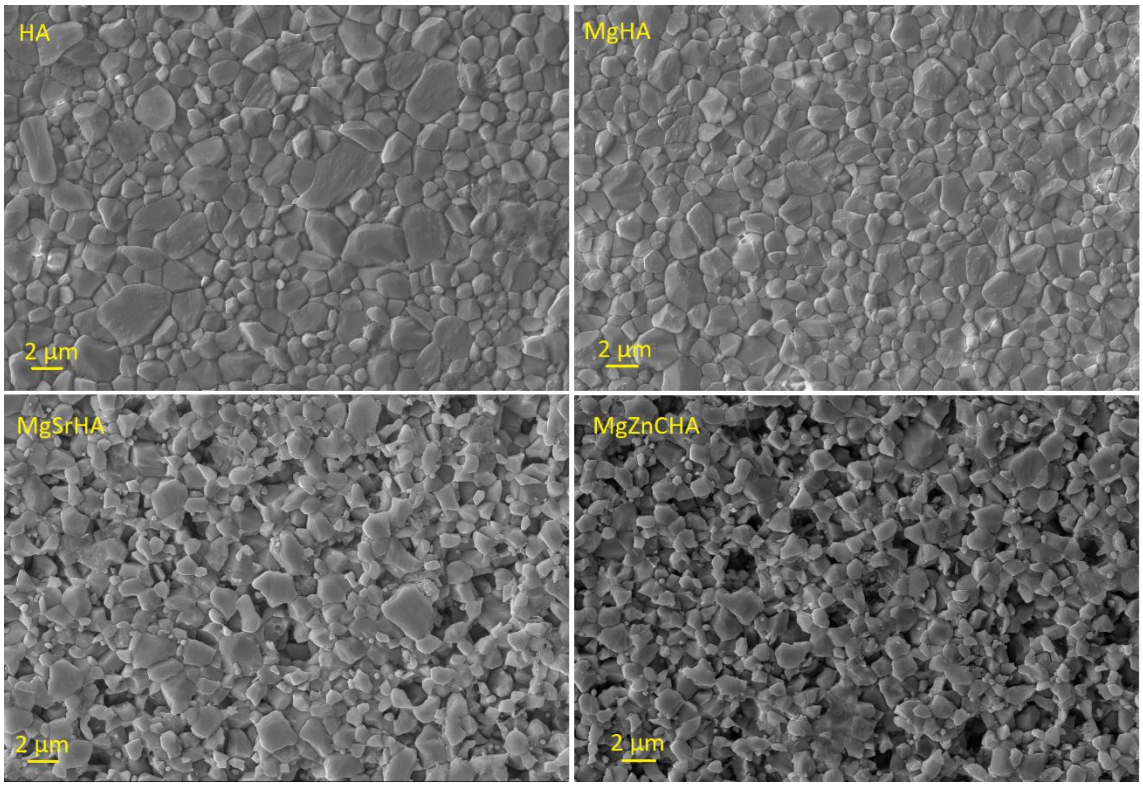

Fig 3.12 – SEM images of the four different hydroxyapatite dense bodies

The average grain sizes are listed in Table 3.7. The grain size of HA is larger than the grain size of the doped HA (about 30%), while there is no significant differences between the MgHA and the MgZnCHA. The MgSrHA results the material with the smallest grain size. These results are consistent with the values of Young's modulus and resistance to flexural strength, indeed we can hypothesize that the reduction of the grain size is a major source of the increased mechanical properties of these materials, in terms of Young's modulus, hardness and resistance to flexural strength, in respect to

the undoped HA. A main reason for this effect is likely the introduction of doping ions into the HA lattice who may have hampered the crystal development and growth during the sintering process, in respect to the undoped HA.

Samples	**Average Grain Size**
HA	1.33±0.08µm
MgHA	0.99±0.05µm
MgSrHA	0.88±0.04µm
MgZnCHA	0.95±0.06µm

Table 3.7 – Average grain sizes of HA dense scaffolds after sintering in air@1250°C

3.5 Conclusion

New multi-substituted nanocrystalline apatites were synthesized by direct introduction of carbonate, magnesium, strontium and zinc ions into the apatite crystal during its formation in aqueous medium. The effective entering of doping ions is confirmed by XRD and chemical analyses (see ICP-OES results at Table 3.3) and confirmed by the changes of the lattice parameters, reporting alteration of the crystal structure (see Table 3.2). These results confirm the ability of the apatite structure to easily accommodate the introduction of multiple foreign ions, therefore permitting the design of biomaterials with enhanced mimicry of natural bone tissue or endowed with specific biofunctionalities.

Thermogravimetric, FTIR and crystallographic analyses (see Table 3.2) confirm the ability of carbonate to enter in the structure of HA; as well, strontium take easily the place of Ca^{2+} inside the structure while Mg^{2+} and Zn^{2+} have more difficulty to enter in the HA structure, indeed the crystallographic analysis of the sintered HAs (see Table 3.4) suggests the absence of Mg^{2+} and Zn^{2+} ions inside the HA lattice, but their segregation in secondary phases like β-TCP and MgO, upon sintering.

It is not possible to prevent the complete loss of carbonate from HA structure (see Fig. 3.3 and 3.4) and at the same time obtain a scaffold with good properties. Indeed, only with a sintering under CO_2 flux below 900°C it was possible to prevent the loss of more than 60% of the initial content of carbonate. But the sintering at that

temperature resulted not effective because the ceramic obtained by this thermal route presents poor mechanical properties due to incomplete densification (see Fig. 3.7), so that such conditions are not useful to obtain ceramics suitable for practical clinical applications.

The mechanical tests carried out on dense ceramics sintered at 1250°C in air show some interesting results (see Figs. 3.8, 3.9, 3.10 and 3.11). The incorporation of Mg^{2+}, Sr^{2+} and Zn^{2+} seems to influence the mechanical properties of HAs scaffolds, indeed the multi-doped HAs scaffolds (MgSrHA and MgZnHA) show different behaviour from pure HA scaffold and from MgHA scaffolds. Multi-doped scaffolds present better mechanical properties in terms of resistance to flexure, Young's modulus and hardness. Such improved properties can be ascribed to the reduction of the grain size related to the ion doping. All the sintered samples show the formation of secondary phases, however this occurrence is common among most of the studied materials, so that this should not be a major factor for the increased mechanical properties. Therefore, it can be concluded that sintered ion doped hydroxyapatite ceramics are promising biomaterials for application as bone scaffolds intended to regenerate bone regions subjected to mechanical loads. To this, the investigation on the mechanical and biologic performance of macroporous ceramic scaffolds with such compositions is for sure a topic of interest.

References

1. Cazalbou, S.; Eichert, D.; Ranz, X.; Drouet, C.; Combes, C.; Harmand, M. F.; Rey, C., Ion exchanges in apatites for biomedical application. *J Mater Sci Mater Med* **2005,** *16* (5), 405-409.
2. Bigi, A.; Foresti, E.; Gregorini, R.; Ripamonti, A.; Roveri, N.; Shah, J. S., The role of magnesium on the structure of biological apatites. *Calcif Tissue Int* **1992,** *50* (5), 439-44.
3. LeGeros, R., Apatites in Biological Systems. *Progress in Crystal Growth and Characterization of Materials* **1981,** *4* (1-2), 1-45.
4. Tampieri, A.; Celotti, G.; Landi, E.; Sandri, M., Magnesium Doped Hydroxyapatite: Synthesis and Characterization. *Key Engineering Materials* **2004,** *264* (3), 2051-2054.
5. E., L.; A., T.; M., M.-B.; G., C.; M., S.; A., G.; P., F.; G., B., Biomimetic Mg- and Mg,CO3-substituted hydroxyapatites: synthesis characterization and in vitro behaviour. *J. Eur. Ceram. Soc.* **2006,** *26* (13), 2593-2601.
6. Landi, E.; Logroscino, G.; Proietti, L.; Tampieri, A.; Sandri, M.; Sprio, S., Biomimetic Mg-substituted hydroxyapatite: from synthesis to in vivo behaviour. *J Mater Sci Mater Med* **2008,** *19* (1), 239-47.
7. Li, Y. W.; Leong, J. C.; Lu, W. W.; Luk, K. D.; Cheung, K. M.; Chiu, K. Y.; Chow, S. P., A novel injectable bioactive bone cement for spinal surgery: a developmental and preclinical study. *J Biomed Mater Res* **2000,** *52* (1), 164-70.
8. Landi, E.; Tampieri, A.; Celotti, G.; Sprio, S.; Sandri, M.; Logroscino, G., Sr-substituted hydroxyapatites for osteoporotic bone replacement. *Acta Biomater* **2007,** *3* (6), 961-9.
9. Ni, G. X.; Lu, W. W.; Chiu, K. Y.; Li, Z. Y.; Fong, D. Y.; Luk, K. D., Strontium-containing hydroxyapatite (Sr-HA) bioactive cement for primary hip replacement: an in vivo study. *J Biomed Mater Res B Appl Biomater* **2006,** *77* (2), 409-15.
10. Ni, G. X.; Chiu, K. Y.; Lu, W. W.; Wang, Y.; Zhang, Y. G.; Hao, L. B.; Li, Z. Y.; Lam, W. M.; Lu, S. B.; Luk, K. D., Strontium-containing hydroxyapatite bioactive bone cement in revision hip arthroplasty. *Biomaterials* **2006,** *27* (24), 4348-55.
11. Montesi, M.; Panseri, S.; Dapporto, M.; Sprio, S., Sr-substituted bone cements direct mesenchymal stem cells, osteoblasts and osteoclasts fate. *PLoS ONE* **2017,** *12* (2).
12. C., C.; S., C.; C., R., Apatite Biominerals. *Minerals* **2016,** *6* (2), 34.
13. Thian, E. S.; Konishi, T.; Kawanobe, Y.; Lim, P. N.; Choong, C.; Ho, B.; Aizawa, M., Zinc-substituted hydroxyapatite: a biomaterial with enhanced bioactivity and antibacterial properties. *J Mater Sci Mater Med* **2013,** *24* (2), 437-45.
14. Yamaguchi, M., Role of Zinc in Bone Metabolism and Preventive Effect on Bone Disorder. *Biomedical Research on Trace Elements* **2007,** *18* (4), 346-366.
15. Plum, L. M.; Rink, L.; Haase, H., The essential toxin: impact of zinc on human health. *International journal of environmental research and public health* **2010,** *7* (4), 1342-1365.
16. Miyaji, F.; Kono, Y.; Suyama, Y.; Formation and structure of zinc-substituted calcium hydroxyapatite. *Mater. Res.Bull.* **2005,** *40* (2), 209-220.
17. Ren, F.; Xin, R.; Ge, X.; Leng, Y., Characterization and structural analysis of zinc-substituted hydroxyapatites. *Acta Biomater* **2009,** *5* (8), 3141-9.
18. Iafisco, M.; Ruffini, A.; Adamiano, A.; Sprio, S.; Tampieri, A., Biomimetic magnesium-carbonate-apatite nanocrystals endowed with strontium ions as anti-osteoporotic trigger. *Mater Sci Eng C Mater Biol Appl* **2014,** *35*, 212-9.
19. Landi, E.; Sprio, S.; Sandri, M.; Celotti, G.; Tampieri, A., Development of Sr and CO3 co-substituted hydroxyapatites for biomedical applications. *Acta Biomater* **2008,** *4* (3), 656-63.
20. Elliott, J. C., *Structure and Chemistry of the Apatites and Other Calcium Orthophosphates*. Elsevier: 1994; Vol. 18.
21. Sprio, S.; Tampieri, A.; Landi, E.; Sandri, M.; Martorana, S.; Celotti, G.; Logroscino, G., Physico-chemical properties and solubility behaviour of multi-substituted hydroxyapatite powders containing silicon. *Materials Science and Engineering: C* **2008,** *28* (1), 179-187.

22. Li, M.; Xiao, X.; Liu, R.; Chen, C.; Huang, L., Structural characterization of zinc-substituted hydroxyapatite prepared by hydrothermal method. *J Mater Sci Mater Med* **2008,** *19* (2), 797-803.
23. Hayakawa, S.; Ando, K.; Tsuru, K.; Osaka, A.; Fujii, E.; Kawabata, K.; Bonhomme, C.; Babonneau, F., Structural characterization and protein adsorption property of hydroxyapatite particles modified with zinc ions. *Journal of the American Ceramic Society* **2007,** *90* (2), 565-569.
24. Landi, E.; Celotti, G.; Logroscino, G.; Tampieri, A., Carbonated hydroxyapatite as bone substitute. *Journal of the European Ceramic Society* **2003,** *23* (15), 2931-2397.
25. Sprio, S.; Preti, L.; Montesi, M.; Panseri, S.; Adamiano, A.; Vandini, A.; Pugno, N. M.; Tampieri, A., Surface Phenomena Enhancing the Antibacterial and Osteogenic Ability of Nanocrystalline Hydroxyapatite, Activated by Multiple-Ion Doping. *ACS Biomater. Sci. Eng* **2019,** *5* (11), 5947-5959.
26. Ruys, A.; Weu, M.; Sorrell, C.; MR, D.; Brandwood, A.; Milthorpe, B., Sintering effects on the strength of hydroxyapatite. *Biomaterials* **1995,** *16* (5), 409-415.
27. Prokopiev, O.; Sevostianov, I., Dependence of the mechanical properties of sintered hydroxyapatite on the sintering temperature. *Materials Science and Engineering: A* **2006,** *431* (1-2), 218-227.
28. Muralithran, G.; Ramesh, S., The effects of sintering temperature on the properties of hydroxyapatite. *Ceramics International* **2000,** *26* (2), 221-230.
29. Martin, R.; Brown, P., Mechanical properties of hydroxyapatite formed at physiological temperature. *Journal of Materials Science: Materials in Medicine* **1995,** *6* (3), 138-143.

Chapter 4
Osteoinductive Character and Anti-infective Properties of the Novel Nanocrystalline Multi-doped Hydroxyapatites

Cell–material interaction has been proved to occur through a combination of biochemical and biophysical signals, including interfacial presentation of molecular, topographic and mechanical cues. Indeed, both biochemical and biophysical material features have been reported to affect and somehow influence cell functions by triggering specific molecular events at the cell–material interface. Cellular activities that are mostly influenced by material properties are adhesion, spreading, migration, proliferation and differentiation. Specifically engineered surfaces displaying selected biofunctional groups or micrometre-scale patterns have been used in order to study signal interactions in a systematic way. Cell-instructive materials are envisioned as nanofeatured materials expressly programmed to impart even complex commands or instructions to cells with the aim of directing, guiding and controlling their fate. The realization of these attractive materials relies upon a deep understanding of the mechanisms that regulate cell–material interactions and, in particular, upon the disclosing of the complex molecular machinery of recognition and decoding that occurs at the interface between the cell membrane and materials. Recent literature has described the phenomenon of crosstalk at the cell– material interface as being mostly influenced by the dynamics of large macromolecular complexes across the cell membrane whose formation and extension depend on material properties. According to this vision, properties such as mechanical, topographical and biochemical influence cell–material interaction by affecting in different ways the dynamics of these macromolecular complexes. Therefore, mechanical, topographical or biochemical signals may not represent separate or different cues, as suggested by some reports, but rather produce a different effect on the macromolecular complex dynamics.[1]

Implantation of medical devices is a frequent surgical practice which, however, is a gateway for pathogen contamination and infections that are often at the basis of the implant failure. Nowadays, this problem raises great concern, mostly due to the bacterial resistance to antibiotic drugs, which is increasing at an alarming rate. Owing to this, it is expected that in the coming decades, nosocomial infections will not be effectively treated by current drug-based protocols, thus leading to negative impact on the clinical outcome of a steadily growing number of patients, particularly those subjected to orthopedic prosthetic surgery, in terms of longer hospital stays, higher medical costs, and increased mortality.[2, 3] In this scenario, the development of drug-free solutions as an alternative to systemic and intensive administration of antibiotics and associated with therapeutically effective biomaterials is increasingly demanded. Most of these solutions are based on the functionalization of biomaterials with elements having antibacterial properties, prominently silver or heavy metal nanoparticles.[4] However, if overdosed, these materials can result into cytotoxic and genotoxic effects on healthy cells, and the correct dosage and distribution of antibacterial nanoparticles are quite difficult to define and apply.[5-7] A recent study highlighted the potential of calcium phosphates as potential antibacterial agents, both against various Gram-positive and Gram-negative strains, including their multidrug-resistant analogues.[8] Previous studies reported the development of HA doped with ions such as silver, copper, gallium, or zinc to improve antibacterial properties and, particularly, in the case of zinc, to provide additional therapeutic effects.[9-12]

The present work describes a nanocrystalline HA, prepared doping with Zn^{2+}, Mg^{2+} and Sr^{2+} ions, to promote osteo-differentiation and to give additional protection against microbial proliferation. The effect of the doping ions on the physicochemical properties and, in turn, on the HA bioactivity is evaluated in terms of proliferation. In a parallel experiment, in vitro cultures of two pathogens, that is, Gram-positive bacteria Staphylococcus aureus and Gram-negative bacteria Escherichia coli, which are among the most common agents involved in nosocomial infections,[13-16] are carried out to assess the antimicrobial ability of the new materials.

4.1 Materials and Methods

Materials

The materials tested were 4 different HAs dense bodies sintered at 1250°C: undoped HA (as control material), MgHA, MgSrHA and MgZnCHA. The synthesis of powders, the consolidation method and the characterization of that materials are reported in chapter 3.

The samples for in biologicals tests were sterilized by γ-ray irradiation and preconditioned for 72 hours in standard cell culture medium.

Characterizations of the Materials

Energy Dispersive X-Ray Spectrometry (Oxford Scientific, OXFORD INCA Energy 350 X-Max 50, Oxford, United Kingdom) associated with Scanning Electron Microscopy (SEM) (Zeiss, EVO MA10-HR "dual gun", Oberkochen, Germany) at 20 kV, investigated the percentage of the elements present on the surface of undoped and doped hydroxyapatite (HA). Moreover, it was important to map the position of the elements present on the surface.

Ion Release Test

The evaluation of the ion release with time was made by immersing tablets (1 g of powder each) into 5 ml of pH=7.4 buffer solution (Ca and Mg free Hank's Balanced Salt solution) and maintained at 37°C under gentle shaking. At scheduled times (i.e. after 1, 2, 3, 7, 11 and 15 days) the solution was removed and 5ml of fresh solution was added to the tablets. The liquids containing the ions released after the prefixed times were analyzed by ICP-OES for the quantitative determination of Ca, Mg, Zn and Ga. The results were presented as cumulative data. All the experiments were made in triplicate.

4.1.1Biological Tests

Cell culture

Mouse pre-osteoblast cell line MC3T3-E1 Subclone 14 (OBs), obtained from ATCC cell bank (Manassas, VA, USA), was used as a model of osteoblasts[17]. 3×104/plate of OBs were cultured in αMEM containing ribonucleosides, deoxyribonucleosides (GIBCO), and

Lglutamine, 10% FBS and 1% Penicillin-Streptomycin and osteogenic factors (10 mM β-glycerophaspate, 50 µg/ml ascorbic acid).

Cell viability and proliferation

The viability and proliferation were measured by evaluating metabolically active cells at 1 and 3 days. The MTT reagent (3-(4,5-dimethylthiazol-2-yl)-2,5 -diphenyltetrazolium bromide) is reduced to formazan dye in metabolically active cells. The formazan production can be observed at λmax of 570 nm, using a Multiskan FC Microplate Photometer (Thermo Scientific), and the absorbance is directly proportional to the number of metabolically active cells. The reagent was prepared at 5 mg/mL in 1x PBS. Cell were incubated with the MTT reagent 1:10 for 2 h at 37°C. Medium was collected and cells incubated with dimethyl sulfoxide for 15 min. In this assay, the mean values of absorbance were determined.

For qualitative evaluation of cell viability after 3 days Live/Dead assay kit (Invitrogen) was used according to the manufacturer's instructions. Briefly, the samples were washed with 1× PBS for 5 min and incubated with calceinacetoxymethyl (Calcein AM) (2 µM) plus ethidium homodimer-1 (EthD-1) (4 µM) for 15 min at 37 °C in the dark. Images were acquired using an inverted Ti-E fluorescence microscope (Nikon).

4.1.2 Antimicrobial Tests

The antimicrobial tests of ions-doped HA scaffold were performed in Prof. Visai's laboratory (Department of Molecular Medicine, University of Pavia, Italy).

Bacterial strains and culture conditions

The microorganisms used were Escherichia coli ATCC 25922 and Staphylococcus aureus ATCC 25923, kindly obtained from the laboratory of Prof. R. Migliavacca (Department of Clinical-Surgical Diagnostic and Pediatric Sciences, Unit of Microbiology and Clinical Microbiology, University of Pavia, Italy). Bacteria were grown in 10 ml of appropriate medium, overnight, under aerobic conditions at 37°C using a shaker incubator (VDRL Stirrer 711/CT, Asal Srl, Italy). E. coli was inoculated in Luria Bertani

broth (LB) (ForMediumTM, UK) whereas S. aureus in BHI (Brain Heart Infusion broth) (Scharlab S.L., Spain).

Bacterial growth

Serial dilutions of bacterial strains were performed in LB medium for both strains to reach 1x105/200 µl concentration. 200 µl of diluted bacterial suspension were inoculated onto ions-doped HA scaffolds (MgHA, MgSrHA and MgZnCHA) and on the undoped HA used as the control, contained into 48-well flat-bottomed sterile polystyrene microplates (Euroclone S.p.a, Italy), incubated overnight at 37°C. The experiment was carried out in triplicate.

Bacterial viability

It was investigated by MTT 3-(4,5-dimethylthiazol-2-yl)-2,5-diphenyltetrazolium bromide) colorimetric assay (Sigma-Aldrich®, USA) on the HA scaffolds (1) and on the supernatant (2) previously removed.

(1) HA scaffolds were washed in sterile Phosphate Buffer Saline (PBS 1X), and bacterial adhesion was carried out by adding 20 µl of MTT to 180 µl of PBS 1X into a 48-wells plate, incubated for 3h at 37°C. Later, 100 µl have been transferred into a 96-wells plate.

(2) 10 µl of MTT (5 mg/ml in PBS 1X) were added to 90 µl of bacterial suspension, previously transferred into a 96-wells plate, incubated for 3h at 37°C.

At the end, after 3 hours of incubation at 37°C the MTT reaction has been stopped by adding 100 µl of solution C (2-propanol, HCl 0.04 N), incubated for 15 minutes at 37°C.

The plates were read at CLARIOstar (BMG Labtech, Germany) at 570 nm and as a reference wavelength 630 nm. Finally, data were analyzed thanks to GraphPad Prism 5 software.

Statistical analysis

To evaluate the differences between the means of the results for the control and the ions-doped hydroxyapatite, an unpaired, two-sided Student t test has been

performed (thanks to GraphPad Prism 5 software). P values of less than 0.05 were considered significant.

4.2 Characterizations of the materials

Analysis about the composition of the HA scaffolds was carried out using an Inca Oxford Instrument (EDS) with a beam of electrons accelerated by a 20 kV voltage. SEM images of the materials allowed the observation of their morphology. Furthermore, EDS provided maps of the elements distribution on the hydroxyapatite surface of the different samples (Fig. 4.1).

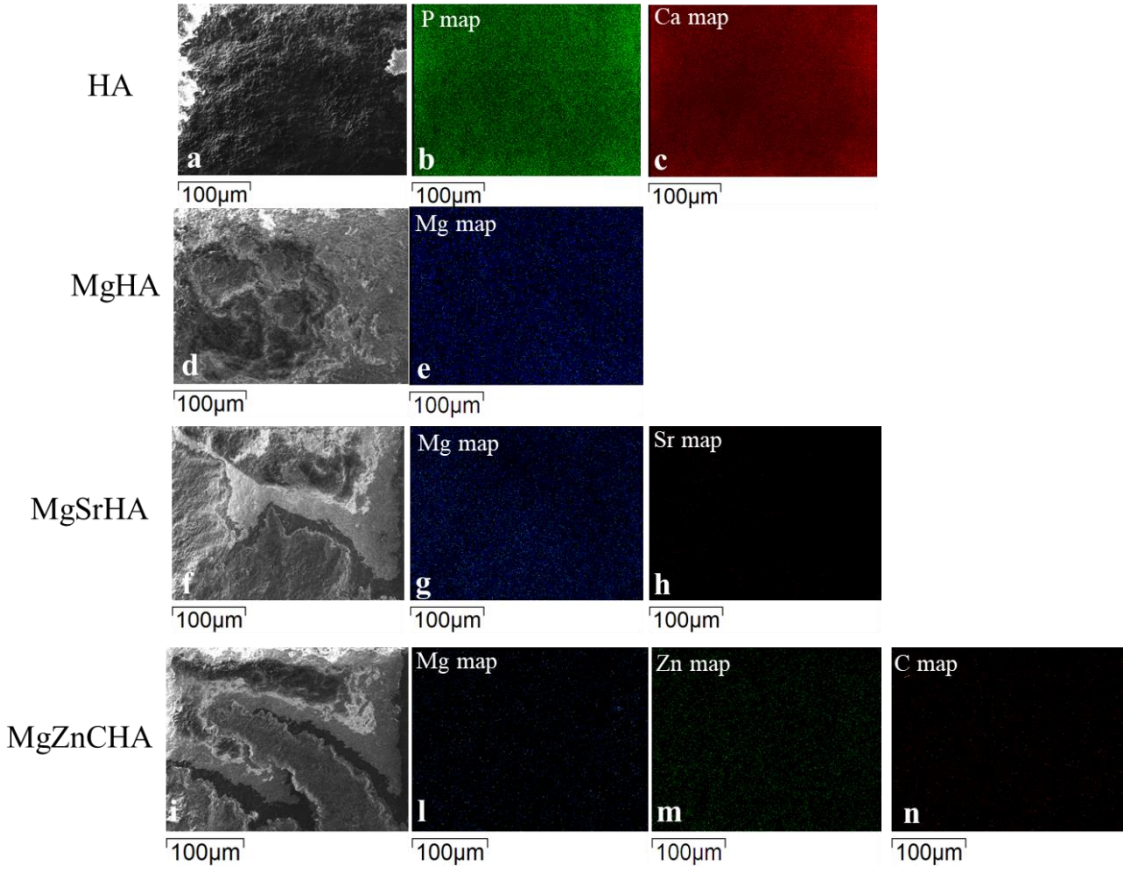

Fig 4.1 - SEM images obtained through EDS analysis. 20kV, 1000X magnification.

It is important to remark that this technique can measure only the superficial distribution of the elements. Indeed, it provides quantitative data regarding the composition of the material and in particular the percentage of weight of each detectable element on the surface. Moreover, the results showed that the highest Mg

content (on the surface) is in MgSrHA. However, the Sr has not been detected. Instead, the zinc has been detected in MgZnCHA in concentration~ 0.2 wt% (Fig. 4.2).

(a) HA

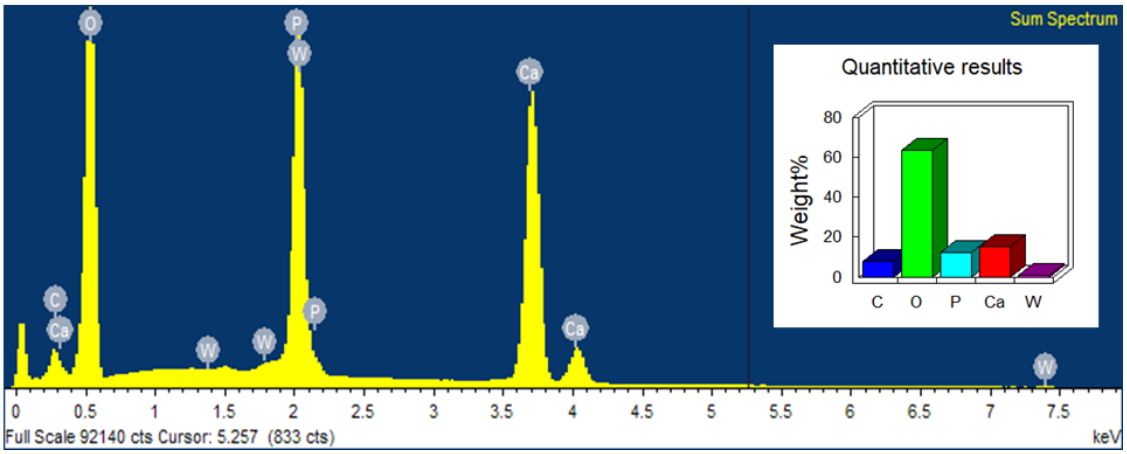

(b) MgHA

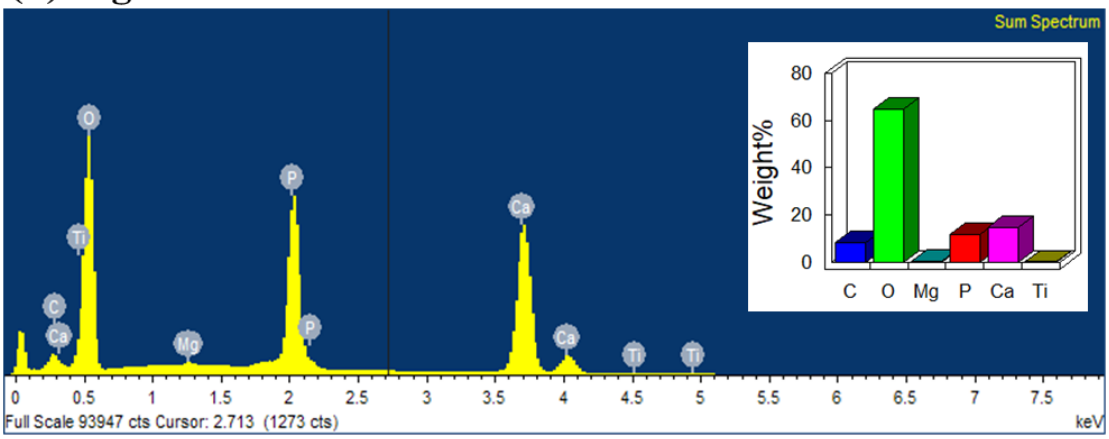

(c) MgSrHA

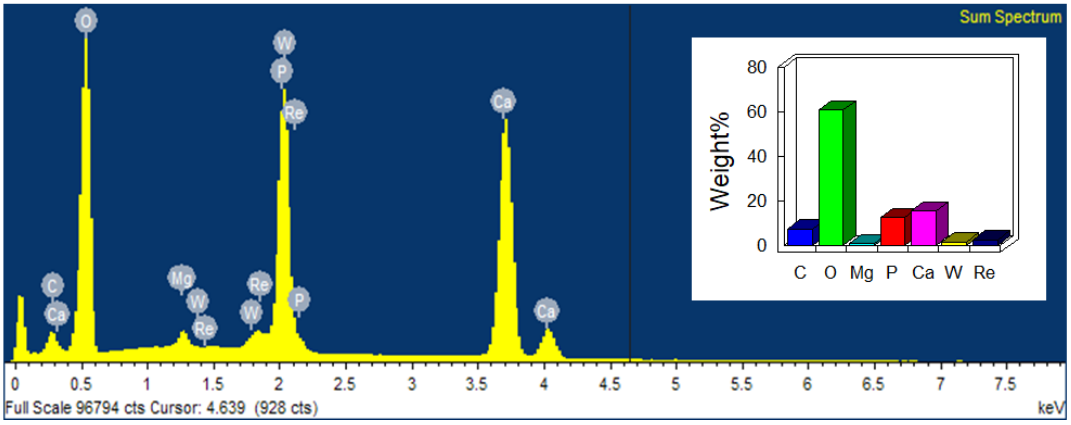

(d) MgZnCHA

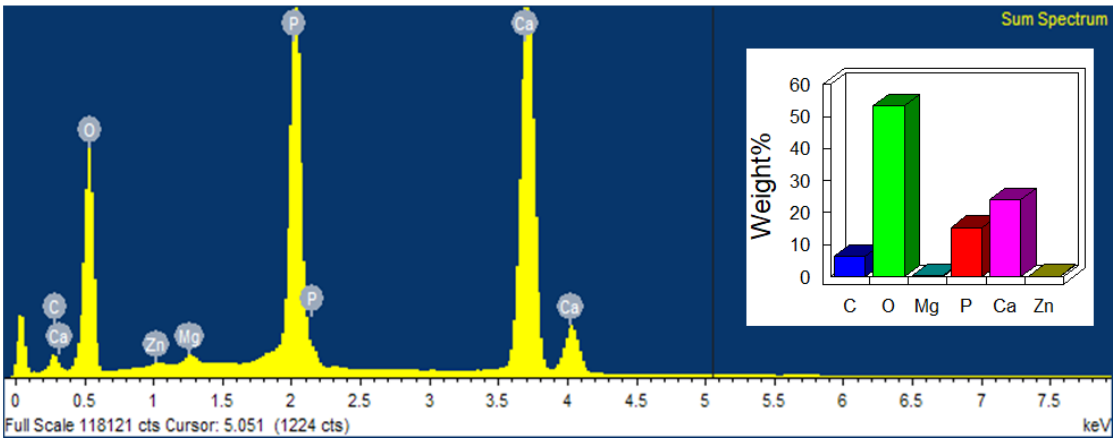

Fig. 4.2- Spectrum obtained through EDS- representing the composing elements of the materials. (a) HA; (b) MgHA; (c) MgSrHA; (d) MgZnCHA.

4.3 Ion release test

The release of ions from the undoped HA, MgHA, MgSrHA and MgZnCHA was investigated to obtain the bio-solubility profile in physiological environment (Hanks' Balanced Salt solution). Figures 4.3-4.4 shows the release profile of Ca^{2+}, Mg^{2+} and Zn^{2+} ions in Hanks' solution, expressed in absolute values (Figure 4.3) and as a percentage of the initial ion content in the material (Figure 4.4). No detectable release of Sr^{2+} ions was observed along the whole experiment; conversely, Mg^{2+} ions were released in relatively large extent over time, also Zn^{2+} were released but in minor extent than Mg^{2+} and Ca^{2+}. The release of Ca^{2+}, Mg^{2+} and Zn^{2} ions can be described by two distinct mechanisms. In fact, a burst ion release was detected during the first 3 days, followed by a slower release kinetic, suggesting that within this stage the release process involves ions characterized by relatively weaker chemical bonds. It is possible to hypothesize that such ions are likely located in surface regions characterized by reduced binding energy in respect to the bulk. In the subsequent stage (i.e. days 3-14) the release of both Ca^{2+}, Mg^{2+} and Zn^{2+} ions slackened, therefore it can be ascribed to the dissolution of inner, more crystalline and stable regions. Taking into account that no Sr^{2+} ions release was detected but it's presence it's certain thanks to ICP analysis made on dense bodies after sintering (Tab 3.6), we can hypothesize that Sr^{2+} ions are entirely located in energetically stable substitutional positions in the HA lattice.

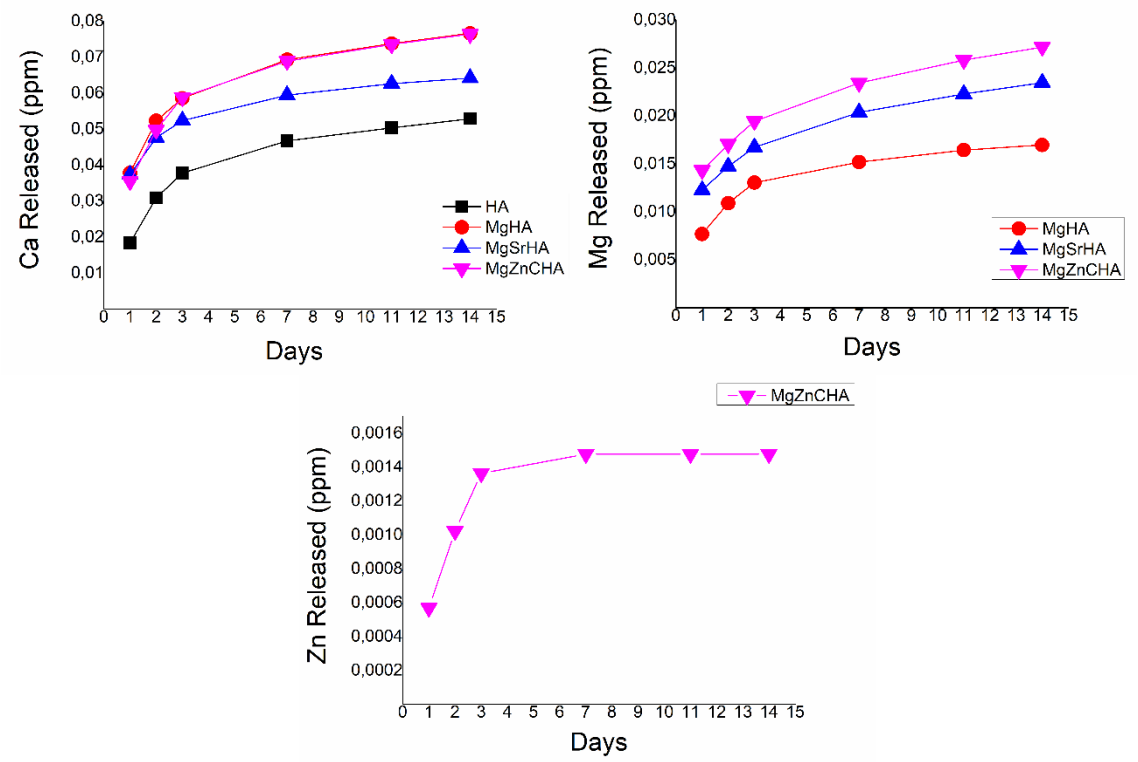

Fig 4.3 - Ion release in physiological fluid: absolute values of released ions. Note that no Sr release could be observed in any materials.

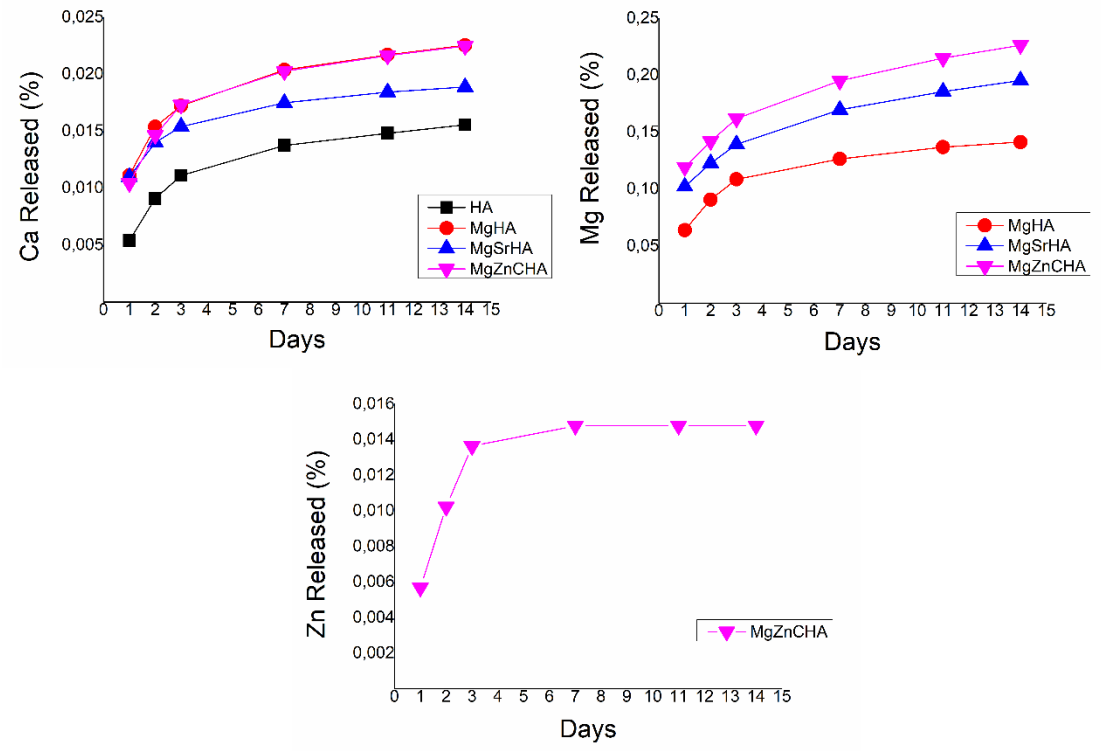

Fig. 4.4 - Ion release in physiological fluid: percentage values of released ions in respect to those present in the the startingas-obtained material. Note that no Sr release could be observed in any materials.

4.4 Biological Tests

The cell cultures have been analyzed for cell viability with the Live/Dead assay based on the simultaneous determination of live and dead cells with two probes, Calcein and EthD-1, that measure recognized parameters of cell viability: i.e. intracellular esterase activity and plasma membrane integrity, respectively. A very high ratio of viable cells is observed, with no significant differences among the groups (Fig. 4.5). Moreover, a quantification of metabolically active cells has been performed for each time point. MTT test results demonstrated an increase in cell proliferation from day 1 to day 3 for all the samples highlighting the absence of cytotoxicity (Fig. 4.6).

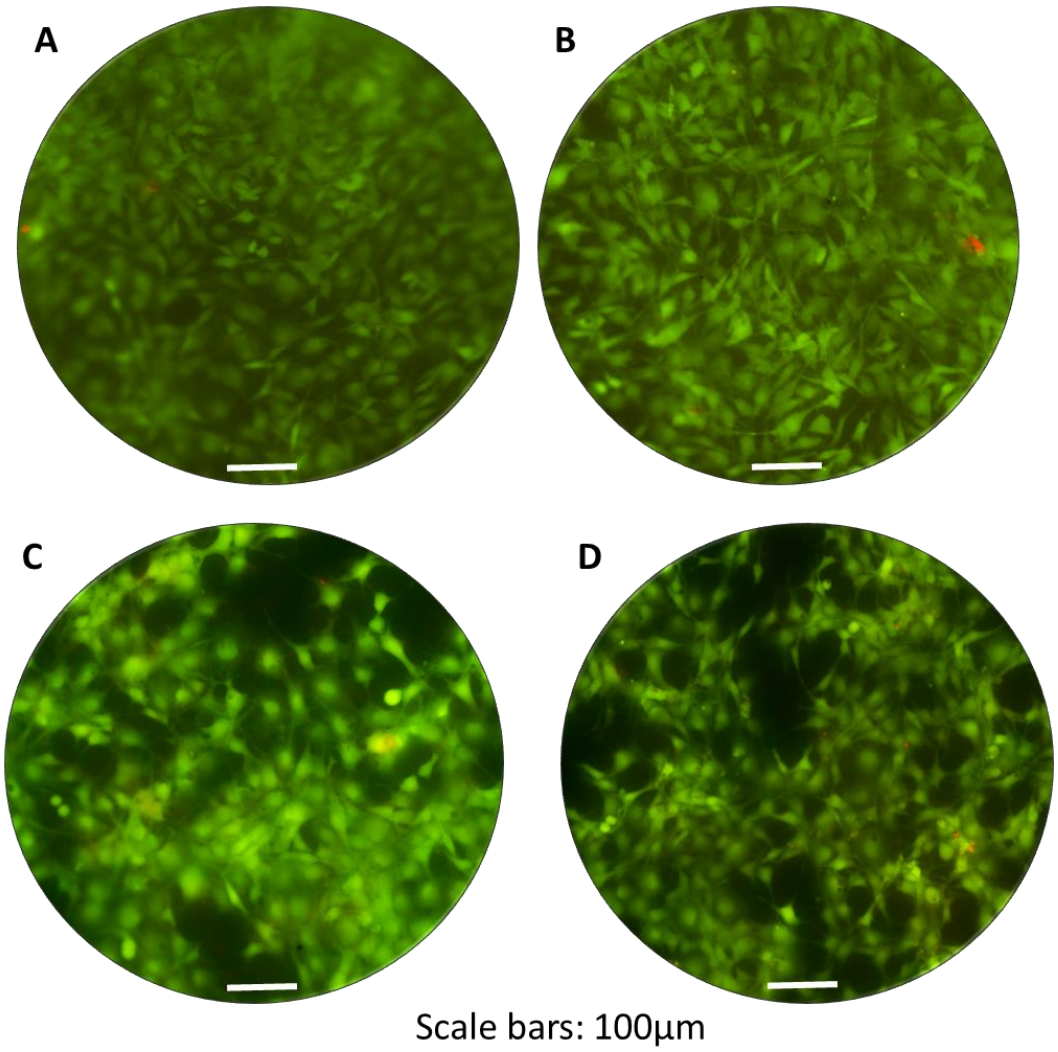

Fig. 4.5 – Live/Dead assay of the 4 different materials: A) HA; B) MgHA; C) MgZnCHA; D) MgSrHA

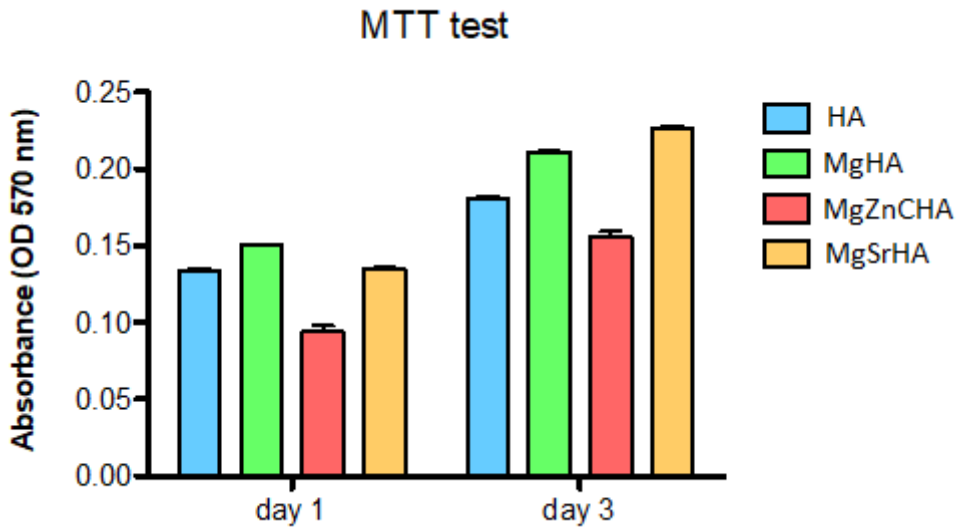

Fig. 4.6 – MTT test results

4.5 Antibacterial tests

The antimicrobial tests of ions-doped HA scaffold were performed at the Department of Molecular Medicine, University of Pavia, Italy, by the research group of Prof. L. Visai, through the MTT 3-(4,5-dimethylthiazol-2-yl)-2,5-diphenyltetrazolium bromide) colorimetric assay.

The bacterial viability was investigated on (1) the ions-doped HA scaffolds to evaluate the adhesion ability of E. coli and S. aureus and on (2) the supernatant (previously removed) to evaluate the inhibitory effect of these materials.

Fig. 4.7 shows the percentage of viability of both strains, considering as positive control the TC (tissue culture) set as 100 % (Panel A) and HA (hydroxyapatite) as positive control (Panel B).

Student t test has been performed to evaluate the statistical differences between the controls and the samples. However, all the values for adhesion were less than 0.05, thus statistically significant (data not shown).

The adhesion of both strains, considering TCP 100%, is the lowest on MgSrHA scaffold, in particular showing the best performance with S. aureus (Figure 4.7b) in comparison to E. coli (Figure 4.7a). Figure 3, panel B, shows the results reported setting HA as 100%. In both strains, again the MgSrHA scaffold retains its inhibitory activity compared to the other HA ion-doped scaffolds (MgHA, MgZnCHA) showing a better effect for S. aureus (Figure 4.7d) than for E. coli (Figure 4.7c).

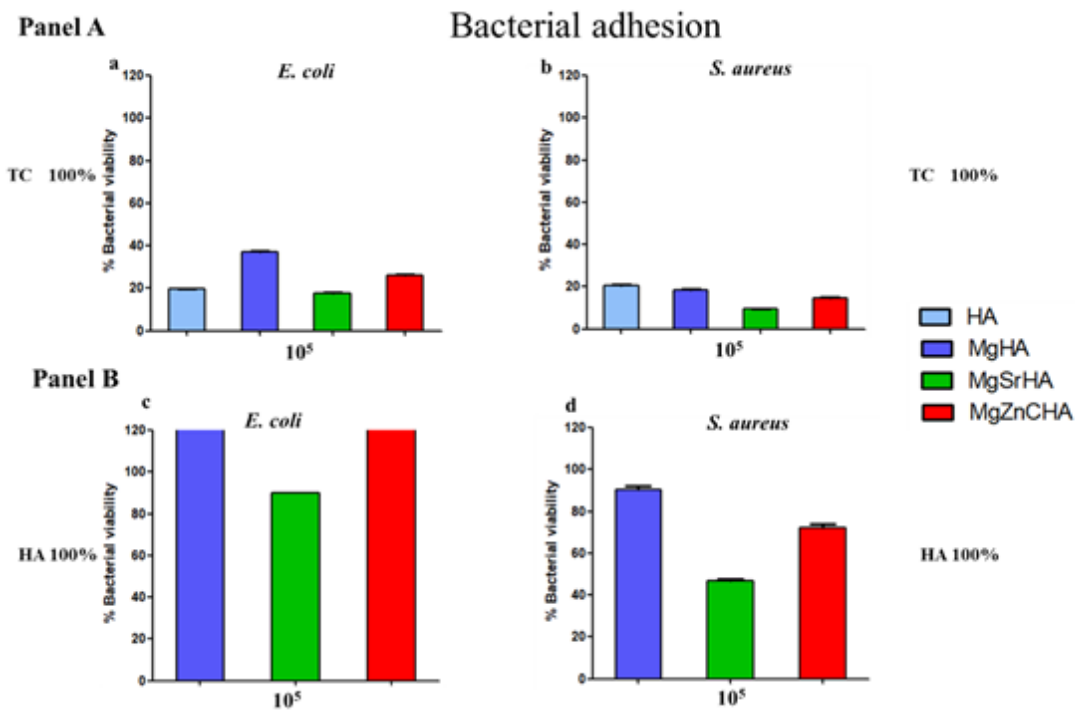

Fig. 4.7- Bacterial adhesion onto HA and HA ion-doped scaffolds. Percentage of both bacterial strains viability related to TCP (tissue culture plates) set as 100% (Panel A) and HA (hydroxyapatite) set as 100% (Panel B). P < 0.05 related to TCP 100% (Panel A) and to HA 100% (Panel B). a, c- Escherichia coli ATCC 25922 at 105/sample concentration. b, d- S. aureus ATCC 25923 at 105/sample concentration.

Figure 4.8 reports data of the viability of the supernatant, considering the bacteria grown on TCP as 100% (Panel A) and on HA (Panel B). The statistical analysis performed demonstrated how the differences between controls and samples were statistically significant ($P < 0.05$) with the exception of the proliferation of E. coli on HA (considering TCP 100%)). In the latter case, P value was > 0.05.

Figure 4.8 Panel A shows a comparison between E. coli (a) and S. aureus % viability (b) related to TCP set 100% as positive control. Hence, the most effective material on E. coli is MgZnCHA instead of MgSrHA, which showed a better inhibition on E. coli adhesion Figure 3A (a). Similar trend is observed in Figure 4 Panel B.

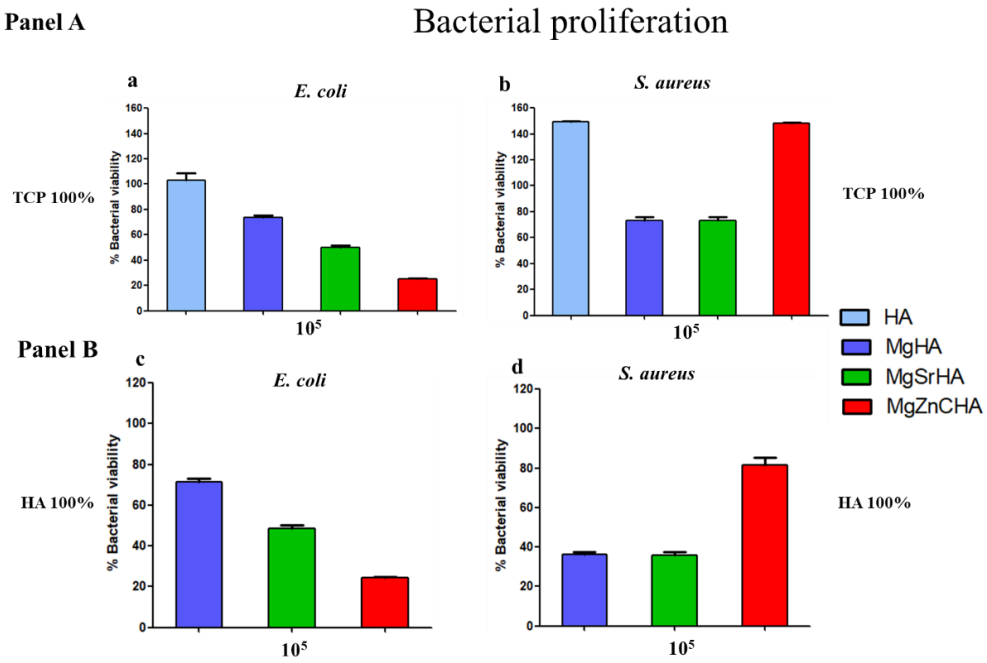

Fig. 4.8- Bacterial viability after direct contact with HA and ion-doped HA scaffolds. Percentage of both bacterial strains viability related to TCP (tissue culture plates) set as 100% (Panel A) and HA (hydroxyapatite) set as 100% (Panel B). P < 0.05 in both panels except for E. coli on HA (Panel A, a). a, c- Escherichia coli ATCC 25922 at 105/sample concentration. b, d- S. aureus ATCC 25923 at 105/sample concentration.

The inhibition data are also reported in the following tables (Table 4.1).

Bacterial inhibition

A — TPC 100% adhesion

% inhibition of bacterial adhesion		
Materials	*E. coli* $10^{\wedge 5}$	*S. aureus* $10^{\wedge 5}$
HA	80%	79%
MgHA	63%	81%
MgSrHA	82%	90%
MgZnCHA	73%	85%

B — HA 100% adhesion

% inhibition of bacterial adhesion		
Materials	*E. coli* $10^{\wedge 5}$	*S. aureus* $10^{\wedge 5}$
MgHA	-	9%
MgSrHA	11%	53%
MgZnCHA	-	27%

C — TPC 100% proliferation

% inhibition of bacterial proliferation		
Materials	*E. coli* $10^{\wedge 5}$	*S. aureus* $10^{\wedge 5}$
HA	-	-
MgHA	26%	26%
MgSrHA	49%	27%
MgZnCHA	75%	-

D — HA 100% proliferation

% inhibition of bacterial proliferation		
Materials	*E. coli* $10^{\wedge 5}$	*S. aureus* $10^{\wedge 5}$
MgHA	28%	65%
MgSrHA	51%	65%
MgZnCHA	75%	21%

Table 4.1 - Tables representing the percentage of inhibition for bacterial adhesion (A) and (B) and bacterial proliferation (C) and (D).

A, C- % inhibition of adhesion and proliferation respectively, considering as positive control TCP 100%

B, D- % inhibition of adhesion and proliferation respectively, considering as positive control HA 100%

These data, considering the TCP and HA as positive controls, show that the ions-doped HA scaffolds are more effective against S. aureus ATCC 25923 than to E. coli ATCC 25922.

In particular, bacterial adhesion resulted more reduced on MgSrHA scaffolds (TC 100% adhesion) ~ 90% in S. aureus whereas ~ 80% in E. coli (Table A). Considering Table B (HA 100%), the best result is still for MgSrHA scaffolds and S. aureus. It is interesting to note the difference of behavior in adhesion and proliferation (TCP as 100%) (Tables A and C). Our data suggest that the best materials with inhibitory activity against both bacterial adhesions were MgSrHA and MgZnCHA (TC 100%) (Table A). The only material, which retains its effect against E. coli growth in both adhesion (TC as 100%) (Table A) and proliferation (Tables C and D) is MgZnCHA. Our data provided a reduction of proliferation of 75% with the respect to the undoped HA control for E. coli ATCC 25922 and a reduction of 21% for S. aureus ATCC 25923 (Table D).

4.6 Conclusions

β-TCP formation, induced by the presence of substituent ions such as Mg and Zn, generates a positive effect on biological properties, both with cells and with infectious strains.

Multi-doping stimulates the release of magnesium and generally improves biological properties.

The presence of strontium, although not released in the surrounding environment and apparently not exposed on the surface, seems to have a positive effect on cell proliferation and antibacterial ability. What is seen is that this sample contains the greatest amount of β-TCP, although not as preponderant compared to other materials. We can therefore hypothesize some effect related, not only to the release of ions but to the composition of the surface so that the presence of β-TCP can be a decisive factor. Keep in mind that the state of the β-TCP phase is linked to the presence of substituent ions which is not easy to evaluate in these complex systems where phases with very similar atomic composition coexist. Therefore, the evaluation of any differences between the various materials could be related to a slight difference in the

composition of the β-TCP that can be evaluated only through sophisticated spectroscopic techniques.

It seems that the coexistence of HA and TCP, induced by HA doping ions, is a factor that promotes antibacterial properties.

References

1. Ventre, M.; Causa, F.; Netti, P. A., Determinants of cell–material crosstalk at the interface: towards engineering of cell instructive materials. *J. R. Soc. Interface* **2012,** *9* (74), 2017-2032.
2. Li, B.; Webster, T. J., Bacteria antibiotic resistance: New challenges and opportunities for implant-associated orthopedic infections. *J Orthop Res* **2018,** *36* (1), 22-32.
3. Hofer, U., The cost of antimicrobial resistance. *Nat Rev Microbiol* **2019,** *17* (1), 3.
4. Slavin, Y. N.; Asnis, J.; Häfeli, U. O.; Bach, H., Metal nanoparticles: understanding the mechanisms behind antibacterial activity. *Journal of Nanobiotechnology* **2017,** *15* (1), 1-20.
5. Gliga, A. R.; Skoglund, S.; Wallinder, I. O.; Fadeel, B.; Karlsson, H. L., Size-dependent cytotoxicity of silver nanoparticles in human lung cells: the role of cellular uptake, agglomeration and Ag release. *Part Fibre Toxicol* **2014,** *11*, 11.
6. Albers, C. E.; Hofstetter, W.; Siebenrock, K. A.; Landmann, R.; Klenke, F. M., In vitro cytotoxicity of silver nanoparticles on osteoblasts and osteoclasts at antibacterial concentrations. *Nanotoxicology* **2013,** *7* (1), 30-6.
7. Vimbela, G. V.; Ngo, S. M.; Fraze, C.; Yang, L.; Stout, D. A., Antibacterial properties and toxicity from metallic nanomaterials. *Int J Nanomedicine* **2017,** *12*, 3941-3965.
8. Wu, V. M.; Tang, S.; Uskokovic, V., Calcium Phosphate Nanoparticles as Intrinsic Inorganic Antimicrobials: The Antibacterial Effect. *ACS Appl Mater Interfaces* **2018,** *10* (40), 34013-34028.
9. Thian, E. S.; Konishi, T.; Kawanobe, Y.; Lim, P. N.; Choong, C.; Ho, B.; Aizawa, M., Zinc-substituted hydroxyapatite: a biomaterial with enhanced bioactivity and antibacterial properties. *J Mater Sci Mater Med* **2013,** *24* (2), 437-45.
10. V., S.; S., D.; J., A.-S.; M., M.; B., J.; B., P. I.; S., R., Synthesis, characterization and antimicrobial activity of copper and zinc-doped hydroxyapatite nanopowders. **2010,** *256* (20), 6083-6089.
11. Ballardini, A.; Montesi, M.; Panseri, S.; Vandini, A.; Balboni, P. G.; Tampieri, A.; Sprio, S., New hydroxyapatite nanophases with enhanced osteogenic and anti-bacterial activity. *J Biomed Mater Res A* **2018,** *106* (2), 521-530.
12. Tapiero, H.; Tew, K. D., Trace elements in human physiology and pathology: zinc and metallothioneins. *Biomed Pharmacother* **2003,** *57* (9), 399-411.
13. Pammi, M.; Liang, R.; Hicks, J.; Mistretta, T. A.; Versalovic, J., Biofilm extracellular DNA enhances mixed species biofilms of Staphylococcus epidermidis and Candida albicans. *BMC Microbiol* **2013,** *13*, 257.
14. Campoccia, D.; Montanaro, L.; Arciola, C. R., The significance of infection related to orthopedic devices and issues of antibiotic resistance. *Biomaterials* **2006,** *27* (11), 2331-9.
15. Wall, D., Kin Recognition in Bacteria. *Annu Rev Microbiol* **2016,** *70*, 143-60.
16. Zajonz, D.; Zieme, A.; Prietzel, T.; Moche, M.; Tiepoldt, S.; Roth, A.; Josten, C.; von Salis-Soglio, G. F.; Heyde, C.-E.; Ghanem, M., Periprosthetic joint infections in modular endoprostheses of the lower extremities: a retrospective observational study in 101 patients. *Patient safety in surgery* **2016,** *10*, 6-6.
17. Wang, D.; Christensen, K.; Chawla, K.; Xiao, G.; Krebsbach, P. H.; Franceschi, R. T., Isolation and characterization of MC3T3-E1 preosteoblast subclones with distinct in vitro and in vivo differentiation/mineralization potential. *J Bone Miner Res* **1999,** *14* (6), 893-903.
18. Sprio, S.; Preti, L.; Montesi, M.; Panseri, S.; Adamiano, A.; Vandini, A.; Pugno, N. M.; Tampieri, A., Surface Phenomena Enhancing the Antibacterial and Osteogenic Ability of Nanocrystalline Hydroxyapatite, Activated by Multiple-Ion Doping. *ACS Biomater. Sci. Eng* **2019,** *5* (11), 5947-5959.

Chapter 5
Development of Macroporous Multi-doped Hydroxyapatite Scaffolds

The development of porous ceramics is a pivotal target for many relevant industrial applications. Particularly in the field of bone surgery, the preparation of macroporous bone substitutes for load-bearing bone parts represents one of the most challenging application, especially due to the difficulty of expressing high bioactivity and bone-like mechanical properties simultaneously. Despite a variety of techniques has been investigated so far, the repeatable and reliable production of macroporous HA scaffolds with bone-mimicking morphology and mechanical strength is still a major challenge.

It is well accepted that bone scaffolds with effective regenerative ability should exhibit a network of interconnected pores permitting extensive bone ingrowth and neovascularization.[1, 2] The optimal pore range and interconnectivity required to achieve osteointegration have been widely studied.[1, 3-5] In this respect, it was observed that a macro-pore range (100–700 µm) should be associated with interconnected micro-pores (0.1–1 µm).[1] The development of bone scaffolds with high porosity associated to bone—like mechanical strength is a key achievement to enable the treatment of clinical problems not solved yet, e.g. the regeneration of critical size load-bearing bone regions such as maxillofacial regions.[6]

In this chapter a forming process based on direct foaming of ceramic suspensions was optimized to produce highly porous calcium phosphate scaffolds starting from magnesium-strontium doped hydroxyapatite (MgSrCHA). This method differs from the other approaches for the use of a high-energy planetary ball milling that allows to obtain stable foamed suspensions and to shorten the whole process. That process was chosen for its ability to introduce air bubbles in the ceramic suspension in tailored volume and size thus giving rise, upon sintering, to HA bodies with open and interconnected porosity associated with remarkable mechanical properties.[7]

Two different scaffolds were developed with the methods of direct foaming: a scaffold made of undoped hydroxyapatite (HA), as a control material, and a scaffold obtained by magnesium-strontium doped carbonated hydroxyapatite (MgSrCHA). The two scaffolds, obtained with the same porosity, were compared in terms of morphology, pores distribution, and mechanical properties, in order to understand if the use of multi-doped hydroxyapatite to obtain highly porous scaffolds could lead to final products with increased mechanical performances, confirming the results obtained with the dense scaffolds as described in Chapter 3.

5.1 Direct Foaming

The production of a scaffold by direct foaming requires the development of a ceramic suspension (Fig. 5.2).

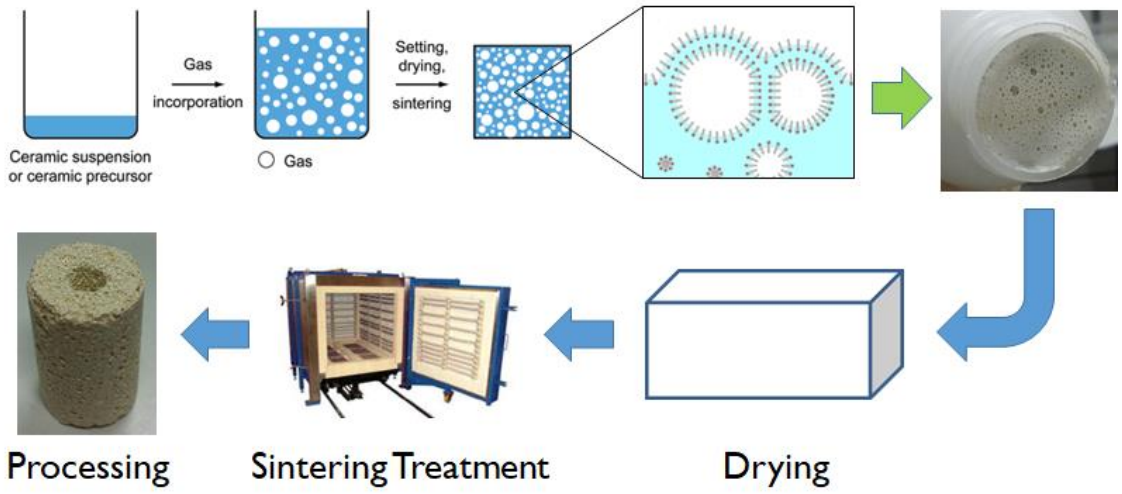

Fig 5.1 – Direct Foaming Process

To produce such a suspension, the two different starting powders of HA and MgSrCHA (Mg=5%mol; Sr=1.5%mol) previously described (see Chapter 3) were calcinated at 1000°C and sieved below 150 µm. Then, the two powders were dispersed in water with a surfactant agent, Dolapix CA (Zschimmer and Schwartz, Germany), according to the weight ratio HA:H_2O:dispersant=73:23:4. A high-energy ball milling treatment, 30 minutes of stirring at 400 rpm (Pulverisette 6, Fritsch, Germany), was used for the preparation of the suspensions in a 250ml zirconia jar with 6 zirconia balls (15mm diameter). Afterwards, in respect to the powder amount, a 2 wt% of Olimpicon A (Olimpia Tensioattivi, Italy) and 0.7 wt% of W53 (Zschimmer and Schwartz, Germany)

were added in the suspensions as foaming agents. Then, after 5 minutes of rapid stirring at 400 rpm the two as-obtained foamed suspensions of HA and MgSrCHA were both poured in 4 different paper molds, 2 for the HA and 2 for the MgSrCHA with dimensions 150x50x30mm. The foamed suspension poured in paper molds were dried for 2 days at room temperature to obtain stable ceramic foams. Finally, the high-temperature thermal treatment (sintering) reported in Table 5.1, including an initial debonding step, was used to consolidate the scaffolds.

Temperature (°C)	Temperature Rate (°C/h)
25-600	30
600-1250	100
1250	1h(dwell time)

Table 5.1 – Sintering process

5.2 Characterization

The 4 different scaffolds (2xHA scaffolds and 2XMgSrHA scaffolds) are visible in Fig. 5.2. The dimensions and the porosity of the 4 scaffolds are listed in Table 5.2.

Fig. 5.2 – Picture of the 4 scaffolds in order from the left to the right: HA-1, HA-2, MgSrCHA-1, MgSrCHA-2

Samples	Length (mm)	Width (mm)	Height (mm)	Volume (cm^3)	Mass (g)	Density (g/cm^3)	Porosity (%)
HA-1	89.10	37.14	21.02	69.56	32.35	0.46	85.28
HA-2	91.10	36.23	20.04	66.14	31.31	0.47	85.02
MgSrCHA - 1	87.66	38.61	22.30	75.46	27.26	0.36	88.57
MgSrCHA - 2	92.18	36.32	19.04	63.76	21.49	0.34	89.33

Table 5.2 – Dimensions of the macroporous scaffolds

The specific surface area (SSA) and the mean particle diameter (d50) of the powders were analyzed before and after the calcination treatment (see Table 5.3). The powders present the same results before and after calcination.

Samples	**SSA** (m^2/g)	$\mathbf{d_{50}}$ (μm)
HA	63.1	0.5
Calcinated HA	3.7	1.7
MgSrCHA	61.2	0.5
Calcinated MgSrCHA	4.2	1.7

Table 5.3 – SSA and d_{50} measurements of HAs before and after calcination

The XRD patterns revealed that each sample is made of only a hydroxyapatite phase (JCPDS Card No.09-0432), only the MgSrCHA scaffolds presents β-TCP (JCPDS Cards No.09-0169) and MgO (JCPDS Cards No.01-1235) as secondary phase (β-TCP 27%vol; MgO 1%vol). As expected, the thermally treated powders exhibited more crystalline patterns, attested by the narrowing of the XRD peaks in respect to the starting powders (Fig.5.3).

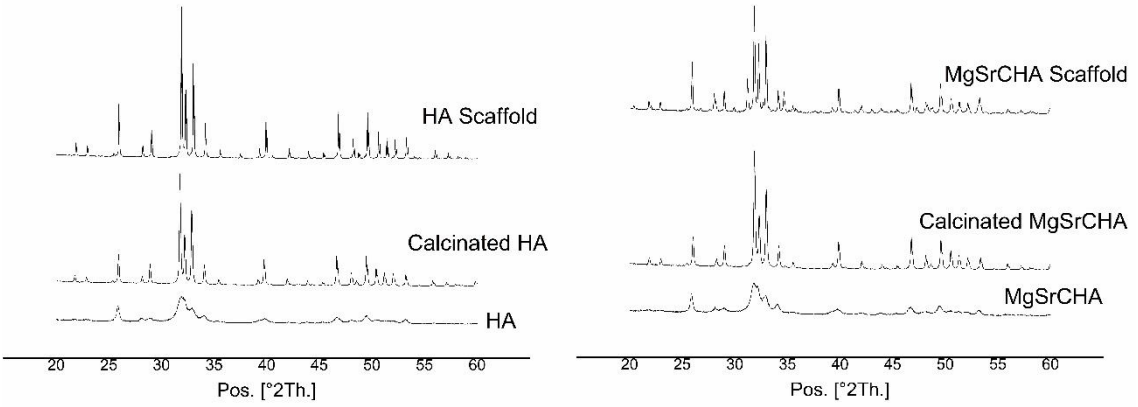

Fig. 5.3 - XRD patterns of the powders, before and after thermal treatments, and the scaffolds

The relative density of the cellular solids was determined by the ratio ρ_c/ρ_s, that is, the density of the cellular material calculated as weight-on-volume ratio (ρ_c), divided by the theoretical density of hydroxyapatite phase (ρ_s=3.16 g/cm^3). The porosity of the structures, Φ, was evaluated as $\Phi = 1-\rho_c/\rho_s$. The porosity of sintered samples was evaluated by both such geometrical method and by the Hg intrusion technique, showing comparable results (Table 5.4).

Sample	Porosity Φ (%)	Φ by Hg Intrusion (%)	Total pore volume (mm³/g)	Total pore Surface area (m²/g)	Average Pore diameter (μm)	Median Pore diameter (μm)	Modal Pore diameter (μm)
HA	85.16	83.0	1957.4	4.4	2.0	217.7	742.1
MgSrCHA	88.95	86.3	2018.7	4.9	2.0	218.5	744.3

Table 5.4 – Results of the mercury porosimetry analysis

In order to test the mechanical properties of the multi-doped HA sintered with CO_2 flux, 5 dense scaffolds, for each sample, in form of cylinders with diameter of 10mm and height of 15mm were tested with a universal testing machine (MTS Insight 5, Minnesota, USA) in a compression test with the crosshead speed was 2mm/min (Table 5.4).

Sample	**Compressive Strength** (MPa)
HA	1.3±0.4
MgSrCHA	0.7±0.3

Table 5.5 – Results of compressive strength test on HA and MgSrCHA scaffolds

There is not a big difference in the results of compression test. MgSrCHA scaffolds result a little weaker than HA scaffolds, but probably this difference is due to the small difference in porosity, indeed MgSrCHA scaffolds are slightly more porous than HA scaffolds (see Table 5.4).

In the article of Dapporto et al[7], the porosity is related to compressive strength (Fig. 5.4) by the formula:

$$\sigma = 10554e^{-0.103\emptyset}$$

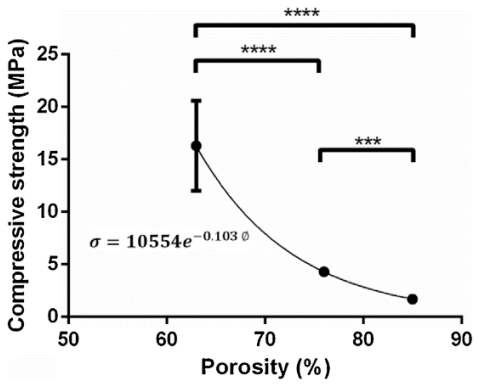

Fig 5.4 – Graphs of the article of Dapporto et al[7], in which porosity is related to compressive strength.

Considering that formula, where σ indicated the compressive strength and ϕ indicated the porosity, the value of compressive strength expected for MgSrCHA scaffolds is 1.10. The value obtained is 0.7±0.3, similar to that expected by the formula.

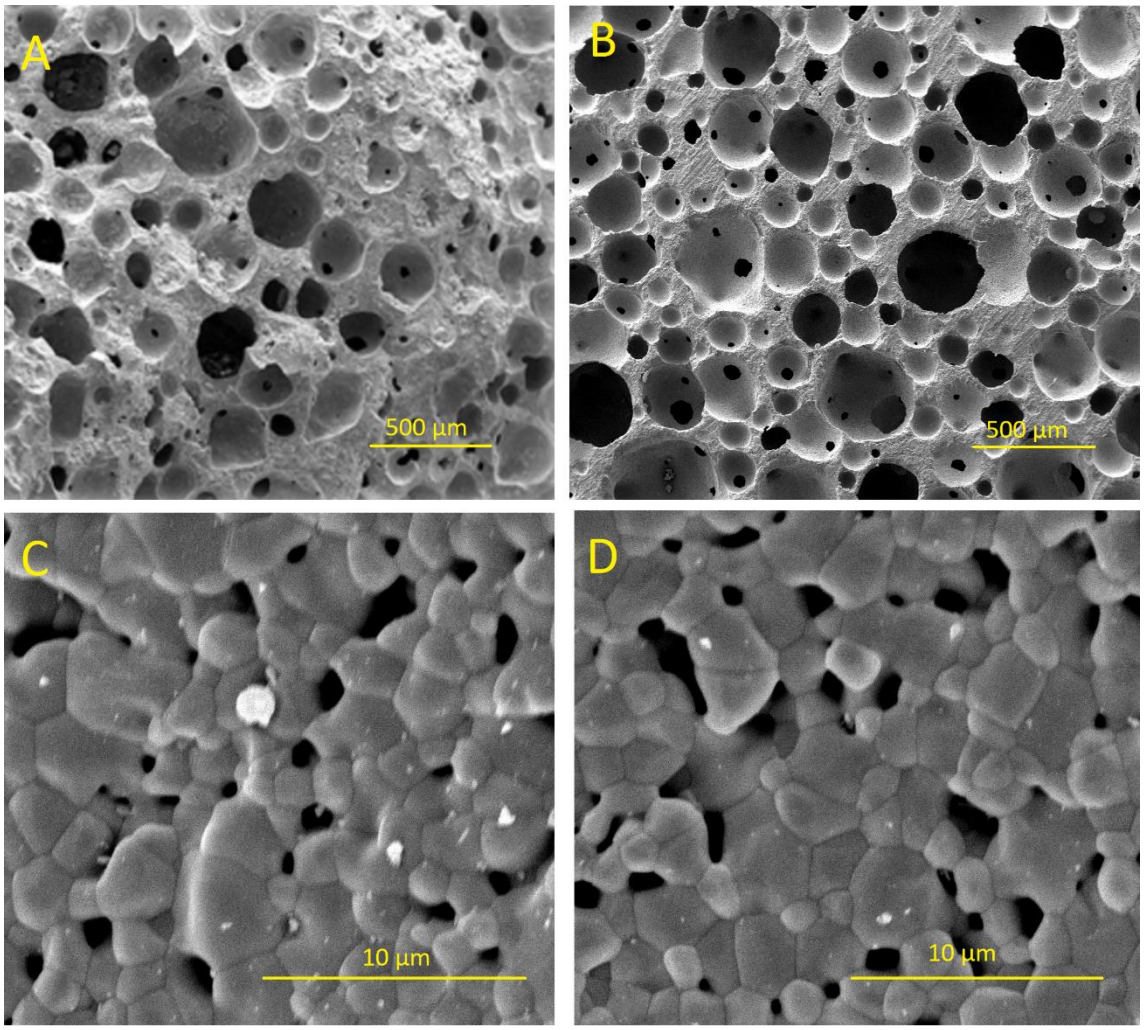

Fig 5.5 - SEM images of the two macro-porous HAs scaffolds at two different magnification. The figures (A) and (C) show pure HA scaffolds while figures (B) and (D) show MgSrCHA scaffolds.

The SEM micrographs of the two scaffolds showed samples very similar in morphology, both samples showed highly interconnected pores with spherical shape (Fig. 5.5A-B). The good consolidation of the struts is clearly visible (Fig. 5.5C-D). Well-coalesced HA grains are intercalated to micron-size pores as detected by SEM investigation at higher magnifications (Fig.5.5C-D), also supporting the results of mercury porosimetry (Table 5.5A-B). A tight cohesion of apatite grains, together with a spherical pore architecture, is evident in sintered scaffolds, thus showing that the calcination treatment was effective in preserving adequate driving energy to yield extensive surface and grain-boundary diffusion towards full neck growth between particles (see Fig. 5.5C-D).

5.3 Conclusion

A direct foaming method carried out with high-energy planetary ball milling was optimized to develop highly porous multi-doped hydroxyapatite-based scaffolds. The method permits to modulate the porosity and the composition, also in terms of the doping ions, thus opening to the possibility to obtain implantable devices with well-defined features for new personalized therapies.

The multi-doped HA scaffolds presents similar morphology, in comparison with simple HA porous scaffolds obtained by the same way. The presence of Mg^{2+} and Sr^{2+} lead to the formation of β-TCP as a secondary phase during the sintering process. The presence of β-TCP could be helpful, improving the release of elements ($Ks_{B\text{-}TCP}$=28.9; Ks_{HA}=58) such as calcium, phosphorus and other bioactive ions providing chemical signals to the cells, relevant for the bone regeneration process, as has been shown in chapter 4.

The mechanical properties of the two scaffolds seems to be similar. The presence of a high porosity (>85%vol) gives scaffolds with low value of mechanical properties, furthermore it’s difficult to discriminate two different materials on the basis of mechanical properties when there is a big content of pores inside it.

References

1. Andrade, J. C.; Camilli, J. A.; Kawachi, E. Y.; Bertran, C. A., Behavior of dense and porous hydroxyapatite implants and tissue response in rat femoral defects. *J Biomed Mater Res* **2002,** *62* (1), 30-6.
2. Yamasaki, H.; Sakai, H., Osteogenic response to porous hydroxyapatite ceramics under the skin of dogs. *Biomaterials* **1992,** *13* (5), 308-12.
3. Cardoso, L.; Fritton, S. P.; Gailani, G.; Benalla, M.; Cowin, S. C., Advances in assessment of bone porosity, permeability and interstitial fluid flow. *J Biomech* **2013,** *46* (2), 253-65.
4. Chang, B. S.; Lee, C. K.; Hong, K. S.; Youn, H. J.; Ryu, H. S.; Chung, S. S.; Park, K. W., Osteoconduction at porous hydroxyapatite with various pore configurations. *Biomaterials* **2000,** *21* (12), 1291-8.
5. Kuhne, J. H.; Bartl, R.; Frisch, B.; Hammer, C.; Jansson, V.; Zimmer, M., Bone formation in coralline hydroxyapatite. Effects of pore size studied in rabbits. *Acta Orthop Scand* **1994,** *65* (3), 246-52.
6. Herring, S. W.; Ochaeron, P., Bone – special problems of the craniofacial region. *Orthodontics & Craniofacial Research* **2005,** *8*, 174-182.
7. Dapporto, M.; Sprio, S.; Fabbi, C.; Figallo, E.; Tampieri, A., A novel route for the synthesis of macroporous bioceramics for bone regeneration. *J. Eur. Ceram. Soc.* **2016,** *36* (9), 23823-2388.

Final Conclusions

In the present thesis various multi-doped nanocrystalline hydroxyapatites were synthesized and used for the development of macroporous scaffolds by direct foaming process. The multiple ions doping induced phase transformations so that the final scaffolds were composed of calcium phosphate HA-TCP composites. The study highlighted that the phase transformations induced by the ionic substitutions in the starting materials induced superior biological and mechanical properties in the final devices. Particularly, bioactive ions exposed or released in physiological media could be the source of improved behaviour of cells and also provided improved ability to inhibit bacterial proliferation, this latter a feature relevant to design new drug-free bio devices, able to contrast the raising resistance of bacteria to antibiotics. From a mechanical perspective, the formation of secondary phases containing part of the introduced doping ions yielded microstructural changes, namely a reduction of mean grain size, in turn inducing enhanced fracture strength. The obtained results show that the new calcium phosphate composites obtained with this approach are promising as porous implantable devices suitable for application in bone regeneration, also in load-bearing sites, and potentially able to contrast the ever raising incidence of nosocomial infections which is among the most critical concerns in medicine nowadays.